AIAA Undergraduate Design Team Project

Final Design Report

Team Hydra: QF-49 Dragonfly

Madi Whitlock, Josh Loeh, Josh Gierut, Thomas Folan, Simon Rodriguez, Nicole Artemyev, Maggie Ni, Alden Yasuda

AE443 - Aerospace Systems Design II

Department of Aerospace Engineering

University of Illinois Urbana Champaign

May 7th, 2025

Madison Whitlock | **Josh Loeh** | **Josh Gierut** | **Thomas Folan**

Simon Rodriguez | **Nicole Artemyev** | **Maggie Ni** | **Alden Yasuda**

Figure 1. Team Hydra Headshots

Table 1. Team Member Discipline Assignments

Team Member	Primary Discipline(s)	Secondary Discipline(s)	Signature
Madison Whitlock 1810727	Team Lead & Systems	Avionics	
Josh Loeh 1810758	Performance	Cost & Ordnance	
Josh Gierut 1810762	Aerodynamics	Landing Gear	
Thomas Folan 1538824	Stability and Control	Configuration	
Simon Rodriguez 1810761	Propulsion	Survivability	
Nicole Artemyev 1810763	Mass Properties	Certification	
Maggie Ni 1339564	Structures	Interior Design	
Alden Yasuda 1810287	Loads and Dynamics	Repair and Maintenance	
Jason Merret	Faculty Advisor	-	

Table of Contents

Nomenclature

b	=	wing span
B	=	wheelbase
$c/4$	=	quarter chord
C_D	=	coefficient of drag
C_{D_0}	=	parasitic drag coefficient
$C_{D_{\text{wave}}}$	=	wave drag coefficient
C_{HT}	=	horizontal tail volume coefficient
C_{VT}	=	vertical tail volume coefficient
C_{l_p}	=	roll damping coefficient
C_{L_0}	=	coefficient of lift before angle of attack
C_{L_α}	=	coefficient of lift as a function of angle of attack
C_L	=	coefficient of lift
$C_{L_{max}}$	=	max coefficient of lift
$C_{l_{\delta a}}$	=	aileron control power
$C_{L_{\alpha VT}}$	=	vertical stabilizer's coefficient of lift
C_{L_f}	=	lift coefficient of flaps
$C_{L_{\delta e}}$	=	effect of elevator deflection on lift
$C_{l_{\delta x}}$	=	power of some control x over roll
C_{l_p}	=	roll damping coefficient
C_{m_0}	=	coefficient of moment before AoA
C_M	=	moment coefficient
C_M	=	moment coefficient about aerodynamic center
C_{M_α}	=	change in coefficient of moment as a function of angle of attack
C_{m_f}	=	moment coefficient of flaps
$C_{m_{\delta e}}$	=	effect of elevator deflection on moment
C_{n_b}	=	body yaw coefficient
C_{n_β}	=	directional stability coefficient
$C_{n_{\delta x}}$	=	power of some control x over yaw
H	=	gear height
I	=	moment of inertia
L	=	lift
l_f	=	distance from vertical tail AC to CG.
M	=	Mach number
M_f	=	distance between the aft center of gravity and main gear
M_{ult}	=	ultimate bending moment
n	=	load factor
P_s	=	excess power
q	=	dynamic pressure
q	=	shear flow
R_e	=	Reynolds number
$S_{flapped}$	=	flapped wing area
S_{ref}	=	wing reference area
t_{rib}	=	rib thickness
V	=	velocity
V_a	=	maneuvering speed
V_c	=	cruise speed
V_d	=	max design dive speed
V_H	=	horizontal tail volume coefficient
V_s	=	stall speed
V_{ult}	=	ultimate shear load
V_v	=	vertical tail volume coefficient
W	=	weight
X_{CG}	=	CG Location
$X_{\text{nose gear}}$	=	position of the nose gear
$X_{\text{main gear}}$	=	position of the main gear
X_{np}	=	Neutral Point Location
X_{SM}	=	CG Location
α	=	angle of attack
β	=	side-slip angle
δ_x	=	deflection of some control surface x
ϵ	=	downwash angle

$\eta_{overall}$	=	overall efficiency
η_p	=	propulsive efficiency
$\theta_{overturn}$	=	overturn angle
$\theta_{tailstrike}$	=	tailstrike angle
$\theta_{tipback}$	=	tipback angle
λ	=	taper ratio
$\Lambda_{H.L.}$	=	angle of the hinge line
μ_B	=	braking coefficient
ρ	=	density
$\dot{\psi}$	=	turn rate

Acronyms

A/B	=	Afterburner
AC	=	Aerodynamic Center
$AIAA$	=	American Institute of Aeronautics and Astronautics
AR	=	Aspect Ratio
AAM	=	Air-to-Air Missile
AoA	=	Angle of Attack
APU	=	Auxillary Power Unit
AVL	=	Athena Vortex Lattice
BFL	=	Balanced Field Length
$BLOS$	=	Beyond Line of Sight
BPR	=	Bypass Ratio
BVR	=	Beyond Visual Range
CAD	=	Computer Aided Design
CFD	=	Computational Fluid Dynamics
CFT	=	Conformal Fuel Tank
CFR	=	Code of Federal Regulations
CG	=	Center of Gravity
CoM	=	Center of Mass
$DAPCA$	=	Development and Production Costs for Aircraft
$DCAP$	=	Defensive Counter Air Patrol
$DISA$	=	Temperature Change from International Standard Atmosphere
DRR	=	Design Readiness Review
DSI	=	Diverterless Supersonic Inlet
ECS	=	Enviornmental Control System
EHA	=	Electro-hydraulic Actuator
EW	=	Empty Weight
FAA	=	Federal Aviation Administration
FEA	=	Finite Element Analysis
FH	=	Flight Hour
FW	=	Fuel Weight
GCS	=	Ground Control Station
GD	=	General Dynamics
GFE	=	Government Furnished Equipment
GPS	=	Global Positioning System
HLD	=	High Lift Device
$ICNIA$	=	Integrated Communication, Navigation, and Identification Avionics
IE	=	Intercept/ Escort Mission
IFF	=	Identification Friend or Foe
$INEWS$	=	Integrated Electronic Warfare System
$IRSTS$	=	Infrared Search and Track System
JFS	=	Jet Fuel Starter
$KEAS$	=	Knots Equivalent Airspeed
L/D	=	Lift to Drag Ratio
LFL	=	Landing Field Length
LG	=	Landing Gear
LOS	=	Line of Sight
MAC	=	Mean Aerodynamic Chord
MMH	=	Maintenance Man-Hour
MSL	=	Mean Sea Level
$MTOW$	=	Max Takeoff Weight
MS	=	Margin of Safety
$MZFW$	=	Max Zero Fuel Weight
$NATO$	=	North Atlantic Treaty Organization
NDT	=	Non-Destructive Testing
OEW	=	Operating Empty Weight
$O\&M$	=	Operations and Maintenance
$OMSI$	=	Operations, Maintenance, Spares, and Infrastructure
OPR	=	Overall Pressure Ratio
PDI	=	Point Defense Intercept
PC	=	Power Condition
PRV	=	Pressure Relief Valve
RAM	=	Radar Absorbing Material
$RANS$	=	Reynolds Average Navier Stokes
RCS	=	Radar Cross Section
$RDT\&E$	=	Research, Development, Test, and Evaluation
RFP	=	Request For Proposal
$SABR$	=	Scalable Agile Beam Radar
$SATCOM$	=	Satellite Communications
SFC	=	Specific Fuel Consumption
SLS	=	Sea Level Static
SM	=	Static Margin
TDL	=	Tactical Data Link
$TOFL$	=	Takeoff Field Length
T/W	=	Thrust to Weight Ratio
UTS	=	Ultimate Tensile Strength
VMS	=	Vehicle Management System
$VTOL$	=	Vertical Takeoff and Landing
W/S	=	Wing Loading
$WUTTO$	=	Warm Up, Taxi, Takeoff

List of Figures

List of Tables

Table 2. RFP Requirements/ Compliance Checklist

Category	Requirements	Dragonfly	Section
Perf.	Perform 3 missions (see Figs. 2, 3, and 4).	Met	VII.C
	Must operate in all weather from existing NATO runways. (BFL ≤ 8,000 ft)	3,900 ft	VII.A
	Must be capable of all-weather interception and weapon delivery.	Met	XII.D
	Max Mach Number at 35,000 ft = 1.6	1.6	VII.D
	Maximum Instantaneous Turn Rate = 18.0 deg/s	18.0 deg/s	VII.D
	1-g Specific Excess Power– Military Thrust - 0.9M/ Sea Level = 200 ft/s - 0.9M/ 15,000 ft = 50 ft/s	 232 ft/s 173 ft/s	V.D
	1-g Specific Excess Power– Maximum Thrust - 0.9M/ Sea Level = 700 ft/s - 0.9M/ 15,000 ft = 400 ft/s	 788 ft/s 607 ft/s	V.D
	5-g Specific Excess Power - Maximum Thrust - 0.9M/ Sea Level = 300 ft/s - 0.9M/ 15,000 ft = 50 ft/s	 510 ft/s 330 ft/s	V.D
	Sustained Load Factor - Maximum Thrust - 0.9M/ 15,000 ft = 5.0 g's	 Met	VII.D
Systems	All Systems must be designed for remote pilot operation.	Met	XII.E.2
Maint.	The design must allow easy access to and removal of primary elements of all major systems.	Met	XVI.B
Structure	Design limit load factors are +7 and -3 vertical g's in the clean configuration with 50% internal fuel.	+8 and -3	IX.A
	The structure should withstand a dynamic pressure of 2,133 psf (M=1.2 at sea level).	Met	IX.A
	A factor of safety of 1.5 should be used on all design ultimate loads.	Met	IX.A
	Primary structures should be designed for durability and damage tolerance.	Met	IX.H
	Design service life is 2,000 hours.	Met	IX.I
Fuel	Primary design fuel is standard JP-8 or Jet-A.	Met	XII.B
	All fuel tanks will be self-sealing.	Met	XII.B
	External fuel tanks may be carried for design missions, but must be retained for the entire mission.	Met	XII.B
Stability	Unaugmented subsonic longitudinal static margin shall be no greater than 10% and no less than -10%.	(-9.1, 8.2)	VIII.E
	A digital flight control system is mandatory for designs that are statically unstable in the longitudinal axis.	Met	XII.E
Cost	Flyaway cost per aircraft for a 1000 aircraft buy will not exceed $25 million in 2024 US dollars.	$24.97 mil	XIII.A
	All practical measures will be taken to minimize total life cycle costs.	Met	XIII.A
Weapon Carriage	Trade the number of AIM-120.	4	XIV.A.1
	Trade the internal and external carriage.	No M61	XIV.B
Prop.	Environmental control systems and the avionics liquid cooling system require 2% of engine mass flow.	Met	V.D
	A derivative of the engine should currently be in production or forecast to be in production by 2027.	In service	V.A

Executive Summary

The AIAA Design Competition RFP asks for a low-cost, homeland defense interceptor capable of executing three distinct missions, achieving an instantaneous turn rate of 18 deg/s, and meeting several other performance requirements [1]. The Dragonfly is the solution to this problem, a simple, no-frills design that meets all requirements and stays under budget at $24.97 million. The Dragonfly features cropped delta wings, conventional horizontal stabilizers, and a single vertical stabilizer aft of the wing. The wing area is 495 ft^2 and the AR is 4.0. Control surfaces include flaps, ailerons, slats, all-moving stabilators, and a rudder. Below the fuselage, the Dragonfly accommodates landing gear with a split inlet that leads into a single F110 engine. The aircraft's maximum fuel capacity is determined by the demands of the DCAP mission; however, over-wing conformal fuel tanks can be removed for better performance during lower-fuel missions such as the PDI mission. To successfully carry out its missions, the Dragonfly achieves the RFP-mandated speed of Mach 1.6 at 35,000 ft and is equipped to carry four AIM-120 AMRAAMs, mounted under the wings.

I. Introduction

The September 11th attacks proved the extreme impact an air attack could have on the United States. International political tensions are continuously on the rise, and with that comes the threat that the United States could be forced into a defensive position by an air attack mirroring the September 11th attacks. This threat could manifest in a number of ways, as large hijacked airliners or small autonomous cruise missiles. To combat this potential air threat, homeland defense is looking for a high performance aircraft that is simple and cost-effective in order not to pull away too much money from offensive forces. This dictates a flyaway cost budget of $25 million [1], which is significantly less than the $143 million flyaway cost of the F-22 [2] or $80-110 million for the F-35 [3]. Additionally, in order to minimize pilot safety risks and have quicker response times, the new aircraft must be remote piloted.

Team Hydra fulfills this niche by introducing the QF-49 Dragonfly. Designed to prioritize a low-cost, no-frills design, the Dragonfly is still built to keep up with other modern fighters. The Dragonfly has cropped delta wings with a wing area of 495 ft^2 and an aspect ratio of 4.0, conventional horizontal stabilizers, and a single vertical stabilizer aft of the wing. The Dragonfly also features removable conformal tanks to allow it to meet demanding performance requirements across a variety of missions. During these missions, the Dragonfly can achieve dash speeds of Mach 1.6 at 35,000 feet and is armed with four AIM-120 AMRAAMs.

II. Concept of Operations

A detailed list of requirements set by the RFP can be seen above in Table 2. The most constraining requirements from this list were the maximum instantaneous turn rate of 18.0 deg/s and the max flyaway cost of $25 million. In addition to these requirements, the Dragonfly must complete three missions. The first mission that the Dragonfly must perform is a defensive counter-air patrol mission (Fig. 2), where the Dragonfly cruises for 300 nmi, performs a four hour combat air patrol, dashes 100 nmi, performs prescribed combat maneuvers, then cruises back 400 nmi. The second mission is a point defense intercept mission (Fig. 3), where the Dragonfly dashes out 200 nmi at max speed, performs the prescribed combat maneuvers, then cruises 200 nmi. The final evaluated mission (Fig. 4) consists of the Dragonfly dashing out at max speed, escorting 300 nmi at a practical airspeed, and then cruising back.

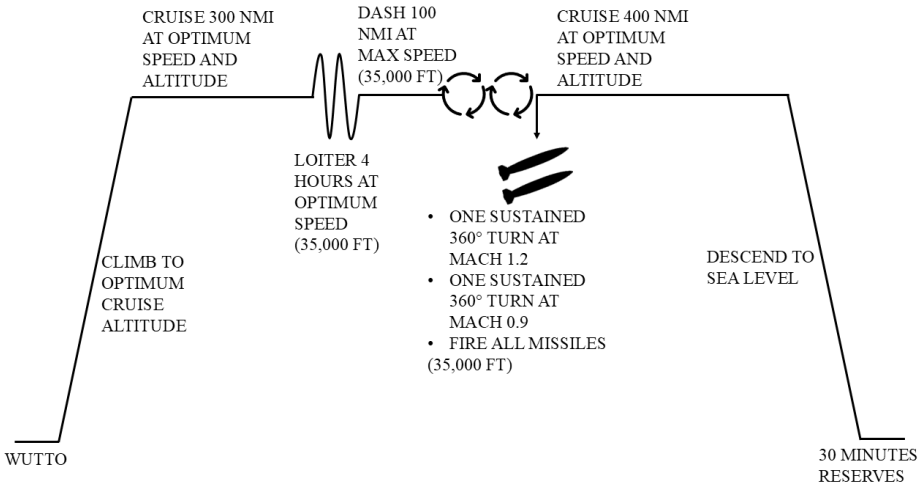

Figure 2. Mission 1: Defensive Counter Air Patrol

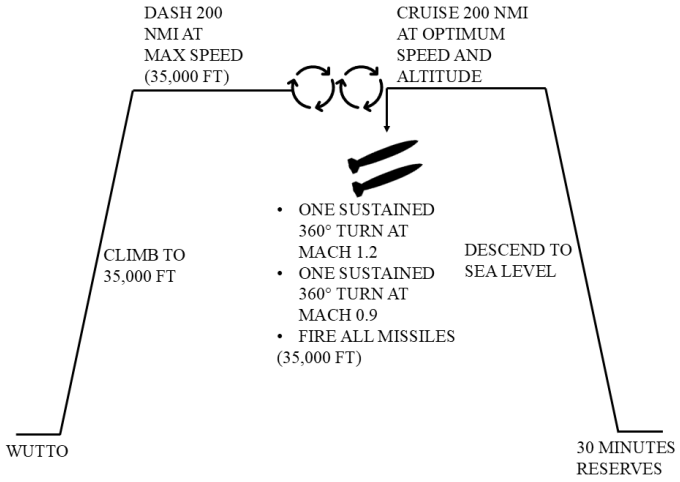

Figure 3. Mission 2: Point Defense Intercept Mission

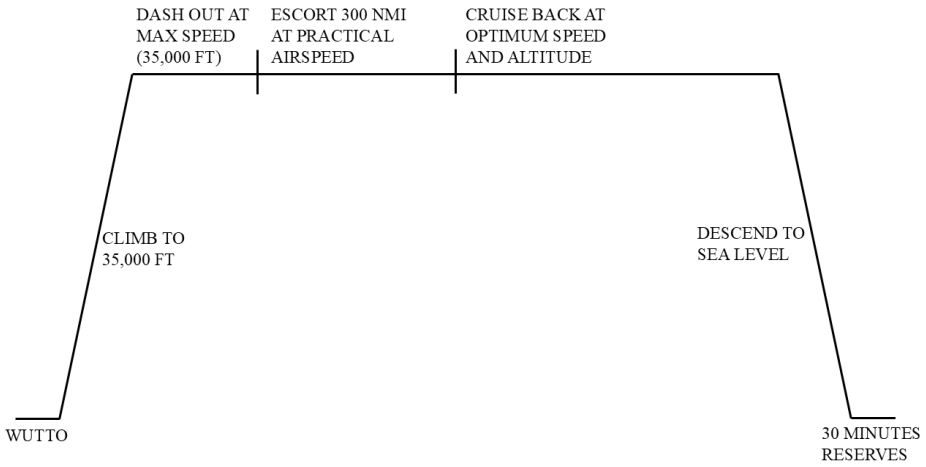

Figure 4. Mission 3: Intercept/ Escort Mission

The most constraining mission was found to be Mission 1, the Defense Counter Air Patrol mission, due to its high fuel requirements for a four-hour loiter (discussed in more detail in Section VII.C.1). However, the Dragonfly requires significantly less fuel for mission 2 (see Section VII.C.2), so the Dragonfly's conformal tanks were designed to be removed depending on the mission.

The operation of the Dragonfly can be seen in the OV-1, Fig. 5. The Dragonfly is capable of taking off and landing from all NATO runways in any conditions, not just designated Ground Control Stations (GCS). Although the Dragonfly's conformal tanks are removable, they are not designed to be quickly installed or removed in scramble situations. The conformal tanks require a crane to be removed, so it is expected that the Ground Control Station will have both versions available at any time. As per the RFP, the Dragonfly will be remote piloted. The Dragonfly will use Line of Sight communications when possible, and satellite communications otherwise. One of the Dragonfly's autonomous capabilities is that it can perform waypoint navigation on its own. In case of emergency, if communications are lost, the Dragonfly will navigate back to the Ground Control Station, another designated landing site, or a designated crash site away from civilian infrastructure, depending on the situation. In accordance with the RCC-323 Range Safety Criteria for Unmanned Aerial Vehicles, chapter 3, section 1 states that there shall be no risk to the public during instances of hazardous operations. During the case of an emergency, the aircraft termination route will adhere to these regulations to ensure the vehicle remains inside the assigned airspace over an unpopulated area on loss of control link. Although ideally the Dragonfly will survive and return from any combat situation, the Dragonfly is seen as a first line of defense aircraft that is more expendable than a regular fighter due to its remote piloted nature and lower cost.

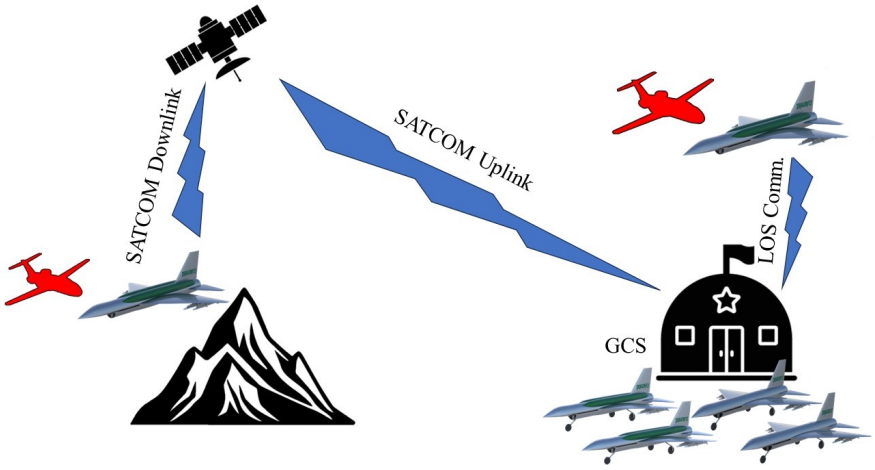

Figure 5. Communications Methodology

III. Sizing Analysis

A. Similarity Analysis

The initial sizing of the Dragonfly was primarily based on the F-16 Fighting Falcon. The F-106 Delta Dart and MiG-25 Foxbat were also considered. The major drawback of the F-16 is that its cost, performance, and complexity, due to being a multirole aircraft, exceed what is required by the RFP. The F-106 is a true interceptor aircraft, but is significantly older than other aircraft considered and in need of updates for modern technology. The major drawback of the Mig-25 is its size, its high MTOW will make it very challenging to stay within the cost requirement since cost is directly proportional to weight. The F-16, F-106, and MiG-25 are compared in Table 3. Green, yellow, and red cells dictate whether or not the aircraft meet RFP requirements. All aircraft specifications are found in *Jane's All the World's Aircraft 1963-1964* [4] or *1977-1978* [5] unless specified within the table.

Table 3. Similarity Analysis

	F-16	F-106	MiG-25
Max Take Off Weight [lb]	33,000	35,000	79,800
Max Speed [Mach]	1.95	2.1	3.2
TOFL [ft]	1,750	6,000	4,525
Wing Area [ft^2]	300	700	603
AR	3	2.2	3.3
Taper Ratio	0.39	Delta Wing	0.36
Overall Length [ft]	47.64	70.7	73.17
Max Thrust	26,950	24,500	24,700
SFC [lb/lbf-hr]	0.68-2.55	1.16	1.25-2.7 [6]
Flyaway Cost [millions][2024 US Dollars]	$28.6 [7]	$35.7 [8]	N/A

B. Constraint Diagram

The constraint diagram for the Dragonfly is shown in Fig. 6. Each curve represents a specific constraint due to a part of a mission or a requirement listed in the RFP [1]. The most constraining requirements are the 18 deg/s instantaneous turn, the Mach 1.6 at 35,000 ft dash, and the climb to 35,000 ft, all mentioned in the RFP. The region above all curves indicates combinations of T/W and W/S that satisfy all design constraints, as shown by the yellow-colored region. The Dragonfly is successfully within the feasible region and satisfies all design constraints.

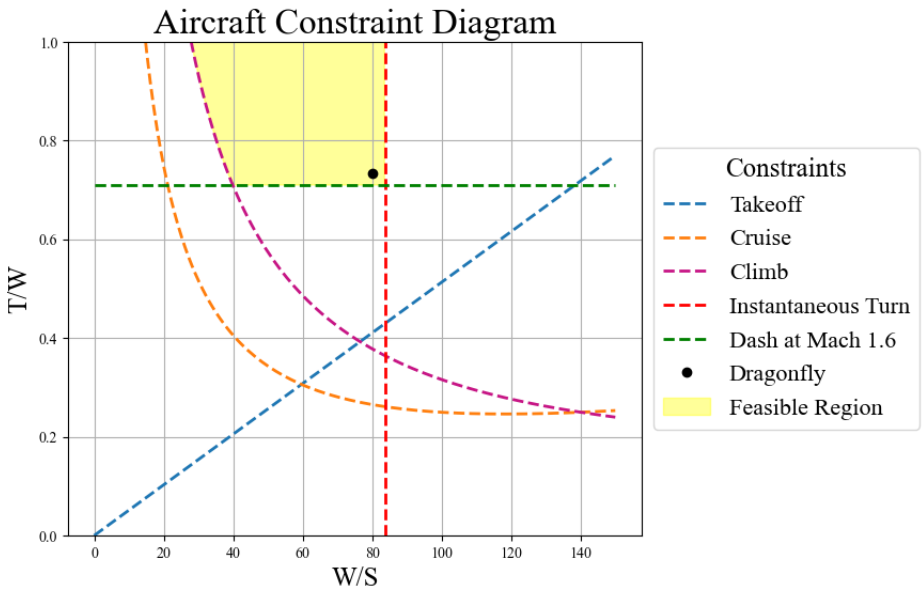

Figure 6. Dragonfly's Constraint Diagram

C. Sizing Iterations

In order to speed up iteration cycles and approach an ideal design in the fastest possible manner, an automatic sizing simulator was created. Through a series of intermeshed functions, constraint tests, and simulations, the sizing tool automatically calculated the minimum required performance characteristics and designed an aircraft to meet them. The program would then run the new design through the same tests and continue the iteration process until converging upon an ideal solution. While the F-16's features were used for initial seed inputs, such a quantity of modifications were made to the design that none of the seed inputs remained in use by the end of the project, being usurped by more optimal design choices. The sizing system was adapted and expanded continuously throughout the aircraft design process, serving to seamlessly join the work of multiple disciplines.

Due to the RFP specification that the 18 deg/s performance characteristic was to be achieved with 50% internal fuel, it was decided that external fuel carriage was optimal. The instantaneous turn was largely a function of wing area, C_L, and weight, so reducing the weight present during the turn was extremely beneficial in lessening the other requirements.

The instant turn rate requirement was in such excess in comparison to all other wing-loading-based criteria that the shrunken wing still met every other performance requirement. High-lift devices were employed to maximize $C_{L_{max}}$ during the instantaneous turn without increasing drag during other mission segments.

Once the design had reached a consensus on the aircraft size and requirements, engine sizing was switched from rubber to fixed, satisfying the RFP desire that the engine is a non-developmental item [1].

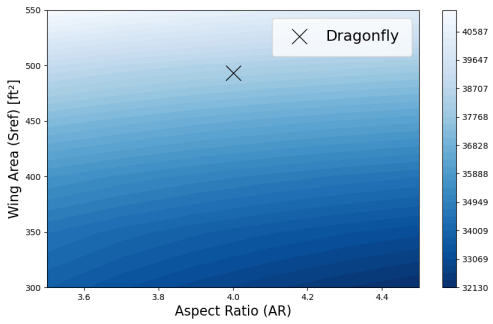

(a) MTOW

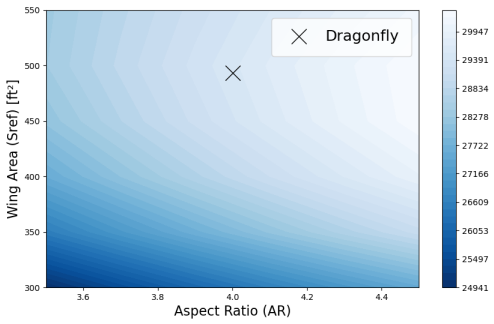

(b) Thrust Required

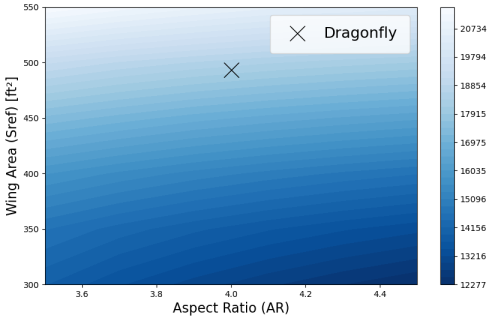

(c) Empty Weight

Figure 7. Contour Plot of Wing Area vs Aspect Ratio

IV. Configuration

A. Investigating Alternative Configurations

In selecting a configuration, the primary concerns were CG management, accommodation of internal configuration, increase of C_L, and reduction of weight, drag, and developmental risk. Of particular concern was the need to accommodate a significant amount of fuel ($12 - 18$ thousand lb) to complete the required set of missions from the RFP, as identified during preliminary sizing analysis.

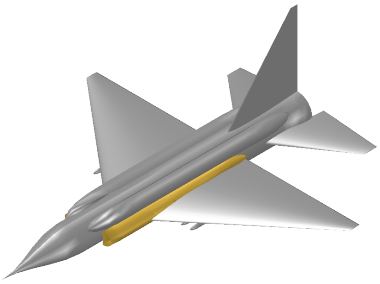

Figure 8. Side Intakes

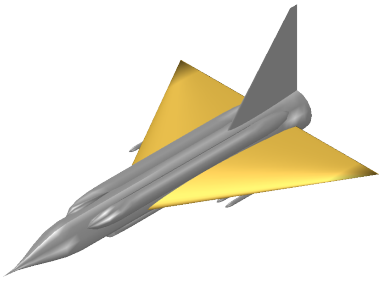

Figure 9. Tailless Delta

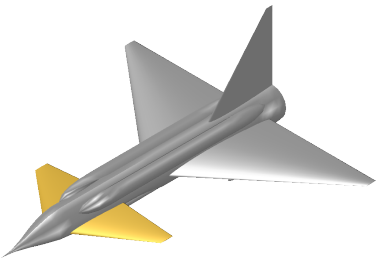

Figure 10. Delta Canard

1. Side Intakes

A configuration variant with side intakes can be seen in Fig. 8. Side inlets offered the configuration and stability benefits of a more symmetrical layout, in addition to freeing up the underside of the nose for simpler landing-gear integration. However, the issue of pressure instability stemming from the joining of the split intakes made this a riskier choice [9]. In addition, there were concerns about structural complexity stemming from the joining of the wing with the fuselage and needing to accommodate the intake's ducting.

2. Tailless Delta

A tailless delta such as the configuration seen in Fig. 9 was initially promising, offering the elimination of the tail's weight and drag penalties [9]. However, difficulties in finding sufficient volume for fuel tanks during internal configuration design led to non-ideal placements of tanks, resulting in a significant CG shift on the order of 16% MAC between the takeoff and empty weights. After trial and error, no effective method to reduce the CG shift could be found without inducing significant drag losses or shifting to a less ideal engine configuration. With these issues identified, the tailless delta concept was ultimately disregarded.

3. Delta Canard

A variant with a delta canard configuration is seen in Fig. 10. The delta canard design promised benefits in terms of increasing the maximum C_L during the 18 deg/s turn requirement of the RFP, as a result of producing lift during a pitching-up maneuver [1]. The instantaneous turn rate of an aircraft, assuming it can maintain trim during the turn, depends upon W/S, $C_{L_{max}}$,ρ_∞ , n, and V [9]. A higher $C_{L_{max}}$ during pull-up would result in a higher possible W/S and a lower necessary n, reducing structural weight significantly. However, the subject of CG placement is again an issue.

By removing the tail and substituting it with a canard in the front of the aircraft, the main wing would have to move aft to keep X_{np} near the CG. This series of changes would have resulted in a rearward shift of the empty CG. In order to meet the RFP requirement of a stability margin within the range of ±10%, this would have required the fuel tanks to be moved aft to reduce the overall movement of the CG. The rear volume of the fuselage is dominated by the engine and

intake; thus, finding volume for fuel in this section would have required the fuselage to be expanded, increasing drag and empty weight. In addition, there were concerns about the structural loads of having a control surface so far forward on the aircraft, away from other significant structural members. Due to the issues with CG placement and structural concerns, the delta canard configuration was deemed unsuitable for meeting RFP requirements.

B. Selected Configuration

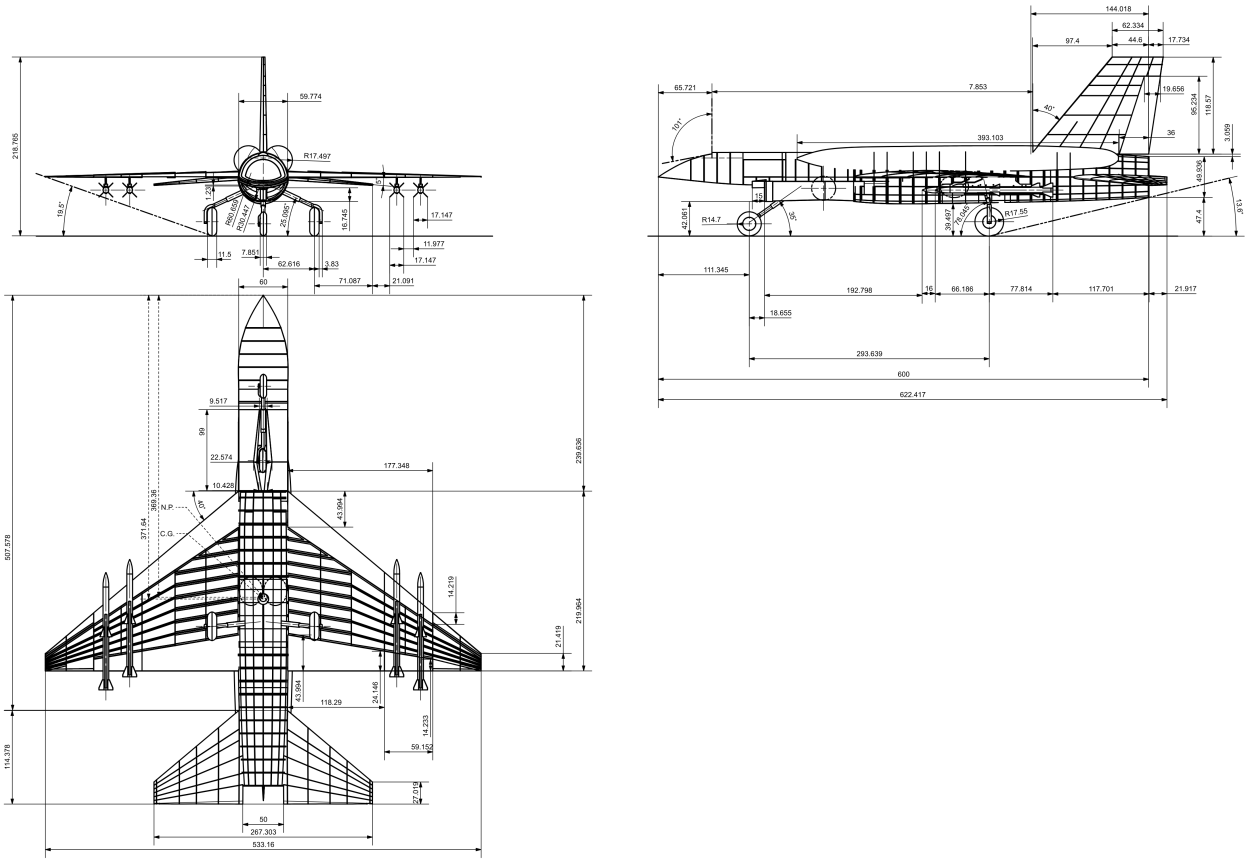

Figure 11. 3-View Drawing of the Dragonfly's External Configuration

The selected configuration for the Dragonfly, shown in Fig. 11, utilizes a single-engine, conventional tail, cropped-delta-wing, chin-inlet design. For propulsion, a single afterburning F-110-GE-129 is installed in the rear of the aircraft, supplied by a chin inlet, which is split in the front to accommodate a nose landing gear within the split. Conformal fuel tanks are utilized along the top of the fuselage to enable missions with higher fuel requirements without compromising performance in those not requiring such tanks. The fuselage is designed with a largely tubular cross-section fuselage to simplify construction, structures, and to minimize the wetted area to volume ratio. The stabilizing surfaces take the form of one vertical fin and two horizontal tail surfaces.

In order to maximize lift without bloating the size of the wing, high-lift devices in the form of slats and Fowler-flaps are utilized. An all-moving horizontal tail is used for pitch control, dedicated ailerons are used for roll control, and a rudder is used for yaw control. Dedicated flaps and aileron systems were utilized instead of combined flaperons in order to minimize control surface area whilst also ensuring sufficient lift and roll control during such high-lift conditions as landing and takeoff.

Four AMRAAM missiles can be carried on pylons beneath the wing, simplifying construction and maintenance in comparison to a proprietary internal system or partially-embedded carrying configuration such as seen on the F-4 Phantom. The reasoning behind the decision to exclude a gun and carry four AMRAAMs is discussed in XIV.

A larger, unedited version of Fig. 11 can be found in the Appendix.

C. Internal Configuration

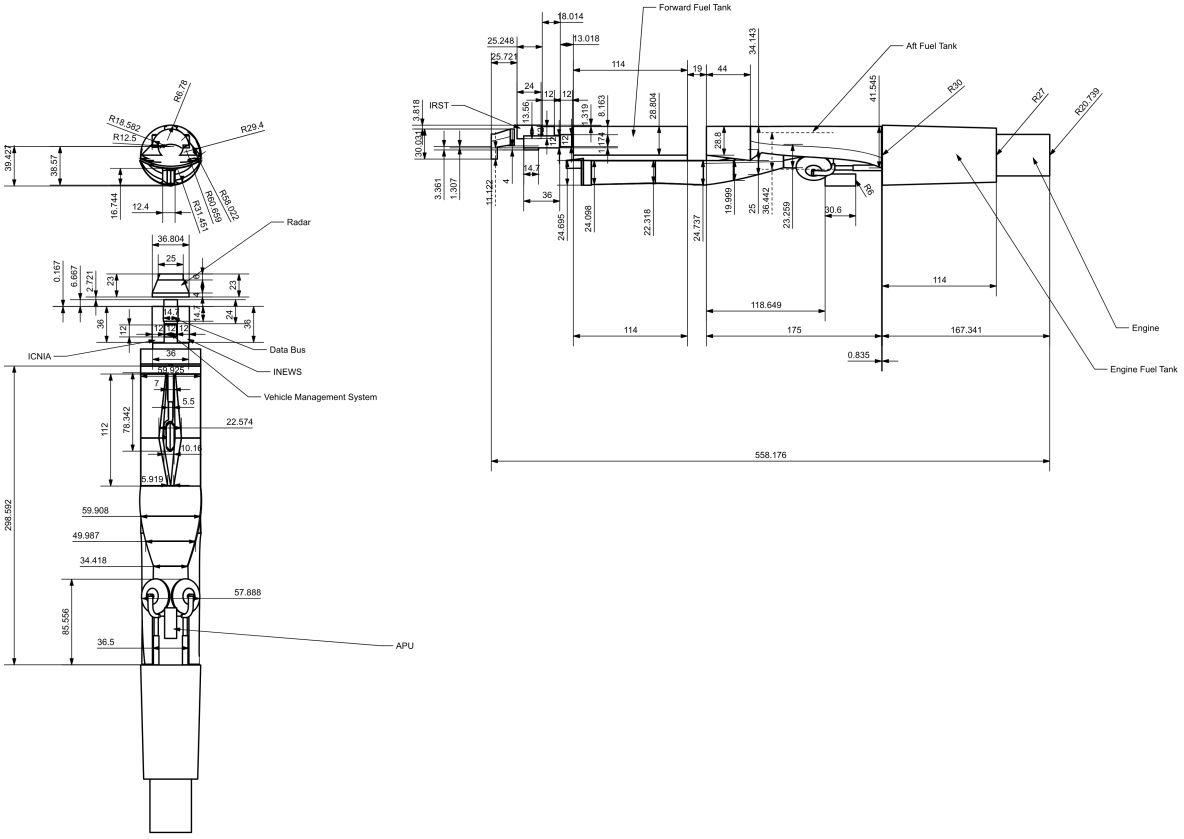

Figure 12. Shrunk 3-View Drawing of the Dragonfly's Internal Configuration

The internal configuration layout of the Dragonfly is shown in Fig. 35. Electronic systems are concentrated in the nose to centralize the electronics placement for ease of connectivity, maintenance, and installation. The sensors, in the form of the radar and IRST systems, are located frontally to ensure a clear line of view for each system. The APU is installed in the belly, near the engine, to simplify its connectivity.

The chin-mounted intake is placed ahead of the wings, landing gears, and other significant obstacles that could induce turbulent airflow, with a gap between the inlet and the body to maximize pressure recovery and clean airflow in spite of the overhanging nose-section. The inlet is split for a short distance right after intake, allowing for the front landing gear to fold in-between the split ducts. However, the distance between these ducts was kept minimal to ease their gentle recombination. This inlet is discussed in more depth in Section V.C. The fuselage was made larger than the engine, its widest interior component, in order to accommodate fuel around the initial stages of the engine, shifting the maximum CG towards the empty CG, which is biased towards the rear of the aircraft.

Three internal fuel tanks are spread throughout the aircraft, with a fuel distribution system capable of distributing the fuel between them to optimize the CG location during the majority of the flight. Meeting requirements in the RFP, all fuel tanks are self-sealing [1]. Fuel volume calculations assumed 14% of each tank's volume was occupied by self-sealing systems. No fuel is required as a ballast in order to maintain static margins during flight. No fuel is stored in the wings as their thin cross-sections and the requirement for self-sealing would have resulted in high surface-area, high-empty-weight tanks with minimal usable fuel volume.

The landing gears are retracted into the body, as it was not possible to fit sufficiently large landing gears into the thin wing-planform without sacrificing structures near the root or adding bulges. The main landing gears are drawn into the space under the rear section of the intake. Countermeasure dispensers can be mounted above the afterburner of the engine to improve survivability. This option is discussed more in section XV.

A larger, unedited version of Fig. 35 can be found in the Appendix.

V. Propulsion

This section covers all propulsion-related aspects of the Dragonfly, including engine selection, inlet design, installation losses, and overall performance analysis. The Dragonfly's fuel system is described in section XII.B. Initial sizing established baseline thrust requirements that could meet the aircraft's mission profile as described in the RFP. These requirements drove the selection of an afterburning turbofan engine with minimal modification needs. Further design efforts focused on integrating the propulsion system efficiently while preserving performance and cost-effectiveness.

A. Engine Selection

Several different engines were evaluated for this aircraft, selected primarily from aircraft with similar roles and mission requirements. Because the aircraft must enter production within the next few years, only engines currently in production or projected to be available by 2027 were considered. As a result, the selected engine is a production-ready design with no resizing applied, though minor modifications remain possible. The propulsion requirements are driven by the aircraft's need to perform supersonic maneuvers, which demand a significant amount of excess thrust. Therefore, only

low-bypass, afterburning turbofans, which are commonplace in supersonic fighters and interceptors, were considered. Candidate engines were compared based on thrust, thrust-specific fuel consumption (SFC), weight, and other categories, as seen in Table 4. Due to limited publicly available data for the F135-PW-100, its SFC values were estimated using empirical methods by Raymer (Equations 10.13 and 10.15) [9]. All SFC values are given for sea-level static conditions, corresponding to PC-50 for maximum dry thrust and PC-100 for maximum afterburner thrust.

Table 4. Afterburning Turbofan Similarity Analysis

Engine	Dry Thrust [lb]	A/B Thrust [lb]	Weight [lb]	SLS Dry SFC [1/hr]	SLS Wet SFC [1/hr]	Max T/W	Bypass Ratio	Fan Diameter [in]	Aircraft
F110-GE-129	17,400	29,500	3,940	0.67	1.85	7.48	0.76	36.1	F-16C/D
F119-PW-100	27,000	35,000	4,700	0.89	1.83	7.45	0.25	40	F-22
F135-PW-100	28,000	43,000	6,422	0.63*	1.96*	6.70	0.57	43	F-35

The precise thrust and power requirements for cruise and dash conditions were determined using a time-step method, accounting for drag and excess power needs throughout the mission profile. Among the candidate engines, the F110-GE-129 was selected due to its proximity to the initially calculated performance requirements in both dry and afterburning modes (around 14,000 and 23,000 lbf, respectively), minimizing the need for scaling or modification. Its baseline configuration provides sufficient thrust margin for maneuvering and supersonic dash, while reducing the penalties of excess weight or fuel burn. Furthermore, the F110-GE-129 is the lightest and most compact of the engines considered, with the smallest diameter and overall length, simplifying integration within the fuselage. It also offers one of the highest thrust-to-weight ratios in its class, enhancing acceleration and climb performance. These advantages, combined with its proven reliability in aircraft such as the F-16C/D, made it the most suitable choice for the design objectives and timeline of this aircraft.

B. Engine Overview

The F110-GE-129 is a low-bypass, axial-flow, afterburning turbofan. It features a two-stage low-pressure turbine that drives a three-stage fan, and a one-stage high-pressure turbine that drives a nine-stage axial compressor. This configuration provides the high pressure ratio and mass flow rate necessary for sustained supersonic flight and maneuvering. A variable-area exhaust nozzle is included as standard, allowing the engine to maintain optimal thrust efficiency throughout varying throttle settings and flight regimes. A jet fuel starter (JFS) is used for engine start-up. The basic engine specifications are summarized in Table 5. The thrust values shown in the data sheet reflect installed performance, with penalties applied to represent expected losses at cruise and dash conditions for dry and afterburning thrust, respectively. The methods used to estimate these installation losses are described in section V.D.

Table 5. F110-GE-129 Engine Data Sheet

Dry Thrust	**Value**	**A/B Thrust**	**Value**
Uninstalled	17,400 lbf	Uninstalled	29,500 lbf
Installed	15,900 lbf	Installed	27,300 lbf
Engine Specs	**Value**	**General Engine Information**	**Value**
Length	15.166 ft	OPR (Overall Pressure Ratio)	30.7
Max Diameter	46.5 in	BPR (Bypass Ratio)	0.76
Fan Diameter	36.5 in	SLS PC-50 Dry SFC	0.67 lb/hr/lbf
Fan Area	7.26 ft^2	SLS PC-100 Wet SFC	1.85 lb/hr/lbf
Weight	3,940 lb	Max Dry T/W	4.47
		Max Wet T/W	7.48

A potential engine scaling effort was considered, given that the F110-GE-129 produces several thousand pounds more thrust than the Dragonfly was calculated to require. Downsizing the engine could have reduced both thrust and weight, aligning more closely with the aircraft's performance needs. However, two key factors led to the decision to retain the full-size engine. First, specific fuel consumption (SFC) generally increases when engines are scaled down, resulting in reduced fuel efficiency [10]. Second, modifying the engine would introduce additional development and manufacturing costs due to design changes and increased labor. Given the Dragonfly's emphasis on simplicity and affordability, it was deemed preferable to use the unmodified engine. This decision is further supported by the fact that GE already holds active production contracts for the F110-GE-129 with the U.S. Air Force [11], allowing production of the Dragonfly to leverage existing supply chains and infrastructure.

C. Inlet Design

Factors considered in the inlet design included weight, cost, complexity, and pressure recovery. According to Raymer [9] and Nicolai [12], pitot inlets, which form a single normal shock at the lip at supersonic speeds, offer acceptable pressure recovery up to approximately Mach 1.6, which matches the aircraft's maximum design speed. While other inlet types such as diverterless supersonic inlets (DSIs) and variable-geometry ramps provide better performance at higher Mach numbers, they come with significant drawbacks. While DSIs can achieve pressure recovery values as high as 0.95 [13] at Mach 1.55-very close to the aircraft's design Mach number-this effort was not prioritized due to greater emphasis on overall integration and design feasibility. Additionally, it cannot adapt to off-design conditions as effectively and has slightly higher weight and cost. The variable-geometry inlet offers the best pressure recovery across supersonic conditions but is significantly heavier, more complex, and introduces a higher radar cross section due to its large adjustable surfaces. Table 6 summarizes the tradeoffs among these three configurations. Where possible, numerical values were used; other categories are represented qualitatively as "low," "moderate," or "high." Considering the project's emphasis on simplicity, affordability, and acceptable performance at Mach 1.6, the pitot inlet was selected as the most appropriate choice.

Table 6. Comparison of Inlet Types with Performance and Integration Attributes

Inlet Type	Pressure Recovery @ M0.8	Pressure Recovery @ M1.6	Weight [lb]	Complexity	RCS Reduction
Pitot	0.99 [12]	0.89 [12]	~500 [12]	Low [9]	Low [9]
Variable Geometry	0.97 [12]	0.94–0.97 [12]	~1600 [12]	High [12]	Moderate [14]
DSI	0.98 [13]	0.90–0.95 [13]	~750 [12]	Moderate [15]	High [16]

The procedure described in Nicolai Chapter 15 [12] was used in combination with compressible flow continuity relations to size the inlet for the engine's airflow requirements across various conditions. The results of this calculation, along with the design cruise and dash points, are shown in Figure 13. Since the dash condition required the highest mass flow rate, the inlet was sized to meet this requirement, resulting in a capture area of 6.9 ft^2. The duct length was also sized using Nicolai's method, yielding a total inlet duct length of 21 ft.

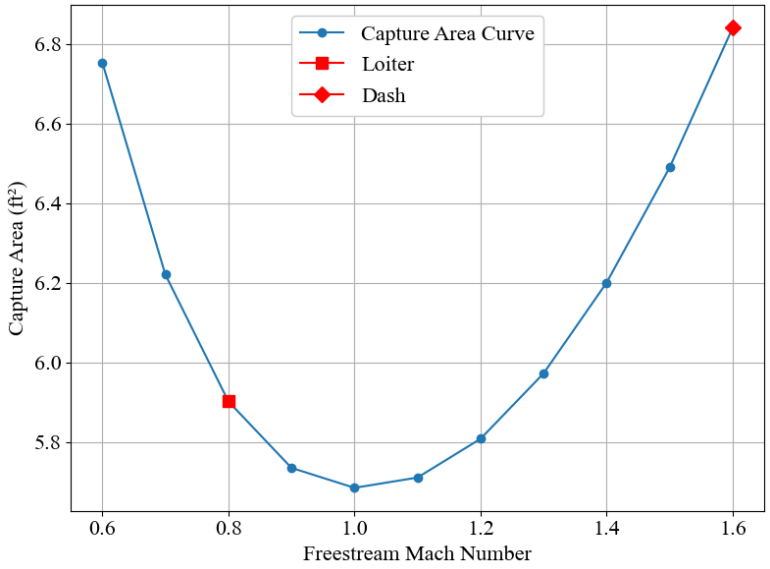

Figure 13. Required Inlet Capture Area vs Freestream Mach Number at 35,000 feet

Following the sizing process, a key integration issue arose: when extended, the nose landing gear would sit directly in front of the inlet, obstructing airflow, which is critical during takeoff. To address this, the inlet was split down the center with a wedge large enough to accommodate the nose gear in its retracted position while minimizing disruption to incoming flow. This design is similar to that of the Eurofighter Typhoon, which similarly integrates its landing gear and inlet. Figure 14a shows a frontal view of the split pitot-style inlet, while Figure 14b highlights the space into which the nose gear retracts.

(a) Dragonfly Inlet **(b) Underside of Inlet and Nose Gear**

Figure 14. CAD views of the pitot-style inlet design.

D. Installed Engine Performance

After finalizing the inlet design, installation penalties were applied to estimate the engine's installed performance aboard the Dragonfly. Four primary penalties were considered: airflow diverted for environmental control and avionics cooling, power extraction for electric and hydraulic systems, boundary layer bleed, and inlet pressure losses. The first two are specified in the RFP [1], though the electrical extraction was increased from the baseline 50 kW to account for the Dragonfly's system demands. The boundary layer bleed was estimated using the method in Nicolai, Chapter 16 [12], resulting in a boundary diverter height of 4.1 inches. Inlet pressure losses were applied to the GasTurb output data to reflect reduced total pressure recovery. These values are summarized in Table 7.

Table 7. Installed Engine Penalties Applied in Analysis

Penalty	**Value**
ECS / Avionics Cooling	2% of airflow
Electric / Hydraulic Systems	75 kW
Boundary Layer Bleed	$\sim$ 1% of airflow
Inlet Pressure Losses	Variable 1–10%

The first three penalties were directly implemented in GasTurb, while inlet pressure recovery losses were applied during post-processing. Because these penalties vary with flight condition, no single value fully captures their impact; however, representative values indicate a thrust reduction of approximately 7% at cruise and nearly 9% at dash. These reductions were deemed acceptable, as the baseline engine provides sufficient excess thrust across the flight envelope, including during combat scenarios where maximum thrust is required.

Performance data for the engine was generated using GasTurb, which can model engine behavior across altitude, Mach number, and throttle setting. Data were plotted for several of the Dragonfly's design flight conditions to visualize the relationship between thrust and SFC. These results are shown in Figs. 15 and 16, corresponding to dry thrust (PC 30/50) and afterburning thrust (PC 80/100), respectively. Each curve represents the engine's performance envelope at a fixed altitude and Mach number as the throttle is increased.

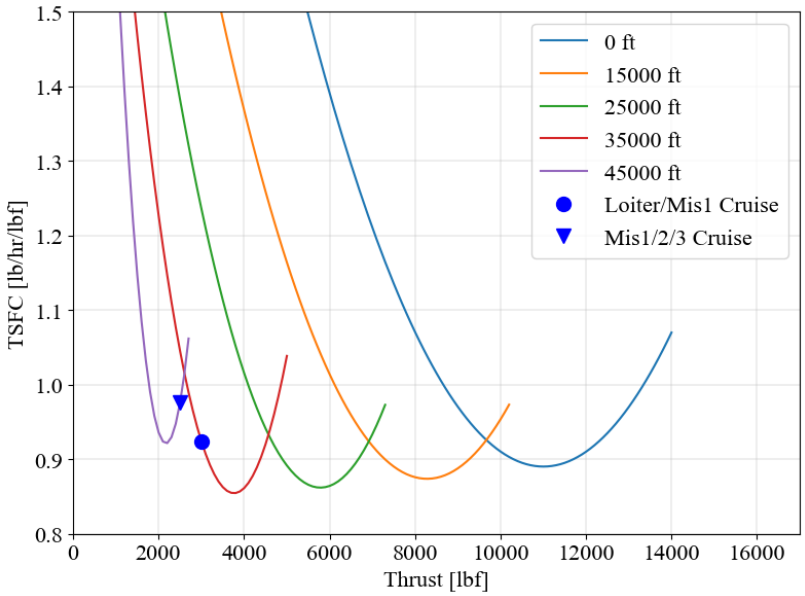

Figure 15. Dry SFC vs Thrust at Mach 0.8

In Figure 15, lines are plotted for different altitudes at Mach 0.8, to demonstrate the engine's subsonic performance throughout the mission profile. Figure 16 shows different Mach numbers for a fixed altitude of 35,000 feet, since this is the altitude at which most of the Dragonfly's afterburner use takes place. Mission segments are overlaid on the plots to demonstrate that the engine can produce sufficient thrust at these conditions while operating close to the lowest SFC possible, minimizing fuel consumption in the subsonic regime.

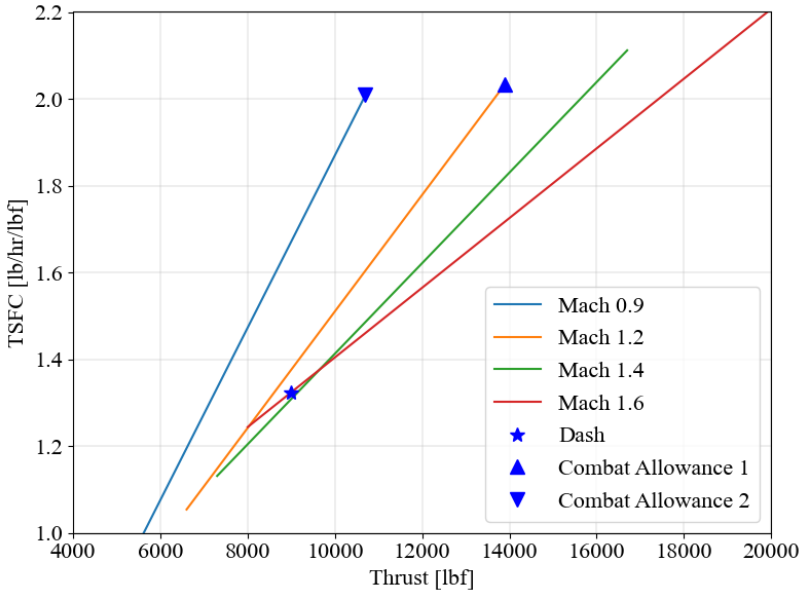

Figure 16. Afterburner SFC vs Thrust at 35,000 feet

Table 8 presents the calculated thrust required to meet the minimum specific excess power conditions outlined in the RFP [1]. These values were determined using the specific excess power expression from Raymer, Chapter 17 [9], and serve to verify that the Dragonfly's propulsion system will not limit its performance. Each condition is assigned a reference number in the table, which corresponds to labeled points on Figs. 17a and 17b. These figures plot thrust versus SFC at sea level and 15,000 feet, both at Mach 0.9, to visualize the throttle setting required to meet each condition.

Table 8. Minimum Specific Excess Power and Net Thrust Requirements at Different Conditions with Mach 0.9

Ref.	Condition	Specific Excess Power Required [ft/s]	Net Thrust Required [lb]	Dragonfly Capability [ft/s]
1	Military, Sea level, 1-g	200	9,670	232
2	Military, 15kft, 1-g	50	7,370	173
3	Max, Sea level, 1-g	700	23,600	788
4	Max, 15kft, 1-g	400	16,660	607
5	Max, Sea level, 5-g	300	20,420	510
6	Max, 15kft, 5-g	50	12,760	330

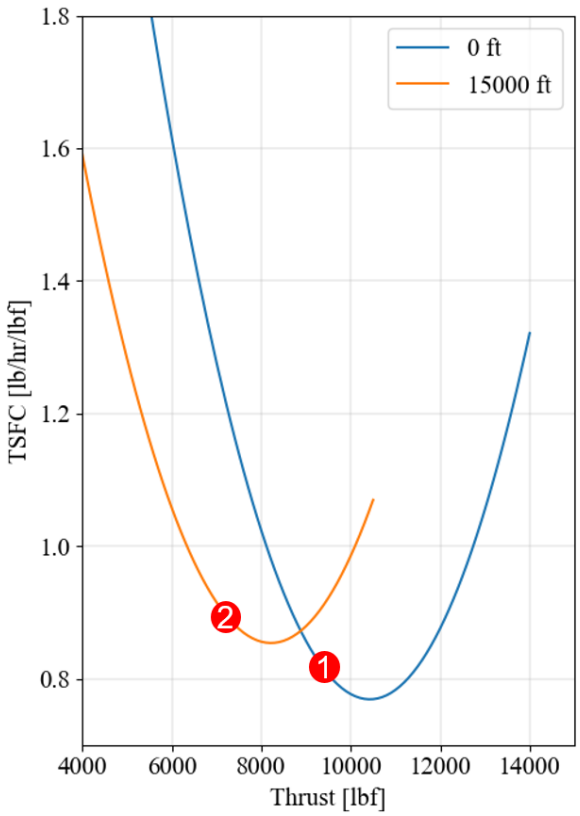

(a) Dry SFC vs Thrust at Mach 0.9

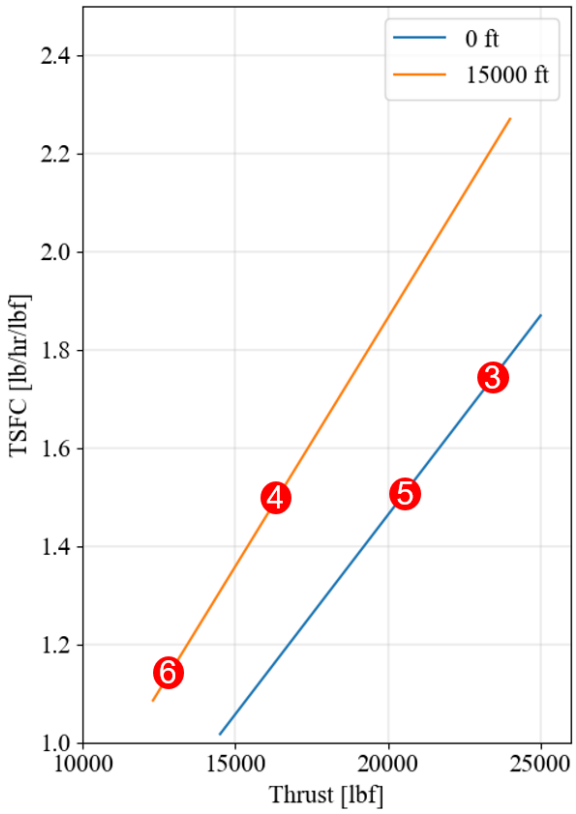

(b) Wet SFC vs Thrust at Mach 1.6

Figure 17. Installed engine thrust vs SFC at specific power conditions.

In Figure 17a, the military (dry thrust) conditions both lie near the lower end of their respective SFC curves, indicating that the engine operates within its available dry thrust margin. The four maximum (afterburning) thrust conditions shown in Figure 17b are more spread out on the plot, but remain within the engine's thrust output at those conditions. The most demanding condition is 3, which demands the highest thrust compared to the other conditions. This confirms that even the most demanding maneuvering requirements can be met without exceeding the engine's capabilities. Together, these plots demonstrate that the selected engine provides sufficient installed thrust for all required power conditions.

Propulsive and overall efficiencies were calculated for representative flight conditions using data from GasTurb, and the results are shown in Table 9. At loiter, the engine achieves a propulsive efficiency of 0.588 and an overall efficiency of approximately 0.27. During dash, propulsive efficiency drops to 0.543, while overall efficiency increases slightly to 0.30. These values fall within the middle-to-lower range of typical aircraft engine efficiencies [17], which is expected given that the engine was not scaled to match the aircraft's lower thrust requirements, resulting in generally off-design operation.

Table 9. Propulsive and Overall Efficiency at Key Flight Conditions

Condition	Mach	Altitude [ft]	Power Setting	η_p	η_{overall}
Loiter / Cruise	0.8	35,000	PC 30	0.588	0.272
Cruise	0.8	45,000	PC 30	0.583	0.271
Dash	1.6	35,000	PC 80	0.543	0.303

Although afterburning is typically associated with lower efficiency, the overall efficiency at partial afterburner during the dash condition was found to be slightly higher than in the cruise condition at dry power. This is due to the engine being better matched to the aerodynamic and mission requirements at dash. In contrast, cruise flight requires operating below the design point, leading to reduced thermal and propulsive efficiency.

VI. Aerodynamics

The aerodynamics section of this report will examine the airfoil selection, drag-build up, wing planform, high lift devices selection, and general aerodynamic performance. In this section, it is demonstrated that the Dragonfly can meet the aerodynamic requirements posed by the RFP and other sections of this report. A main aerodynamic consideration was minimizing the empty weight. The empty weight of the aircraft directly corresponds to cost. Due to budgetary constraints, the design must minimize empty weight where possible. A reduction in drag leads to a reduction in required fuel and structural weight, which would be required to carry the extra fuel volume and weight. For this reason, it is imperative that the fuel required is minimized.

A. Airfoil Selection

To keep the Dragonfly competitive with currently existing designs, a similarity analysis was conducted in Table 10 to determine the airfoils that other fighter aircraft utilize [18]. The similarity analysis determined that fighter aircraft typically use NACA 64- or 65- series airfoils with a thickness to chord ratio between four and ten percent. For fighters, a thickness between four and six percent is optimal due to the fact that thicknesses below four percent increase the wing structural weight significantly, while thicknesses above six percent increase supersonic drag significantly [12]. In the sizing analysis, it was determined that a thickness of four percent was best suited to the design, as smaller thicknesses created structural concerns and larger thicknesses increased the wave drag significantly.

Table 10. Airfoil Similarity Analysis

Airplane	**Wing Root Airfoil**	**Wing Tip Airfoil**
Boeing F-15 Eagle	NACA 64A006.6	NACA 64A203
Boeing F-18 Hornet	NACA 65A005	NACA 64A203.5
Lockheed/Boeing F-22 Raptor	NACA 64A05.92	NACA 64A?04.29
Grumman F-14 Tomcat	NACA 64A209	NACA 64A208.91
Lockheed Martin F-16 Fighting Falcon	NACA 64A204	NACA 64A204

The Dragonfly's airfoil was selected to minimize the drag created in the segment of flight that consumes the most amount of fuel. In Section VII, it was determined that the loiter segment consumed the greatest amount of fuel. Table 11 shows that Dragonfly requires a lift coefficient of 0.352 at the start of loiter and a lift coefficient of 0.251 at the end of loiter. The median of this range is a lift coefficient of 0.3, so the Dragonfly's airfoil has a design lift coefficient of 0.3. The relevant parameters for loiter are tabulated in Table 18

Table 11. Loiter Segment Conditions

	Loiter Start	**Loiter End**
Mach	0.80	
Altitude [ft]	35,000	
Weight [lbs]	36,860	26,250
C_L	0.352	0.251

Figure 18 demonstrates that NACA 64-304 produces the least amount of drag for a given amount of lift within the coefficients of lift experienced during loiter. For this reason, NACA 64-304, as depicted in Fig. 19, was selected as the airfoil for the Dragonfly's main wing planform. The data in the plot were gathered using Reynolds-Average Navier-Stokes computational fluid dynamics.

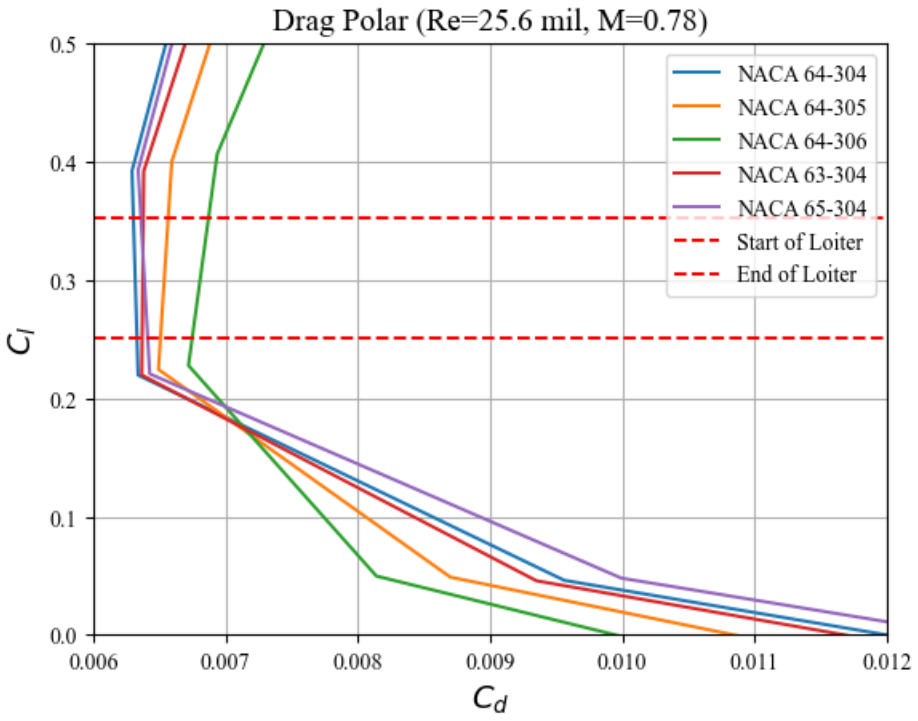

Figure 18. Airfoil Analysis

The tail surface airfoil selection process will be explained in Section VIII of this report. It was determined that a symmetric airfoil with six percent thickness was required to achieve stability and control requirements. The airfoil selected for the tail surfaces was NACA 0006 and is depicted in Fig. 20.

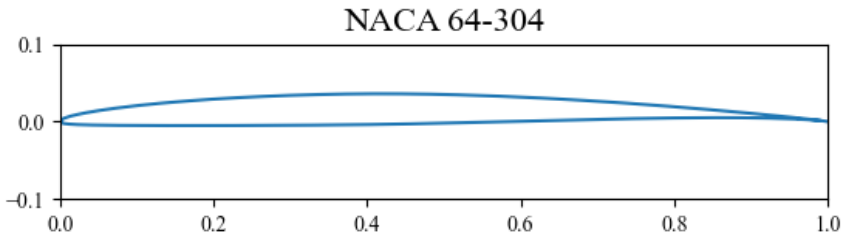

Figure 19. NACA 64-304

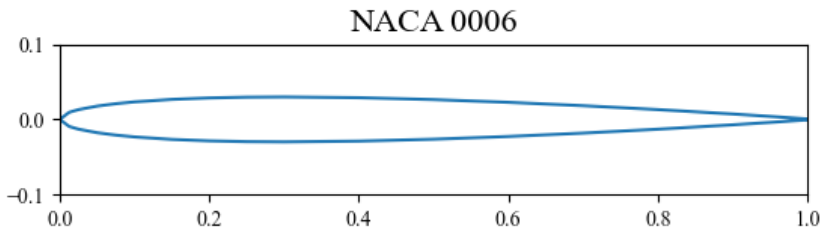

Figure 20. NACA 0006

B. Wing Planform

The wing planform of an aircraft determines an aircraft's lift, stability, drag, wing loading, and many other parameters. The Dragonfly's planform was selected to minimize drag while still meeting the aircraft's structural and performance requirements derived from the RFP. Table 12 tabulates the major characteristics of the Dragonfly's wing planform. Stability and Control as well as Performance determined that the aircraft requires a lift coefficient of 2.0 to achieve an instantaneous turn rate of 18 deg/s as required by the RFP [1]. An area of 494.70 ft^2 was selected to achieve this coefficient of lift. Satisfaction of this requirement will be further discussed in Subsection VI.C of this Section.

Table 12. Wing Planform Geometry

Wing Area [ft^2]	494.70
Aspect Ratio	4
Span [ft]	44.43
Leading Edge Sweep [degs]	40
Quarter Chord Sweep [degs]	32
Taper Ratio	0.0875
Root Chord [ft]	20.43
Tip Chord [ft]	1.79
MAC [ft]	13.71

Various wing sweeps were tested using the Delta Method and Raymer's drag build-up. Figure 21 shows that an increase in sweep leads to a reduction in drag. Since the Dragonfly uses a delta wing for its ease of manufacturing and performance, the increase in sweep also decreases the thickness at the tip of the wing planform. As the sweep approaches 45°, the wing tip becomes a fine point, which is difficult to manufacture in a manner that does not raise structural concerns. 40° of leading edge sweep was selected as it reduces drag while still being able to handle the structural loads of the aircraft as discussed in Section IX. 40° was also selected due to its effects on observability as discussed in Section XV.

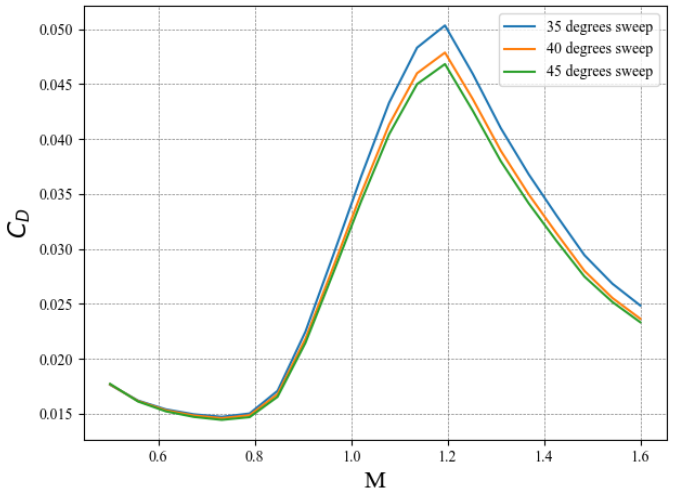

Figure 21. Sweep Trade Study

C. High-Lift Devices

The Dragonfly's high-lift devices will be deployed during takeoff, landing, and other maneuvers required by the RFP. High-lift devices allow the aircraft to achieve a greater amount of lift by increasing the wing area and camber at selected portions of flight. Figure 22 shows the CAD of the high-lift devices. The Dragonfly uses leading edge slats across the entire wingspan that use up 20% of the leading edge chord in combination with Fowler flaps across half the wingspan that use up 20% of the trailing edge chord. These high-lift devices were selected to meet the aircraft's takeoff and instantaneous turn rate requirements specified by the RFP [1].

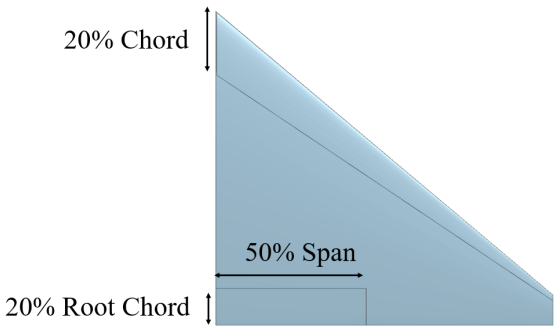

Figure 22. High Lift Devices CAD

Section VII determined that a lift coefficient of 1.6 is required for takeoff. Figure 23 shows that the Dragonfly achieves a $C_{L_{max}}$ of 0.829 during landing when no high-lift devices are applied. This curve was created by running Reynolds Average Navier Stokes computational fluid dynamics on the airfoil to determine C_l, then C_L was determined using equation 12.15 in Raymer [9]. Raymer Chapter 12 was used to determine the $C_{L_{max}}$ the wing planform with flaps extended can produce [9]. Figure 13 demonstrates that the planform can produce a $C_{L_{\text{max with HLDs}}}$ of 2.223 which ensures that 90% of the takeoff lift is generated before the tipback angle [12].

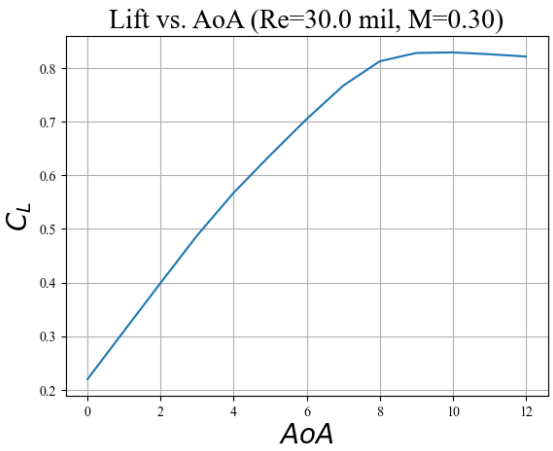

Figure 23. Landing C_L vs. AoA Curve No HLDs

Table 13. Takeoff Flaps Calculations

$S_{\textbf{flapped}}$	289 ft^2
Slats Extension	$1.2\frac{c'}{c}$
Flaps Extension	$1.2\frac{c'}{c}$
$C_{L_{\textbf{max no HLDs}}}$	0.829
$\Delta C_{L_{\textbf{max flaps}}}$	1.128
$\Delta C_{L_{\textbf{max slats}}}$	0.266
$\Delta C_{L_{\textbf{max}}}$	1.394
$C_{L_{\textbf{max with HLDs}}}$	2.223

Figure 24 was created using the Vortex Lattice Method and demonstrates that the $C_L = 1.6$ required for takeoff is produced below the aircraft's tip back angle of 12.2°. Performance determined that a $C_{L_{max}}$ of 2.0 is required during the instantaneous turn rate requirement of 18 deg/s [1]. Figure 25 shows that the wing planform with no high-lift devices can produce a $C_{L_{max}}$ of 1.150. This plot was created using the same method as in Fig. 23.

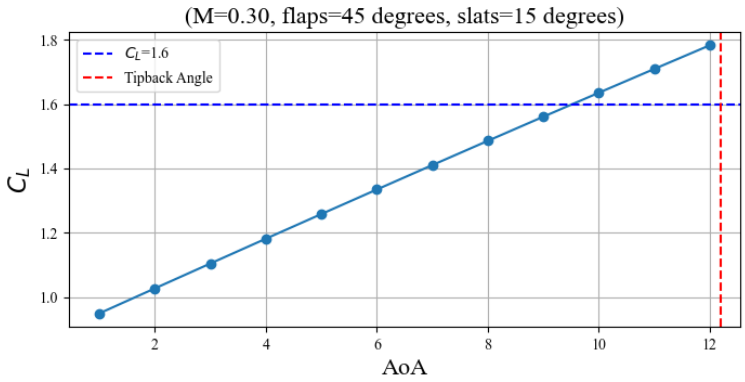

Figure 24. Takeoff C_L vs. AoA Curve With HLDs

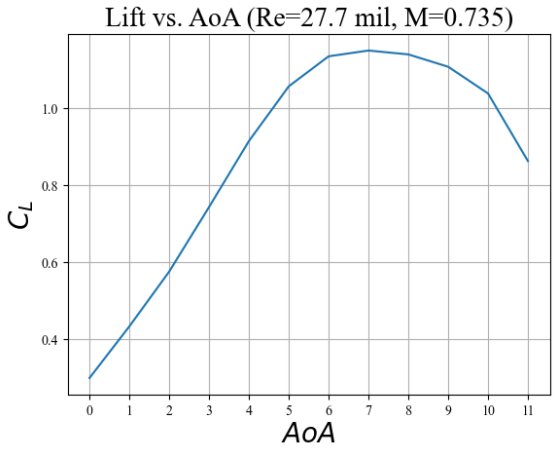

Figure 25. Instantaneous Turn Rate C_L vs. AoA Curve no HLDs

Table 14 was created using Chapter 12 in Raymer [9]. This table demonstrates that the Dragonfly can exceed the $C_{L_{max}}$ of 2.0 performance requirement for the instantaneous turn rate. The turn rate requirement C_L was exceeded to ensure that there is no stall buffeting during the turn. Figure 26 demonstrates that Dragonfly will complete the instantaneous turn rate requirement with an angle of attack of 19.5°. This plot was generated using the same method as described for Fig. 24.

Table 14. Instantaneous Turn Rate Flaps Calculations

$S_{\textbf{flapped}}$	289 ft^2
Slats Extension	$1.2\frac{c'}{c}$
$C_{L_{\textbf{max no HLDs}}}$	1.150
$\Delta C_{L_{\textbf{max flaps}}}$	0.940
$\Delta C_{L_{\textbf{max slats}}}$	0.266
$\Delta C_{L_{\textbf{max}}}$	1.206
$C_{L_{\textbf{max with HLDs}}}$	2.356

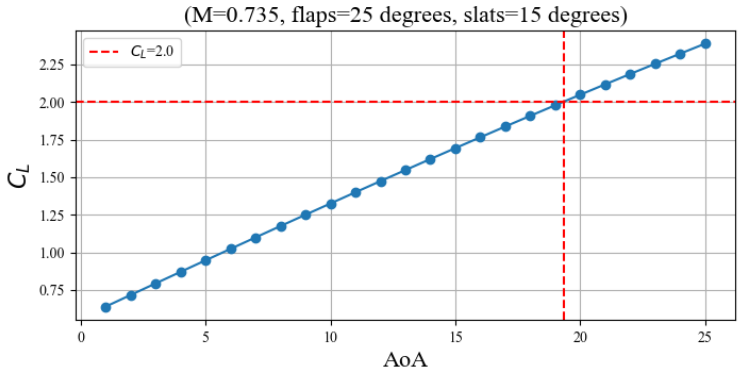

Figure 26. Instantaneous Turn Rate C_L vs. AoA Curve With HLDs

D. Area Ruling

Figure 27 shows the area ruling of the Dragonfly without its conformal tanks compared against a Sears-Haack Body. Placing conformal tanks closer to the front of the aircraft would improve the area ruling, but this would cause the C.G. to shift substantially from the maximum take-off weight C.G. to the empty weight C.G. while fuel is burned. This led to issues with maintaining the static margin. In a future design iteration, the shape of the fuselage and the storage of components would be adjusted to improve the area ruling while still maintaining static margin.

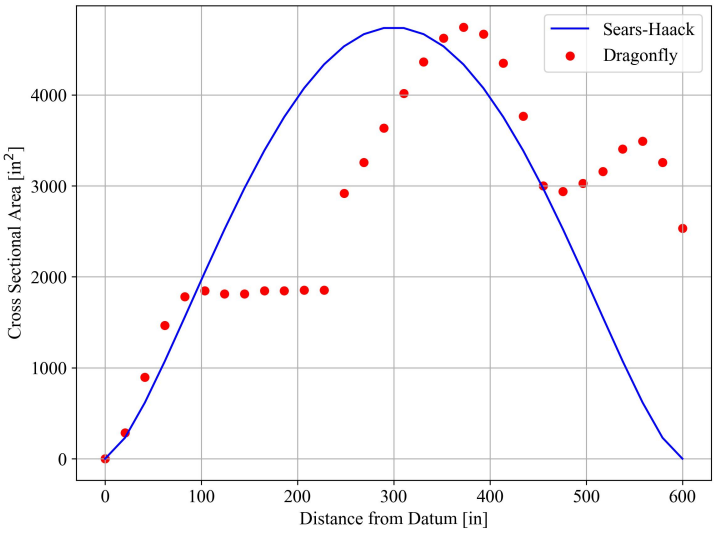

Figure 27. Dragonfly Area ruling

E. Drag Build-Up and Aerodynamic Performance

A drag build-up of the Dragonfly was created using the Delta Method and Raymer's drag build-up to evaluate the aerodynamic performance at various mission segments. Table 15 shows the drag build-up for Mission 1. The greatest amount of drag occurs during Cruise. Lift is greatest during Loiter.

Table 15. Mission 1 Drag Build-Up and Performance

	C_{D_0} wing	C_{D_0} h tail	C_{D_0} v tail	C_{D_0} fuse	C_{D_0} ord	C_{D_0} w	C_{D_0}	C_{D_i}	C_D	C_L
Cruise 1 Start	0.007	0.002	0.001	0.005	0.003	0.002	0.019	0.012	0.031	0.340
Cruise 1 End	0.007	0.002	0.001	0.005	0.003	0.002	0.019	0.011	0.030	0.321
Loiter Start	0.007	0.002	0.001	0.005	0.003	0.000	0.017	0.012	0.029	0.352
Loiter End	0.007	0.002	0.001	0.005	0.003	0.000	0.017	0.006	0.023	0.251
Dash Start	0.006	0.001	0.001	0.004	0.002	0.012	0.026	0.001	0.027	0.060
Dash End	0.006	0.001	0.001	0.004	0.002	0.012	0.026	0.001	0.027	0.055
Cruise 2 Start	0.007	0.002	0.001	0.006	0.003	0.002	0.020	0.010	0.030	0.318
Cruise 2 End	0.007	0.002	0.001	0.006	0.003	0.002	0.020	0.009	0.029	0.292

Table 16 shows the drag build-up for Mission 2. During the dash, lift decreases, leading to most of the drag being produced by parasitic drag. Later on in the mission, the lift increases, leading to an increase in induced drag.

Table 16. Mission 2 Drag Build-Up and Performance

	C_{D_0} wing	C_{D_0} h tail	C_{D_0} v tail	C_{D_0} fuse	C_{D_0} ord	C_{D_0} w	C_{D_0}	C_{D_i}	C_D	C_L
Dash Start	0.006	0.001	0.001	0.004	0.002	0.012	0.026	0.001	0.028	0.073
Dash End	0.006	0.001	0.001	0.004	0.002	0.012	0.026	0.001	0.027	0.065
Cruise Start	0.007	0.002	0.001	0.006	0.003	0.002	0.020	0.015	0.035	0.382
Cruise End	0.007	0.002	0.001	0.006	0.003	0.002	0.020	0.014	0.034	0.369

VII. Performance

The performance analysis of the Dragonfly evaluates key capabilities of the aircraft across all mission sets. Each mission and performance requirement is assessed using the propulsion and aerodynamic models discussed in the previous sections. The objective is to ensure that the vehicle meets or exceeds all mission criteria while remaining safely within its operational limits.

A. Takeoff and Landing

Takeoff operations at MTOW were analyzed using timestep integration at sea level and 4,000 feet MSL under DISA 15°F for standard day, wet, and icy conditions as requested by the RFP [1]. Sea level calculations establish baseline values and represent the best scenario for engine performance. However, 4,000 ft MSL represents a more realistic, moderate-altitude airfield for defense operations. For takeoff analysis, the friction coefficient, μ, is not a driving factor, making the surface condition of the concrete less relevant. The altitude, however, does contribute to the takeoff field length because of the air density and lift generation produced by the wings. The procedure is broken down into three main phases for more accurate analysis: ground roll, rotation, and transition. At the end of the transition phase, the vehicle must be on a set path to clear a 35-foot obstacle at the end of the runway, defined in the FAA 14 CFR Part 25 § 25.115. Table 17 contains the field length distances for each segment of takeoff, which were calculated using timestep integration techniques.

Table 17. Takeoff Distances

Altitude	Ground Roll [ft]	Rotation [ft]	Transition [ft]	TOFL [ft]
Sea Level	1,800	600	800	3,200
4,000 ft MSL	2,300	700	900	3,900

Similar to takeoff, landing procedures were analyzed using timestep integration at sea level and 4,000 MSL with a landing weight of half the MTOW to account for fuel consumption during flight. The total landing field length is broken down into the approach, free roll, and braking distances. During the approach phase, the Dragonfly must be able to clear an obstacle height of 50 feet as described in the FAA 14 CFR Part 25 §25.125. The braking distance varies depending on runway surface conditions and is adjusted using the friction braking coefficient, μ_B. Landing analysis was completed for dry, wet, and icy concrete surface conditions. As shown in Table 18, the aircraft is able to land within standard NATO runways of 8,000 feet during all conditions.

Table 18. Landing Distances at Sea Level and 4,000 ft MSL

Altitude	Surface	μ_B	Approach [ft]	Free Roll [ft]	Braking [ft]	LFL [ft]
Sea Level	Dry concrete/asphalt	0.3	1,400	620	1,730	3,750
	Wet concrete/asphalt	0.225	1,400	620	2,120	4,140
	Icy concrete/asphalt	0.08	1,400	620	3,930	5,950
4,000 ft MSL	Dry concrete/asphalt	0.3	1,570	670	2,010	4,250
	Wet concrete/asphalt	0.225	1,570	670	2,460	4,700
	Icy concrete/asphalt	0.08	1,570	670	4,570	6,810

B. Cruise and Loiter

The cruise and loiter segments of the mission are optimized to produce the largest L/D ratio possible while also minimizing fuel required. Using the drag model described in the aerodynamics section, aircraft performance coefficients were calculated and plotted in Fig. 28 to determine the optimal speeds for cruise and loiter.

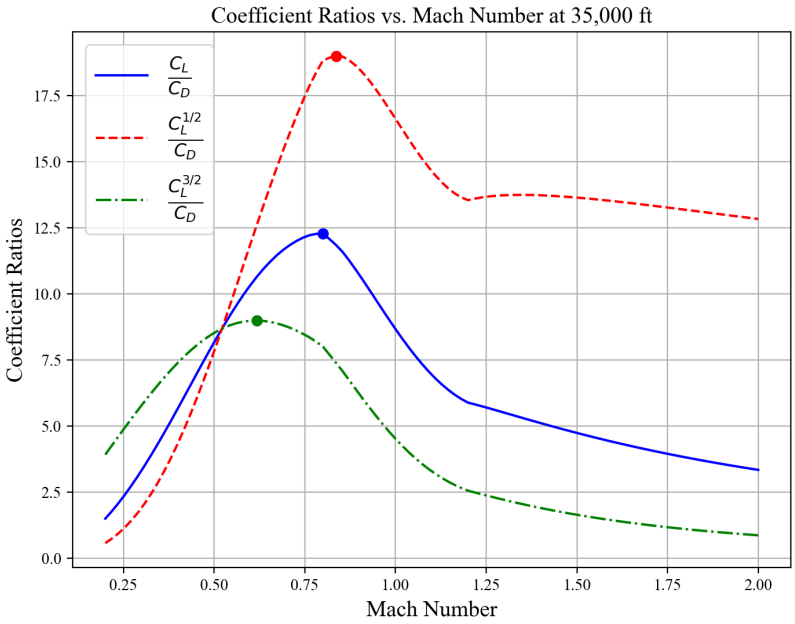

Figure 28. Aircraft Performance Coefficients

After analyzing Fig. 28, the maximum C_L/C_D ratio was determined to be at Mach 0.79. This speed is used for the loiter phase of the flight since it provides the most aerodynamic efficiency per nautical mile. The cruise speed was chosen from the maximum $C_L^{1/2}/C_D$ ratio at Mach 0.84, where endurance efficiency is maximized. Both speeds were proven to minimize fuel consumption in their respective mission segments by running the values through the fuel calculation model. Table 19 displays all maximum aircraft performance coefficients.

Table 19. Maximum Aerodynamic Efficiency Values

Metric	Maximum Value	Mach Number	Phase of Mission
Max C_L/C_D	12.30	0.79	Loiter
Max $C_L^{1/2}/C_D$	19.00	0.84	Cruise
Max $C_L^{3/2}/C_D$	9.00	0.62	-

A trade study was also considered for the altitude of the return cruise for all missions. The fuel burn for the cruise segment, along with the fuel needed to climb to that altitude, was calculated and compared over a range of altitudes in increments of 1,000 feet. The fuel required for these variations in the second cruise and climb phases of the Defense Counter-Air Patrol mission is plotted in Fig. 29. It was determined that the minimum fuel burned for the combined cruise and climb segments was 2,190 pounds at an altitude of 45,000 feet.

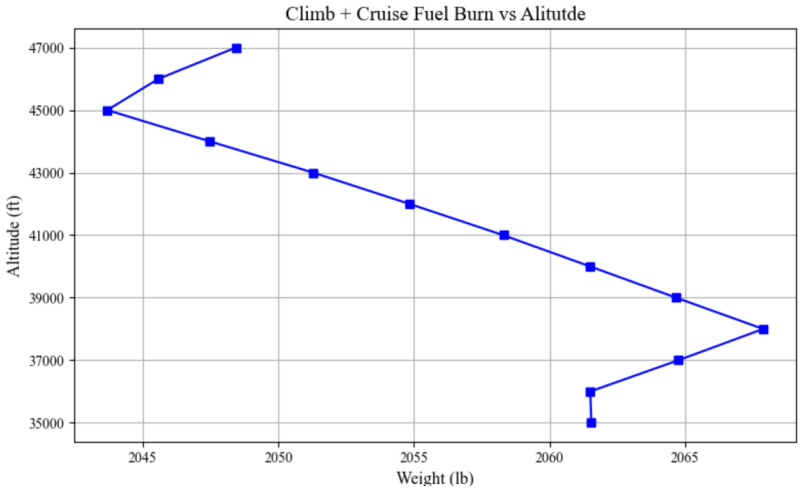

Figure 29. Cruise Altitude Trade

The same method was used for the Point Defense Intercept and Escort missions, where 45,000 feet was also found to be the optimal cruising altitude. This trade study excludes the first climb and cruise segments of the Defense Counter-Air Patrol mission, as it was more efficient to remain at 35,000 feet, where the loiter and dash segments are performed.

C. Mission Performance Analysis

For each mission that the Dragonfly is designed to complete, the fuel weight and fraction for each phase of flight were calculated using a timestep integration technique over 15-second intervals. Since fuel consumption is a continuous process and depends on varying factors such as weight, thrust, altitude, and speed, an incremental approach is necessary. At each timestep, all parameters and performance coefficients were recalculated to obtain more accurate results.

1. Defense Counter-Air Patrol Mission

The most constraining mission in terms of fuel consumption is the Defense Counter-Air Patrol mission due to the four-hour loiter phase. During this segment, the Dragonfly burns 10,600 pounds of fuel, accounting for more than half of the total 19,000 pounds needed for the mission. Since the internal fuel tanks can only hold up to 12,000 lbs of fuel, the remaining 7,000 pounds must be stored in conformal tanks, which will always be required for this mission. Table 20 displays the rest of the breakdown for the entire mission, including fuel fraction for each mission segment. Other notable segments include the cruise phases at optimal speeds and altitudes, and the dash segment at Mach 1.6. These segments each add another 2,000 pounds of fuel to the mission.

Table 20. Segment Fuel Burn for DCAP Mission

Segment	**Fuel Burn [lb]**	**Fuel Fraction [%]**
WUTTO	120	0.63%
Climb	400	2.12%
Cruise	2,200	11.64%
Loiter	10,600	56.08%
Dash	2,000	10.58%
Combat Allowance I	300	1.59%
Combat Allowance II	30	0.16%
Climb	200	1.06%
Cruise	2,000	10.58%
Reserves	1,050	5.56%
Total	**18,900**	**100.00%**

2. Point Defense Intercept Mission

The second mission, a Point Defense Intercept mission, requires significantly less fuel than the Defense Counter-Air Patrol mission. With a total fuel requirement of just under 6,200 pounds, the Dragonfly can carry all necessary fuel internally, eliminating the need for external tanks. This configuration not only reduces weight but also minimizes drag, enhancing performance during the mission. With no loiter phase and a 200 nautical mile dash distance, the dash phase becomes the most fuel-intensive segment at 3,500 pounds of fuel. The full fuel breakdown is shown in Table 21.

Table 21. Segment Fuel Burn for PDI Mission

Segment	Fuel Burn [lb]	Fuel Fraction [%]
WUTTO	80	1.28%
Climb to Cruise Alt	200	3.23%
Dash	3,500	56.45%
Combat Allowance I	200	3.23%
Combat Allowance II	20	0.32%
Climb Back to Cruise	200	3.23%
Cruise Back	1,000	16.13%
Reserves	1,000	16.13%
Total	**6,200**	**100.00%**

3. Escort Mission

The final mission is an intercept and escort mission that redirects enemy aircraft away from critical airspace. For this mission, the dash to intercept and return cruise distances are traded based on required fuel, while the escort distance is fixed at 300 nautical miles. As stated in the RFP, the minimum dash to intercept radius is 200 nautical miles [1, p.7]. Assuming a linear flight path for the dash and escort distances, the return cruise would sum to 500 nautical miles, and the total mission would consume 9,300 pounds of fuel. Table 22 compares these parameters to variations carrying maximum internal and maximum total fuel capacity.

Table 22. Fuel Requirement for Various Escort Mission Profiles

	Dash Distance [nmi]	Cruise Distance [nmi]	Fuel Required [lb]
Min Dash	200	500	9,300
Max Internal	315	615	12,000
Max Fuel	550	850	18,900

Although the variations in Tab. 22 assume a linear flight path between the dash and escort phases, alternative mission profiles exist such that the dash and escort phases are at some angle relative to each other, changing the distance of the return cruise. For instance, a dash leg due east, followed by an escort leg due north, would result in a return cruise oriented southwest. This would reduce the linear distance to return to base. The three variations described, along with all other mission possibilities, are shown in Fig. 30.

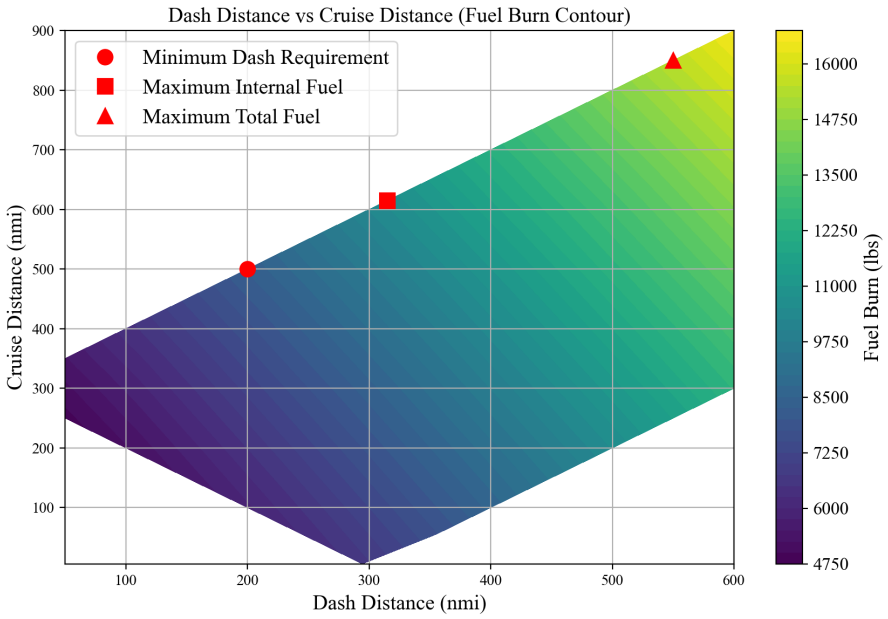

Figure 30. Escort Mission Variations

D. Maneuverability Diagrams

Additional requirements specified for the Dragonfly design include several maneuver capabilities at 50% internal fuel weight and are shown in Table 23. Given an internal fuel capacity of 12,000 pounds, the corresponding maneuver weight was calculated to be 24,700 pounds.

Table 23. Performance at Maneuver Weight (50% Internal Fuel)

Requirement	Condition	Value	Status
Max Mach Number	35,000 ft	Mach 1.6	Met
1-g Specific Excess Power – Max Thrust	0.9M / Sea Level 0.9M / 15,000 ft	700 ft/s 400 ft/s	Exceeded
5-g Specific Excess Power – Max Thrust	0.9M / Sea Level 0.9M / 15,000 ft	300 ft/s 50 ft/s	Exceeded
Sustained Load Factor – Max Thrust	0.9M / 15,000 ft	5.0 g's	Exceeded
Max Instantaneous Turn Rate	35,000 ft	18.0 deg/s	Met

At 35,000 feet, a maximum Mach number of 1.6 and an instantaneous turn rate of 18 degrees per second must be achieved. Figure 31 illustrates that the interceptor meets the Mach and instantaneous turn rate requirements under a limit load factor of 7-g's, which is the aircraft's structural design limit load. Since the aircraft's wing and structural design were sized specifically to meet the instantaneous turn rate requirement, it is reasonable that the Dragonfly achieves this threshold precisely, with limited excess capabilities.

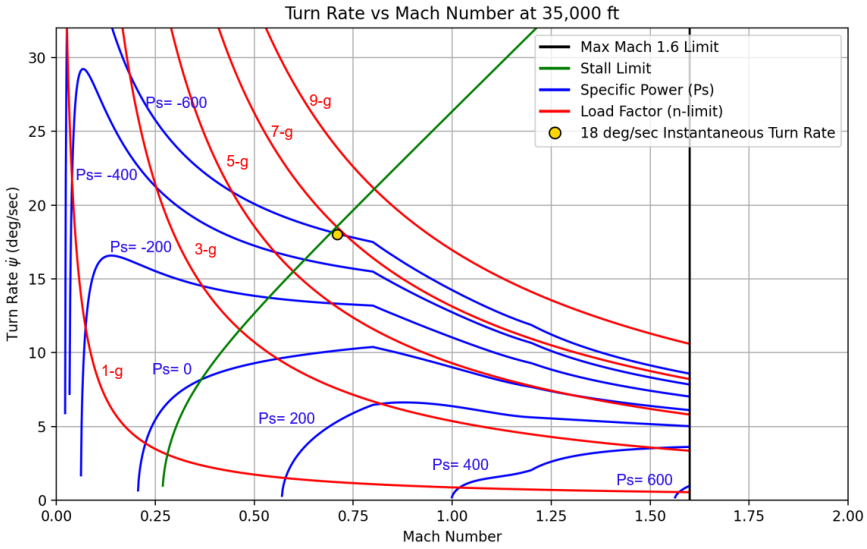

Figure 31. Maneuverability Diagram at 35,000 ft

Figures 32 and 33 confirm that the Dragonfly meets or exceeds all of the performance requirements at sea level and 15,000 feet. At sea level, the aircraft reaches 700 ft/sec of specific excess power at Mach 0.9 and 1-g, and 300 ft/sec at 5-g. At 15,000 feet, it achieves 400 ft/sec at 1-g and 50 ft/sec at 5-g. The red load factor contours show that a sustained 5.0 g turn is achievable at Mach 0.9 and 15,000 feet, satisfying the sustained turn performance requirement. These requirements ensure that the aircraft can accelerate, climb, and maneuver effectively during air-to-air combat at both low and mid altitudes.

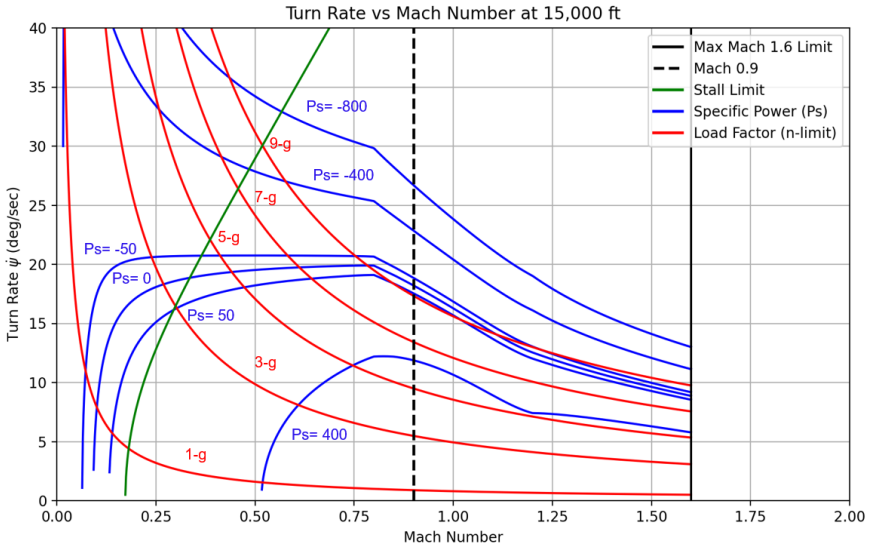

Figure 32. Maneuverability Diagram at 15,000 ft

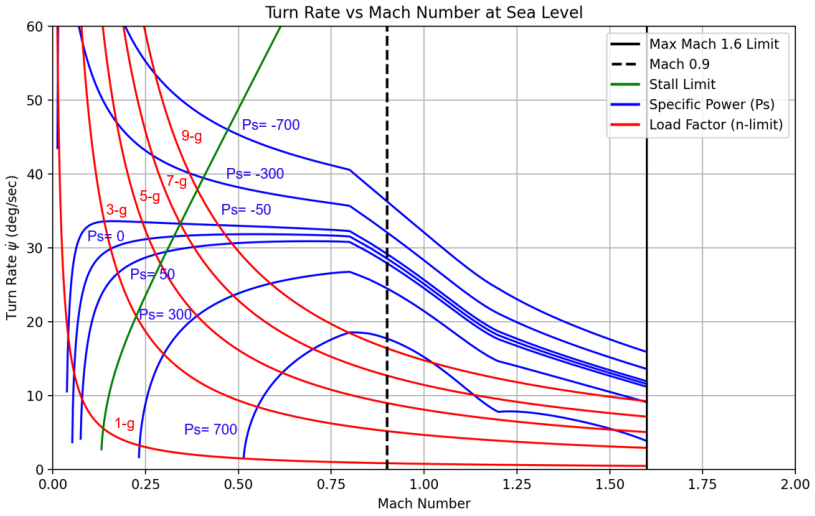

Figure 33. Maneuverability Diagram at Sea Level

E. Flight Envelope

The flight envelope at the MTOW of the Dragonfly interceptor for 1-g is displayed in Fig. 34 and defines the operational limits of the aircraft. The q limit, representing the dynamic pressure constraint, restricts high-speed, low-altitude flight. This constraint limits the maximum speed at sea level to Mach 1.2. On the opposite side of the envelope, the stall limit shows the boundary where the aircraft cannot generate enough lift to sustain flight. Another limiting factor of flight is when the specific power is zero. This limit represents the speed and altitude combinations where the aircraft can maintain level flight without any excess power available for climb and other maneuvers. All missions and flight operations must be conducted within the confines of these performance limits.

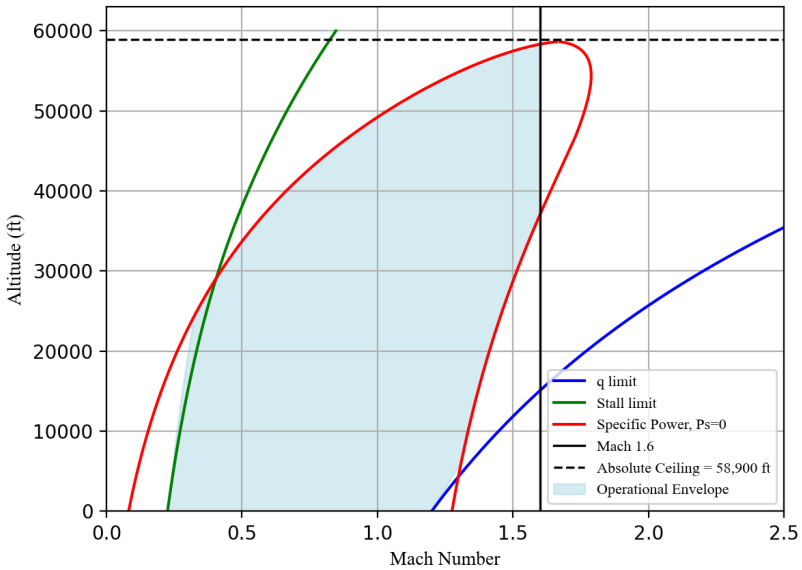

Figure 34. Flight Envelope

VIII. Stability and Control

This sections covers the control surfaces and characteristics of the Dragonfly, providing justification and verification of acceptable stability and control characteristics, meeting all requirements listed in the RFP for maneuverability and static margin [1].

A. Stabilizer Configuration

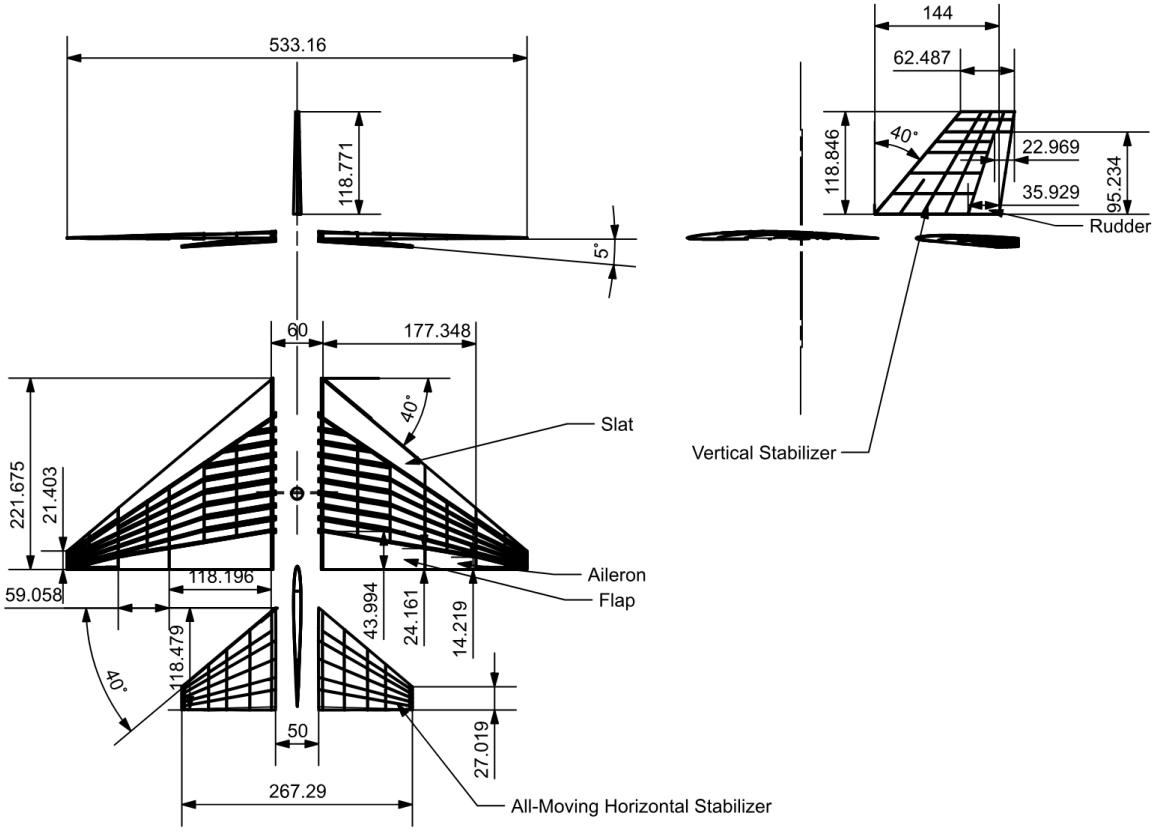

Figure 35. 3-View Drawing of Dragonfly's Stabilizers and Control Surfaces in Inches

Conventional horizontal and vertical tails are used for stabilization and additional control surfaces. Both stabilizers are placed as far aft on the aircraft as possible to maximize their lever arms and stabilizing characteristics. The horizontal tails, on account of their all-moving nature, are only connected to the fuselage at their pivot points. Given their configuration, both stabilizers can extend slightly aft of the end of the tailpipe. The rear of the vertical stabilizer is lightly angled to ease its structural integration with the fuselage. The horizontal stabilizer has an anhedral angle of 5 degrees to minimize the effect of wing-wake upon the tail [12]. The use of separate stabilizers, with their associated control surfaces, allows for minimal control deflection to trim out the aircraft as the CG shifts, therefore minimizing

trim drag. Furthermore, there is no incidence on the wings or stabilizers. Although it might reduce the drag in some particular stage of flight, putting an incidence on the wing was determined unnecessary due to the extensive variations in the Dragonfly's weight and speed during operations. Instead, a cambered airfoil was employed. Another concern was that an excessive incidence angle could require a negative angle of attack to maintain trim, potentially leading to engine intake flow distortion or shrouding. The horizontal stabilizer is an all-moving surface, so it can change its incidence at will. The vertical tail was optimized for laterally symmetric loads, so there was no need to bias it one way or the other with any incidence.

B. Stabilizer Sizing

The final chosen characteristics of the stabilizers are collected in Table 24.

Table 24. Final Stabilizer Characteristics

Characteristic	Horizontal Stabilizer	Vertical Stabilizer
Apex Location Behind Nose [ft]	42	38
AR	3	1.15
MAC [ft]	6.85	9.05
Area [ft^2]	110	85
Span [ft]	18.16	9.89
Taper Ratio	0.228	0.433
Anhedral [deg]	5	0
Leading Edge Sweep [deg]	40	40
Quarter Chord Sweep [deg]	32.18	33.70
Volume Coefficient [V_H, V_v]	0.234	(0.0457, 0.0543)

1. Stabilizer Airfoil Selection

A symmetrical NACA 0006 airfoil was employed for both stabilizers. Symmetry was desired on the vertical stabilizer due to the symmetrical lateral design of the aircraft, resulting in no need to bias the vertical stabilizer one way or the other. Symmetry was also desired on the horizontal stabilizer due to the significant CG shifts, which necessitates both significant positive and negative deflections of the horizontal stabilizer during flight.

In order to minimize parasite drag, thin airfoils were desired, with the selected airfoils having the minimal required thickness to ensure they would not stall during their maximum angles of attack. After calculating various subsonic scenarios in AVL, the highest angle of attack for the vertical stabilizer was set by an 11.5 deg side-slip during landing and takeoff. For the horizontal stabilizers, this was set by trimming during landing with suboptimal CG placement.

Table 25. Max Stabilizer Alpha/Beta

Stabilizer	Maximum Effective Alpha/Beta
Horizontal Stabilizers	12.6
Vertical Stabilizer	11.5

Utilizing both viscous Xfoil simulations and NACA testing on the 0006 airfoil, it was found that this airfoil would stall at 14 degrees with a Reynolds number of 4.5 million [19]. The lowest Reynolds number over the horizontal or vertical tail during the landing approach or takeoff climb is above 10 million. Given the tendency of higher Reynolds numbers to delay flow separation, it can be concluded that the NACA 0006 airfoil will not stall before it reaches the maximum effective Alpha/Beta.

2. Horizontal Stabilator Sizing

The horizontal stabilizer's seed sizing was based upon similarity analysis. However, the scissor plot sizing method was also employed, calculating the minimum V_H necessary to achieve a particular $C_{L_{max}}$ during landing and takeoff, accounting for shifts in CG, the wing's aerodynamic center, and static margin. [20]. Utilizing AVL, it was possible to obtain $C_{M_{ac}}$ at a particular $C_{L_{max}}$, the movement of the CG was given by the distribution of the mass across the configuration, the movement of the static margin is roughly known already, and the movement of the aerodynamic center in AVL is about 0.03 at landing speeds. In addition, using the calculated moment neutral point from AVL, the relationship between the placement of the neutral point and the lift of the tail can be used to extract the ratio of the horizontal tail's lift derivative vs that of the entire system [20]. The planform of the wing is known, so the MAC is also assumed to be known. By testing the effect of α upon the combined lift of the wing and tail, it was possible to derive the value of $d\epsilon/d\alpha$. Therefore the only value unknown is C_{L_h}, which is assumed to be around -0.8 based upon historical precedent [20]. Data used in the calculation of Fig. 36 can be found in Table 26.

Table 26. V_H Sizing Values

Condition	$C_{M_{ac}}$ [1/rad]	$C_{L_{max}}$	Δx_{SM} [ft]	$\overline{c}$ [ft]	$d\epsilon/d\alpha$	Δx_{CG}	$C_{L_\alpha,h}$	$\frac{C_{L\alpha,h}}{C_{L\alpha,h+w}}$
Landing	-0.12	1.2	-0.08	13.71	0.25	0.16	-0.8	0.15
Takeoff	0.08	1.2	0.08	13.71	0.25	0.16	-0.8	0.15

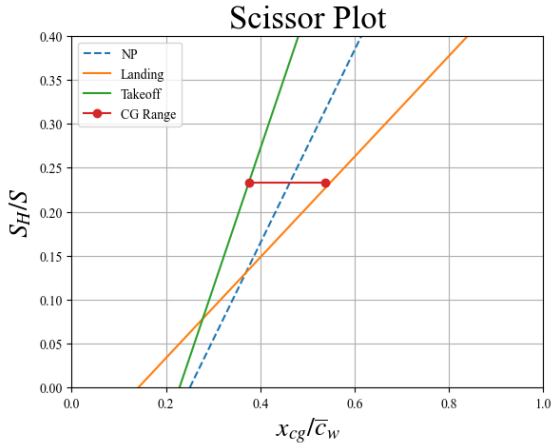

Figure 36. Scissor Plot

Looking at Fig.36, it can be seen that the selected horizontal tail planform and area are very close to the minimum for handling the fore and aft CGs during landing and takeoff.

3. Vertical Stabilizer Sizing

The vertical stabilizer was sized based upon a mixture of similarity analysis surrounding vertical tail volume coefficient, directional stability, and the feasibility of control during cross-wind landing conditions. The vertical tail's volume coefficient was selected based on aircraft with a similar horizontal tail volume coefficient. The vertical tail's planform was initially similar to the wing's, yet modified for better control during cross-wing landing. The aerodynamic center of the wing and vertical tail is assumed to be at the quarter of their MACs. Initial calculations were based upon a CG that was farther forward than the final CG, resulting in the final stability and volume coefficients ending up lower than initially calculated. Simulations still indicate that the vertical stabilizer is sufficient to retain stability throughout flight. The F-4 Phantom was used as the initial target to match directional stability and tail volume coefficient area, with directional stability of $C_{n_\beta} \approx 0.14$ and $V_v = 0.054$ [12]. Using equations from Nicolai to calculate the directional stability of the aircraft (accounting for the tail, wing, and fuselage), it can be seen in Table 27 that the final vertical tail has a slightly lower vertical tail coefficient than the F-4 Phantom. It also has a significantly lower directional stability. The reason for lowering the directional stability by decreasing the AR of the vertical tail is discussed in section VIII.C.2.

Table 27. Vertical Tail Sizing Characteristics

Characteristic	Value
S_{VT} (ft^2)	85
l_f range (ft)	(11.80, 14.00)
V_v range	(0.046, 0.054)
C_{n_β} range experienced during landing and takeoff	(0.075, 0.099)

C. Control Surface Sizing

The positive directions of rotation for the control surfaces are defined in Fig. 37.

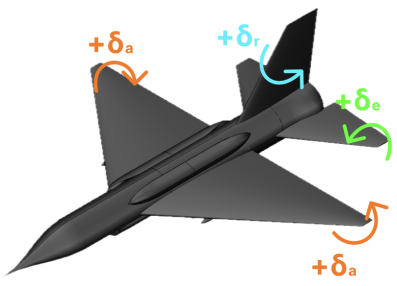

Figure 37. Positive Rotations for Control Surfaces

1. Elevators

Based on similarity analysis with other supersonic fighters such as the MiG-21, F-16, F-4, and more, an all-moving horizontal stabilizer was used for pitch control. As such, the elevator was subservient to the horizontal tail sizing. Using trim analysis, it was then possible to calculate the necessary thickness of the airfoil and the freedom of elevator motion to provide control throughout different flight regimes. The elevator sizing was otherwise designed using the scissor plot sizing in section VIII.B.2.

2. Rudder

The rudder was sized based upon a side-slip condition of $\beta = 11.5$ degrees during landing and takeoff, as suggested by Nicolai [12]. Assuming that the aircraft is not banking into the sideslip, a reasonable assumption considering that most aircraft landing or taking off tend not to want to place excessive force on any one landing gear by touching it down alone, then lateral trim can be calculated as a function of C_{n_β}, β,$C_{n_{\delta r}}$, and δ_r [12]. Nicolai recommends a rudder deflection of no more than ±20 degs [12, p. 597]. The directional stability of the Dragonfly, due to the significant sweep of its wings, is largely a function of C_L at landing and takeoff speeds, and so it is necessary to define not only the speeds of landing, but also the necessary coefficients of lift [12]. The landing and takeoff Mach numbers were provided by Performance. The RFP's requirements of landing and takeoff at 4,000 ft were utilized as the lower density would require a higher C_L, placing a higher requirement on the rudder's control power than sea level takeoff and landing [1]. For landing with cross-winds, it was decided that 125% OEW was a sufficient weight as it allows the Dragonfly to return to land with a full payload and over 2,500 lbs of fuel in reserve, even in cross-winds. Calculations for C_{n_β} were initially performed with both AVL and Nicolai's equations to solve for C_{n_β}. First, Nicolai's empirical calculations were employed, using the situation-specific variables found in Table 29 and the fixed variables found in Table 28.

Table 28. Constant Variables Necessary for C_{n_β}

Characteristic	**Value**
Fuselage Structural Depth [ft]	5
ac_w [ft]	28.0
ac_v [ft]	43.8
β [deg]	11.5

Table 29. Variables Related to Nicolai-Based Rudder Calculations

Characteristic	Takeoff	Landing
M	0.29	0.22
VTAS [ft/s]	322.5	246.6
x_{CG} [ft]	29.75	31.95
Weight [lb]	36,800	20,650
C_{L_α}	2.28	2.29
C_L	0.68	0.65
V_v	0.054	0.046
C_{n_β}	0.099	0.075
δ_r [deg]	20	20
$C_{n_{\delta r}}$ [1/rad]	0.06	0.04
$\tau_{required}$	0.51	0.47

These τ values indicate a rudder area occupying approximately 30% of the tail. However, utilizing AVL's automatic trim calculation system, with 30% tail surface area as an initial guess for the rudder sizing, it was discovered that the empirical equations from Nicolai were underestimating the effects of the rudder. Under the same conditions as used to calculate the values from Nicolai, AVL produced the following differing results found in Table 30.

Table 30. AVL Cross-Wind Rudder Calculations With a 20% Tail Area Rudder

Characteristic	Takeoff	Landing
C_{n_β}	0.11	0.11
δ_r [deg]	20.03	19.94
$C_{n_{\delta r}}$ [1/rad]	0.061	0.060
$\tau_{required}$	0.51	0.47

As can be seen in Table 30, in comparison to Table 29, AVL predicts that just a 20% surface area rudder is sufficient to maintain trim during cross-wind landings and takeoffs. The AVL results, on account of being within AVL's ideal low-subsonic range and AVL's results being specific to the aircraft configuration, will be selected. For structural reasons, the rudder will only extend 80% the span of the vertical stabilizer. As an addition, it was found that reducing the AR of the vertical tail from 2 to 1.15, while lowering directional stability, shrunk the size of the rudder from 25% area to 20% area. This acceptance of lower directional stability was accepted due to the existing flight control computer system, which can handle less stable flight, and because the aircraft remains directionally stable with a similar volume coefficient. This decision reduced the empty weight of the aircraft by making the vertical tail lighter overall.

3. Ailerons

The three major requirements placed upon the ailerons during sizing were the ability to counteract the roll caused by the rudder during trim, the ability to trim out imbalanced payloads, and the ability to sustain a 90 deg/s roll rate as suggested by MIL-HDBK-1797. Limits in aileron deflections were set at, as is typical for such control surfaces. ±20[12]. Utilizing AVL with the dragonfly's current configuration, relevant variables could be extracted at Mach 0.8, 35,000 ft, MTOW. No angle of attack or control inputs were present during the simulation. The results are stored in Table 31.

Table 31. 90 Deg/s Cruise Roll Parameters

Characteristic	**Cruise**
$C_{l_p}[1/rad]$	-0.34
V [ft/s]	778.3
b [ft]	44.4
δ_a (deg)	20
$C_{l_{\delta_a},required}$ [1/rad]	0.044

The most asymmetric loading along the Y-axis would be carrying two AMRAAMs on one side, but not on the other. This will be simulated during landing a heavy aircraft at 4000 ft, assuming MTOW minus the two AMRAAMs missing from one wing. Simulating this condition using AVL, the relevant parameters are displayed in Table 32. As can be seen, the required aileron power to maintain trim, even at the lowest flight speeds, is below that necessary to roll at 90 deg/s during cruise, so it is not the driving motivator behind the aileron sizing.

Table 32. Asymmetric Loading Landing Parameters

Characteristic	**Cruise**
C_L	1.14
V [ft/s]	250.5
W [lb]	36,140
x_{CG}	31.95
y_{CG}	0.27
C_l	0.0069
$C_{l_{\delta_a},req}$ [1/rad]	0.0198

Moving onto the side-slip trim, the same parameters as shown in Tables 28 and 29 shall be utilized for the cross-wind side-slip. The rudder deflection will be identical to the AVL simulation used. Takeoff required the most aileron control power. The results of these simulations can be found in Table 33.

Table 33. Asymmetric Loading Landing Parameters

Characteristic	Value
C_{l_β} [1/rad]	(-0.14, -0.14)
$C_{l_{\delta r}}$ [1/rad]	(-0.02,-0.02)
C_l [1/rad]	(-0.025,-0.024)
$C_{l_{\delta a},req}$ [1/rad]	(0.073, 0.070)

Based upon the results of roll rate, asymmetric loading, and side-slip during takeoff/landing, the most intense requirement for the ailerons was trimming out sideslip on a heavy aircraft taking off. The aileron itself was then sized by starting the control surface after the end of the trailing edge flaps, using the same chord % for structural reasons, and then extending the span of the ailerons. A control power of $C_{l_{\delta a}} = 0.087$ [1/rad] was obtained, which exceeds all requirements and leaves a 19% margin in the worst case. The ailerons were left as such in order to accommodate corner cases where the Dragonfly might need to do multiple roll-heavy acts at once, such as side-slipping with asymmetric ordnance or battle damage.

4. Control Surface Parameters

The physical parameters of all-sized control surfaces can be found in Table 34. Flap deflection was chosen based upon the normal deflection expected to be seen during a landing [9]. The deflection for the slats is based on the typical deflection for a control surface.

Table 34. Control Surface Parameters

Characteristic	Elevator	Aileron	Rudder	Flaps	Slats
Start From Root [ft]	2.5	12.36	0	2.5	2.5
End From Root [ft]	11.58	17.28	7.42	12.36	17.28
Length [ft]	18.17	9.84	7.42	19.72	45.98
Span %	100	22.15	75	44.38	66.53
Chord %	100	20	25	20	20
Area [ft^2]	110	15.734	17.00	55.96	71.7
Deflection Range [+/-]	+20, -12	± 20	± 20	+20, -0	+0, -20

D. Trim Analysis

1. Trim Diagram Plots

In order to look at the capability of the aircraft to trim itself throughout its flight, the weight, CG, and dynamic pressure were shifted in AVL simulations, with the location of the neutral point being automatically calculated by AVL. The specific changes between the different simulations of phases of flight are collected in Table 35. None of these simulations involved side slip.

Table 35. Trim Conditions

Characteristic	Takeoff	Cruise	Landing
X_{np} [ft]	30.86	30.99	30.86
x_{CG} [ft]	29.747	30.85	31.95
W [lb]	36,800	29,440	16,520
C_{L_α} [1/rad]	3.85	4.86	3.90
C_{m_α} [1/rad]	-0.32	-0.05	0.32
$C_{m_{\delta_e}}$ [1/rad]	-0.67	-0.74	-0.567
q $[lbf/ft^2]$	109.8	223.1	64.2
ϵ_{maxC_L}	-7.6	-1.5	-7.0
$\frac{\delta\epsilon}{\delta\alpha}$	-0.27	-0.33	-0.29

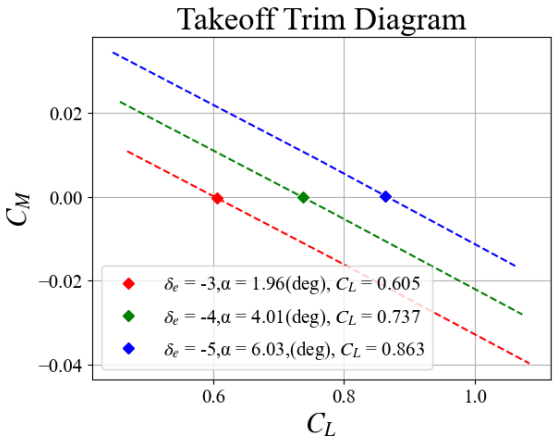

Figure 38. Takeoff Trim

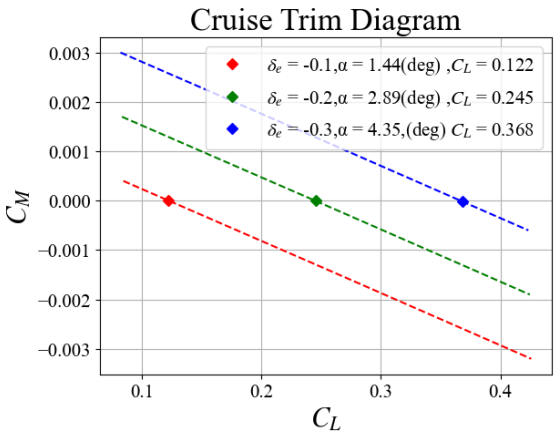

Figure 39. Cruise Trim

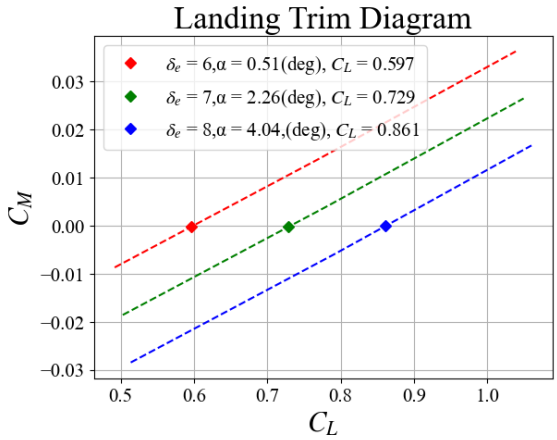

Figure 40. Landing Trim

Looking at Fig. 38, it can be seen that the aircraft is stable during takeoff. It can be seen that two degrees of α can be trimmed out by a negative degree of δ_e. The AVL simulation in this case assumed a slat angle of five degrees and a flap angle of 30 degrees. Using the downwash from table 35 and trim α values, it is possible to determine that at the maximum trimmed C_L, the horizontal tail has $a_{eff} = -6.54$ deg.

Figure 39 represents the trim diagram for an aircraft at 80% MTOW. It can be seen that the required horizontal tail deflection for trim is very small in this state. At the maximum trimmed C_L, the horizontal tail has $a_{eff} = 2.57$ deg. Figure 38 represents an operationally empty aircraft approaching for landing. The aircraft is directionally unstable at this point, represented by the positive slope on the lines, but this plot shows that the aircraft is capable of trimming when completely empty. The AVL simulation in this case assumed a slat angle of five degrees and a flap angle of 30 degrees. At the maximum trimmed C_L, the horizontal tail has $a_{eff} = 5.06$ deg.

E. Longitudinal Static Stability

The neutral point of the Dragonfly was automatically calculated from Mach = 0 to Mach = 0.8 using AVL. The extreme limits of the CG ranges are defined by the MTOW and OEW locations. This is because the fuel distribution system in the aircraft is placed such that the CG can be kept within these two extremes for the entire flight. The neutral point and CG ranges are shown in Table 36, along with the corresponding maximum possible SM values.

Table 36. Longitudinal Stability

Characteristic	Value
X_{np} [ft]	(30.82, 31.00)
X_{CG} [ft]	(29.74,31.95)
SM %	(-9.1, 8.2)

F. Dynamic Lateral Stability Properties

The Dragonfly's lateral stability derivative $C_{l_b} = -0.101$ [1/rad] is negative, implying stability. Comparing the value itself to the T-38, a supersonic trainer, the Dragonfly has higher lateral stability, with its closest match being a Learjet [12].

1. Dynamic Roll Speed

An estimate of the Dragonfly's I_{xx} can be made based upon its weight, wing-span, and similarity to other fighters [9]. Estimating the Dragonfly's inertia about the x-axis when fully loaded comes out to 29,858 slug*ft^2. With this value, it was then possible to solve for roll dynamically using a 1-dimensional differential equation [9]. AVL was used to get the roll-damping coefficient and aileron control power. Table 38 has all variables required to calculate dynamic roll behavior. It was calculated that it takes about 9.25 seconds for the Dragonfly to complete a 60-degree snap roll at cruise speeds.

Table 37. Dynamic Roll Relevant Information

Characteristic	Value
C_{l_p} [1/rad]	-0.34
b [ft]	44.43
V [ft/s]	778.3
q [lbf/ft^2]	223.1
$C_{l_{\delta_a}}$ [1/rad]	0.11
S_w [ft^2]	493.7
δ_a [deg]	20

G. Pull-Up Tail Deflection

Section VIII.D.1 shows that the Dragonfly is capable of maintaining straight and level trim during flight, but there is a need to prove that the tail is sufficient to enable high-G turns. This can be confirmed using an analytical equation [12]. Calculating this value during cruise without any high-lift devices with 50% internal fuel and no ordnance, the following relevant variables were calculated using AVL and preexisting information..

Table 38. Pull-Up Variables

Characteristic	Value
SM	0
ρ [slug/ft^3]	0.00074
S_{ref} [ft^2]	493.7
$\overline{c}$ [ft]	13.71
C_{M_q} [1/rad]	-3.31
C_{M_δ} [1/rad]	-0.74
$C_{L_{n=1}}$	0.21
m (slug)	700.9

Solving the analytical equation with the variables in Table 38, the results indicate that without any high-lift devices deployed, the elevators only need to be deflected 0.47 degrees more than normal cruise flight to achieve a 7-g turn during cruise. There is sufficient control authority in the elevators to achieve high-g maneuvers.

H. Natural Frequencies

To calculate natural frequencies and related characteristics, it is necessary to have estimates for the moments of inertia. As in section VIII.F, approximations shall be used for the moments of inertia[9, p. 623]. $I_{xx}, I_{yy}, I_{zz} = 29,858\ slug-ft^2, 103,218\ slug-ft^2, 172,314\ slug-ft^2$. Eigenvalue analysis was carried out using AVL, which provided the natural frequencies and damping ratios. One phugoid mode was discovered through eigenvalue analysis of the Dragonfly in AVL. Its relevant characteristics are described in Table 39.

Table 39. Phugoid Mode Parameters

Natural Frequency [Hz]	Damping Ratio
0.405	0.213

One dutch-roll mode was discovered. Its relevant characteristics are described in Table 40.

Table 40. Dutch-Roll Mode Parameters

Natural Frequency [Hz]	Damping Ratio
0.009	0.080

One spiral mode was discovered. Its relevant characteristics are described in Table 41. The doubling time was calculated based on the natural frequency [21].

Table 41. Spiral Mode Parameters

Natural Frequency [Hz]	Damping Ratio	Doubling Time [s]
0.317	0.057	38.35

I. Trade Studies

1. Effect of Anhedral on Elevator Control Power

It is a well-known design strategy to add anhedral to fighter-jet horizontal stabilators in order to minimize the effects of wing-wake upon the tail. However, adding anhedral means that less force is directed upwards when the tail is deflected. As such, there is a need to find an intermediate anhedral angle. Utilizing AVL, several simulations were run, with the only difference being changes in the horizontal tail's anhedral. The measure of merit was the required deflection to achieve trim during landing.

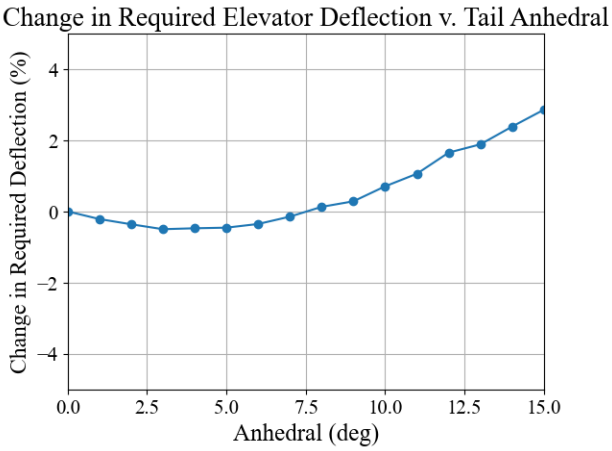

Figure 41. Variation of δ_e Over Changes in Tail Anhedral

Looking at Fig. 41, it can be seen that whilst the reduction in required deflection is small, a definite reduction in required elevator deflection can be achieved by having an anhedral of 3 to 5 degrees. Based upon this information, the Dragonfly's all-moving horizontal tail was given an anhedral of 5 degrees.

2. Drag as a Function of Static Stability With a Stabilator

By shifting fuel between the three main tanks, it became possible to actively control the CG of the Dragonfly. As such, there was interest in the most efficient location for the CG during flight. In order to test this, AVL's automatic trim and induced drag calculators were employed to provide drag data from shifting the CG fore and aft in the fuselage.

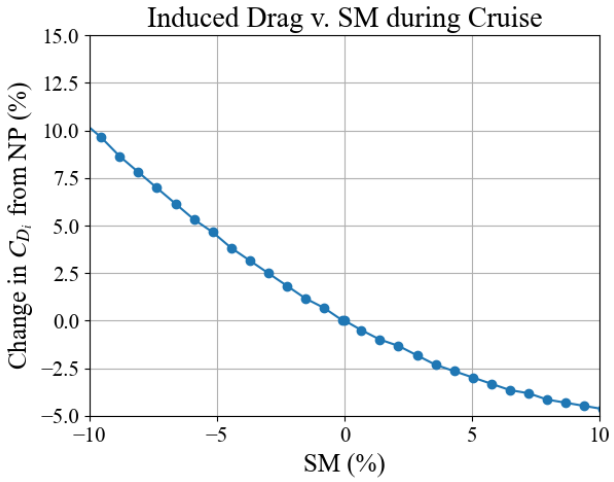

Figure 42. Variation of C_{D_i} With Changes in SM During Cruise

As can be seen in Fig. 42, the simulation indicated that induced drag is minimized when the CG is placed as far forward of the CoG as allowable by SM limits. Compared to placing the CG at the x_{np}, induced drag can be lowered by approximately 5% through shifting the CG forward.

IX. Structures and Loads

A. V-n Diagram

A limit load and ultimate load V-n diagram was created to represent the limitations of the Dragonfly's design. In accordance with 14 CFR § 25.301, structural design loads are based on limit and ultimate conditions, with prescribed load distributions representing realistic operating environments. Data calculated through the sizing analysis and information acquired from military specifications MIL-A-8861 for attack/fighter aircraft were used in the V-n diagrams. The weight used in the V-n diagrams corresponds to a clean configuration with 50 % internal fuel as required in the RFP[1]. All values were calculated in knots equivalent air speed (KEAS) at sea level to exclude the effect of altitude from the loads that the aircraft would experience. Using the equations listed in Roskam [22] and Bruhn [23], the

different significant speed values listed in Table 42 were calculated. The positive limit load was determined as +8g to meet the instantaneous turn rate of 18.0 deg/s requirement, and the negative limit load was determined by the mission requirement of -3g [1]. The maximum limit design dive speed V_D was determined using the requirement of being able to withstand 2,133 psf at Mach 1.2 at sea level. In accordance with 14 CFR Part 25 §25.333, Fig. 43a establishes the necessary boundaries of the representative maneuvering envelope (V-n diagram) as prescribed by the regulations. When determining the ultimate load V-n diagram, the safety factor of 1.5 was used to determine the ultimate load in accordance with 14 CFR Part 25 §25.303. As shown in Fig. 43b, the ultimate positive and negative loads are now +12g and -4.5g. Furthermore, the safety factor was applied to the maximum dynamic pressure as well to get the Dragonfly's ultimate maximum dive speed.

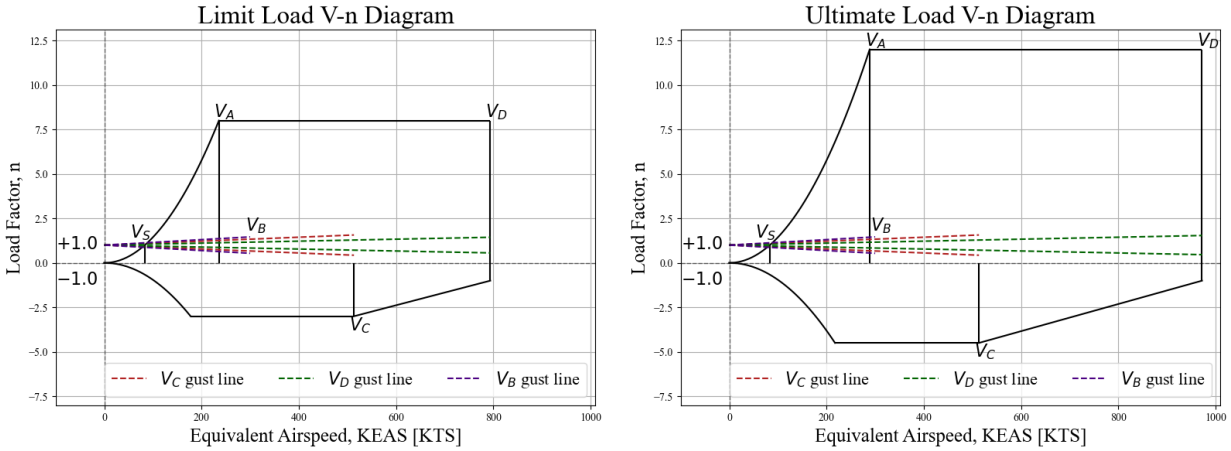

(a) Limit Load V-n Diagram **(b) Ultimate Load V-n Diagram**

Figure 43. Clean Configuration With 50% Internal Fuel V-n Diagram

Table 42. Limit Load V-n Diagram Significant Speed Values

V_S [kts]	V_A [kts]	V_C [kts]	V_D [kts]	n_{pos}	n_{neg}
83.34	235.7	513.4	793.7	8	-3

A gust load analysis is also done at the maximum gust intensity, cruise, and dive. The gust load factor lines were derived using equations given in Roskam [22] and are given in Table 43. As shown in Fig. 43, the gust load factor lines fall well within the V-n diagrams and are not a limit factor to the aircraft design. This is due to the Dragonfly's ability to maneuver at high loads and speeds.

Table 43. Gust Load Factor Line Slopes

V_B	V_C	V_D
0.00153	0.0011	0.000553

B. Selection of Load Cases of Interest

Three specific load cases were analyzed for the Dragonfly due to its significance and limiting factor to the design. One of the load cases is the 18 deg/s instantaneous turn, which is close to the maximum wing loading. This was chosen as one of the limiting load cases as this represents the extreme load factor the structure of the aircraft must withstand during a high-speed turn and generates peak lift coefficients and bending moments that the aircraft must resist without yielding. Another load case is the supersonic cruise and dashing. Sustained flight at maximum continuous supersonic speed exposes the airframe to elevated dynamic pressures and significant aeroelastic effects. This case governs the sizing of skin thicknesses to resist aerodynamic heating and the loads required to maintain stability margins at high Mach numbers. Ensuring structural integrity in supersonic cruise guarantees safe, reliable performance during high-speed dashes. The last load case is the +2.5g landing. This landing case captures the maximum vertical load transmitted through the landing gear and fuselage during a hard landing. Although the load factor is lower than the instantaneous turn load case, the highly concentrated loads on the landing gear tests the structure of the fuselage for any high-stress points or structural damage.

C. Wing Loading

During flight, the wing experiences lift due to air pressure and inertial loads. This can be displayed through the spanwise lift distribution, which describes how the lift per unit span varies from the wing root to the tip. The three main lifts experienced by the wing, the aerodynamic load, the wing weight, and the pylon weight. The aerodynamic load is approximated using Schrenk's approximation, which takes the average of the wing loading from the elliptical method and the trapezoidal method. The spanwise lift distributions for the three specific load cases are shown below in Fig. 44.

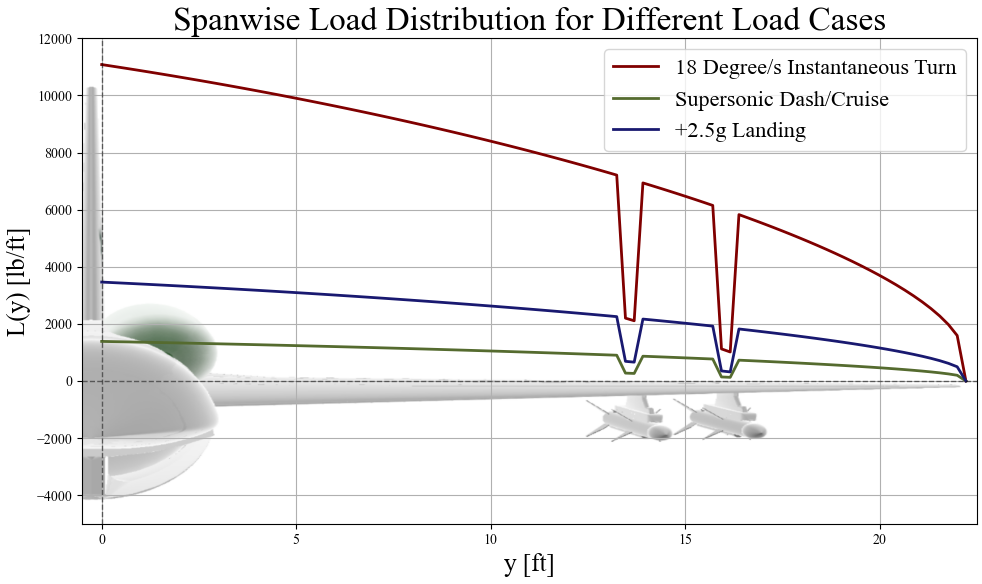

Figure 44. Spanwise Wing Loading

D. Bending Moment and Shear Force

The bending moment and the shear force from the loads on the wing are approximated numerically by integrating the spanwise lift distribution shown in Fig. 44. The shear force diagram and the bending moment diagram for the three load cases are shown in Fig. 45a and Fig. 45b, respectively. As seen in the figures, the magnitude of the shear force and bending moment is greatest at the root of the wing and decreases to zero at the tip of the wing. The ultimate shear force and ultimate bending moment are calculated by the force and moment experienced where the fuselage intersect with the wing. The critical values are given in Table 44.

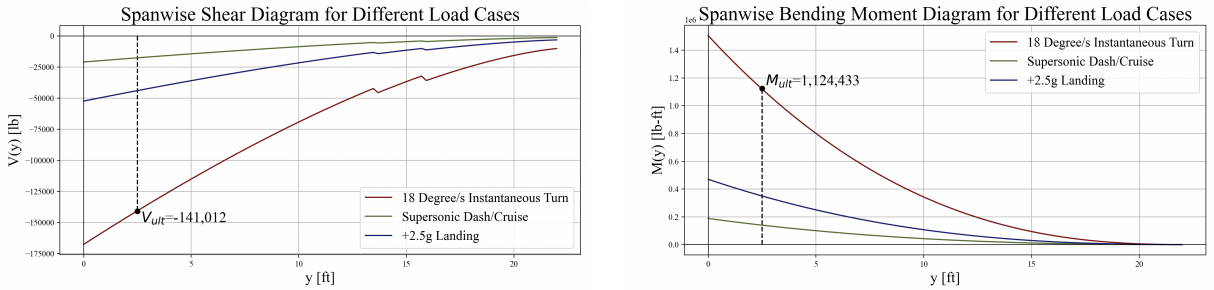

(a) Spanwise Shear Force Diagram **(b) Spanwise Bending Moment Diagram**

Figure 45. Ultimate Shear Force and Bending Moment Diagrams

Table 44. Bending Moment and Shear Force Critical Values

y_{ult} [ft]	V_{ult} [lb]	M_{ult} [lb-ft]
2.5	-141,000	1,124,000

E. Load Paths

The load path diagrams corresponding to the three load cases discussed in Section IX.B are shown below in Fig. 49, each illustrated with idealized point loads. Analyzing load paths is critical in aircraft structural design, as it clarifies how forces are transmitted through the airframe and ultimately to the center of gravity. Proper load paths help stabilize the aircraft and prevent unintended moments about the yaw, pitch, and roll axes. Figure 46 shows the load path for the 18-degree-per-second instantaneous turn. The dominant force in this case is the aerodynamic load, highlighted in yellow. The wing loads are transferred through the ribs and spars into the fuselage, and then to the center of gravity. Figure 47 shows the load path for the supersonic cruise and dashing. The load path is pretty similar to the 18 deg/s load path, but it experiences less aerodynamic load in the wings as it is experiencing a lower load factor. Similarly, the loads experienced in the wing and fuselage transfer their loads through the structure into the center of gravity. Lastly, Figure 48 shows the load path in a +2.5g hard landing. For this load case, the most noticeable load is due to the normal force experienced by the landing gear from the ground. As seen in the figure, the loads from the landing gear transfer to the oleo and into the fuselage. The loads then travel through the fuselage structure into the center of gravity.

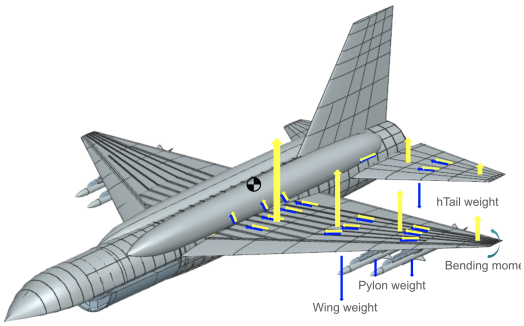

Figure 46. 18 Degree per second Instantaneous turn

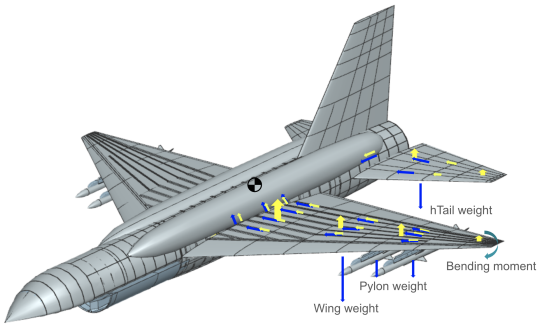

Figure 47. Supersonic Cruise and Dashing

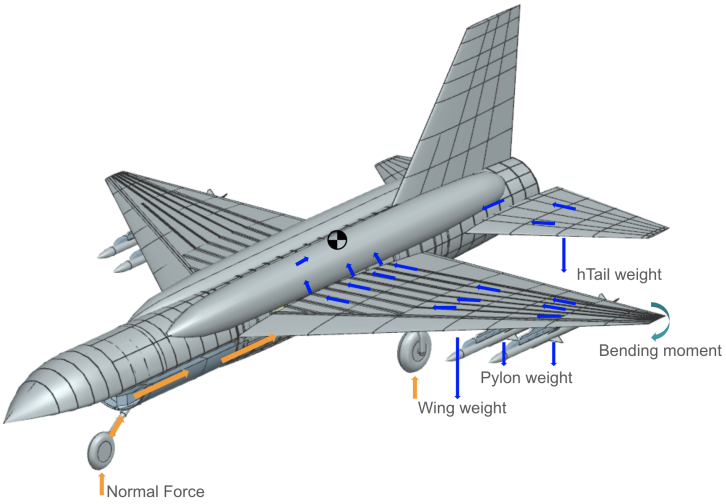

Figure 48. +2.5g Landing

Figure 49. Load paths for different load cases

F. Material Selection

During flight, the Dragonfly is subjected to various forces, including compression, tension, and shear. The structure surrounding the engine must also withstand high burner temperatures, requiring materials with excellent heat resistance. To meet these demands, materials were selected based on an optimal balance of strength, weight, and performance under load. For the fuselage, key properties include stiffness, strength, fatigue, corrosion resistance, and fracture toughness [24]. Wing materials must offer high stiffness, strength, damage tolerance, and durability. The wing skin demands materials with high shear strength, while spars require superior tensile strength. Wing connections experience greater loads than the wing structure itself, necessitating materials with exceptional strength, fatigue resistance, and fracture toughness, making composites an ideal choice. The tail structure, experiencing similar loads, follows a comparable

material selection. Control surfaces face high cyclic stresses during takeoff, landing, and maneuvering, justifying the use of fatigue-resistant composites in these components.

Historically, the material chosen for the spars varies from titanium, steel, composite, and aluminum. In a structural analysis conducted for the F-5E [25], the paper compared eight material compositions for its six spar configurations. Ultimately, aluminum was chosen for its cost and weight savings, ruling out honeycomb titanium and aluminum titanium from the top three. Since the Dragonfly has a thinner wing than the F-5, the same amount of spar will not be used.

The final material selection for the aircraft incorporates high-strength aluminum alloys, titanium, steel, and carbon-epoxy composites. The specific properties of the material [26] are detailed in Table 45. Aluminum 7075-T6, with its relatively low density and high strength-to-weight ratio, was widely used in primary structural elements such as spars, ribs, and skin due to its good yield strength and moderate stiffness. Additionally, aluminum is fairly inexpensive to produce and manufacture, which is favorable given the RFP's cost restriction. The titanium alloy Ti-6Al-4V, though denser, offers excellent strength and is used where high temperature and corrosion resistance are needed, such as in engine integration. For high-impact, high-load components, such as landing gear, AISI 4340 steel is chosen for its superior strength and stiffness, despite its high density. In contrast, composite materials such as epoxy/carbon fiber and E-glass fiber are employed in weight-critical areas; the former combines high tensile and yield strengths with low density, wing-root components, while the latter is suitable for lightweight parts such as bulkheads and nose cones.

Table 45. Material Properties

Material	**Density [lb/in^3]**	**UTS [psi]**	**Yield Strength [psi]**	**Shear Strength [psi]**	**Poisson's ratio**	**Young's Modulus [ksi]**	**Component**
Al 7075-T6	0.1020	83,000	73,000	48,000	0.33	10,400	Spars, ribs, frames, longerons, skin
Ti-6Al-4V	0.1600	170,000	160,000	N/A	0.33	16,500	Engine integration
AISI 4340	0.2840	185,900	125,000	N/A	0.29	29,000	Landing Gear
Epoxy/Carbon fiber composite	0.0513	140,000	182,700	13,000	0.286	14,600	Feathers, wing-root attachment
E-Glass Fiber	0.0920	525,000	290,076	N/A	0.2	10,500	Bulkhead, nose cone

G. Structural Layout

The structural layout of the Dragonfly is observed in Fig. 50. The methods used for this design include similarity analysis, empirical methods, and FEA analysis. Structures were designed to stay within allowable load limits to minimize excess weight.

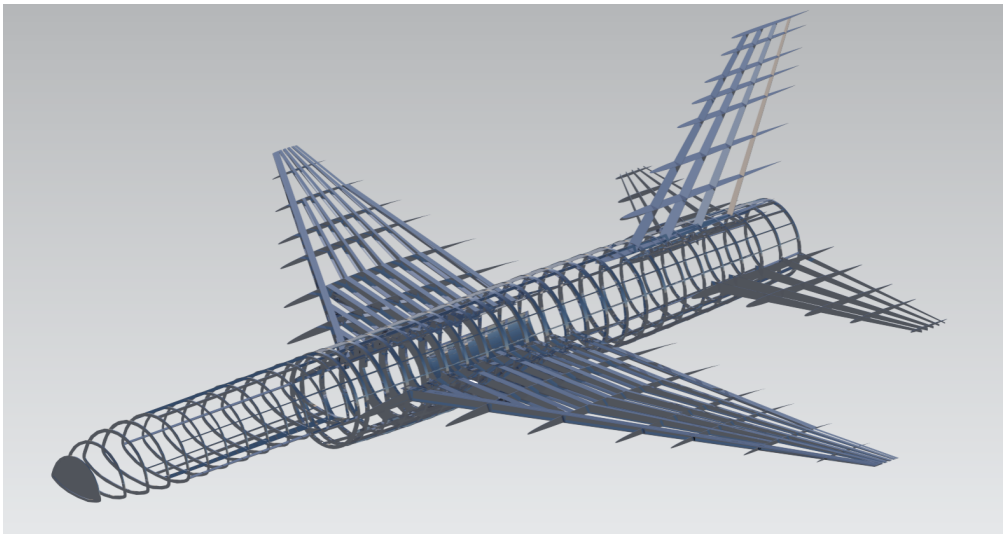

Figure 50. Structural Layout

1. Fuselage

A semi-monocoque fuselage structure was used, consisting of a thin skin that bears shear loads, longitudinal longerons that support tension and compression forces, and frames that help redistribute the overall airframe load. The structural layout for the fuselage is obtained from Chapter 3 of Roskam Part 3 [27]. Bulkheads were placed where the wing attaches to the fuselage to manage the moment about the root chord. The layout of the fuselage is summarized in Table 46. The landing gear retracts into the fuselage into a dedicated bay that is structurally reinforced to handle the high forces generated during takeoff and landing.

Table 46. Fuselage Structural Dimensions and Spacing

Fuselage	
Skin thickness [in]	0.039
Frame thickness [in]	0.700 to 2.500
Frame depth [in]	2.000
Frame pitch [in]	16
Longeron spacing [in]	11.78

The tail was attached to the rear fuselage through reinforced bulkhead frames that interface with the main spars of the vertical and horizontal tails. These attachment points are critical load paths that transmit aerodynamic and control

loads into the fuselage structure. For the vertical tail, the two forward spars are bolted to the fuselage frame, while the aft spars are connected to a load-distributing fitting near the rudder hinge line. For the all-moving horizontal tail, a central pivot shaft connects the tail to a bearing assembly embedded within a load-bearing bulkhead. Actuator mounting points are integrated near this interface to deliver pitch control moments while minimizing eccentric loading on the fuselage.

2. Wing

A multi-cell wing construction was chosen to keep the wing very thin while providing stability in the skin. Additionally, this configuration will reduce wing flutter by adding stiffness and damping properties to help control oscillations. The structural layout of the wing includes ten spars, which reduce to six at the tip, and eight ribs. The location of the front and aft spars is adjacent and parallel to the control surfaces to support the moments about the hinges. The spars are evenly spaced, as is typical for multi-cell construction, and also provide predictable deflection and stress concentrations along the wing. The spars are more severely swept as they approach the tip to follow the angle of the ailerons and slats.

The dimensions of the wing structure are first determined empirically using equations and methods from Megson [28] and Howe [29]. The ultimate shear load and moment from the shear and moment diagram of the wing are used to size the spars by determining the required moment of inertia. The thickness of the airfoil constrains the height of the spars. The other spar cross-section parameters are modified until bending stress and shear stress experienced by the spars comply with their material properties. The wing skin thickness is determined using Eq. 15.11 from Howe [29]. The rib thickness is calculated based on shear flow q distribution within the 10-cell wing from Eq. 23.6 and 23.4 from Megson [28]. The rib spacing is in consideration of the location of ordnance and control surfaces. The dimensions of the wing structure are listed in Table 47.

Table 47. Wing Structural Dimensions

Wing	
Skin thickness [in]	1.000 to 0.056
Spar	
Web thickness [in]	0.573
Flange thickness [in]	0.440
Spar width [in]	4.0 to 2.0
Rib	
Rib Thickness [in]	0.189

Finite Element Analysis (FEA) was conducted, using Abaqus, to simulate wing loading and assess structural performance. The wing was modeled as fixed at the root and free at the tip, subjected to an ultimate load factor of +12g. A pressure field map generated from SU2 was applied to the wing skin to replicate aerodynamic loading. Hinge moments, derived from the hinge coefficient outputted by AVL, were applied at actuator locations. Additionally, point

loads were introduced at the pylon attachment points. As shown in Fig. 51, the resulting stress distribution indicates a maximum stress of 54,600 psi, well below the material's yield strength of 73,000 psi, where permanent deformation would occur. This maximum stress represents approximately 70% of the yield limit, providing a conservative safety margin to account for unexpected or higher-than-anticipated loading and fatigue, albeit with some added structural weight.

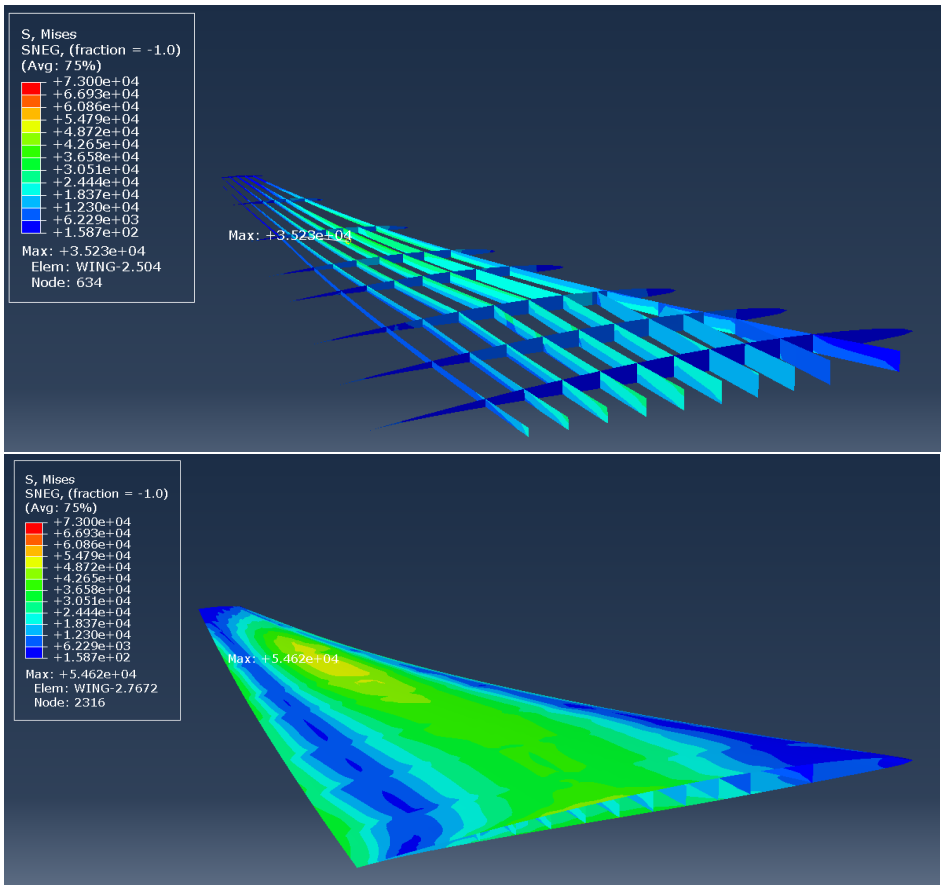

Figure 51. Stress Concentration with Ultimate Loading on Wing

3. Tail

The tail structure chosen is also a multi-spar configuration, as is typical for fighters. The structural layout of the vertical tail includes four spars and eight ribs. Similarly to the wing, the spar of the vertical tail runs parallel and adjacent to the rudder. Ribs were concentrated at the tip, where greater deflection and torsional loading are expected. For the horizontal tail, five spars and five ribs were used, with ribs closer to the root to support the mechanics of the all-moving stabilizer. The dimensions of the tail structures are listed in Table 48, which were derived using a combination of FEA results and similarity analysis.

Table 48. Tail Structural Dimensions

	Vertical Tail	Horizontal Tail
Skin thickness [in]	0.250 to 0.026	0.075 to 0.026
Web thickness [in]	0.200	0.100
Rib Thickness [in]	0.150	0.150

Similar to the wing, the tail was subjected to an ultimate load factor of +12g. Pressure loads obtained from SU2 were mapped onto the tail surfaces, and the hinge moment was applied at the rudder actuator. The stress distribution on the vertical tail is shown in Fig. 52, with a maximum von Mises stress of 34,450 psi. The horizontal tail's stress distribution is shown in Fig. 53, with a maximum stress of 38,690 psi. Both values remain below the material's yield strength, corresponding to approximately 47-52% of the yield limit.

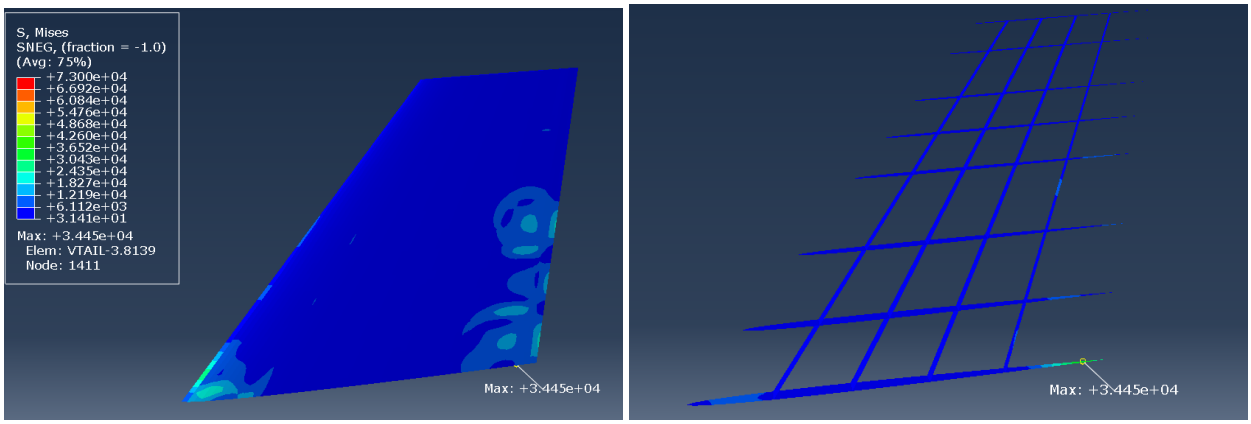

Figure 52. Stress Concentration with Ultimate Loading on Vertical Tail

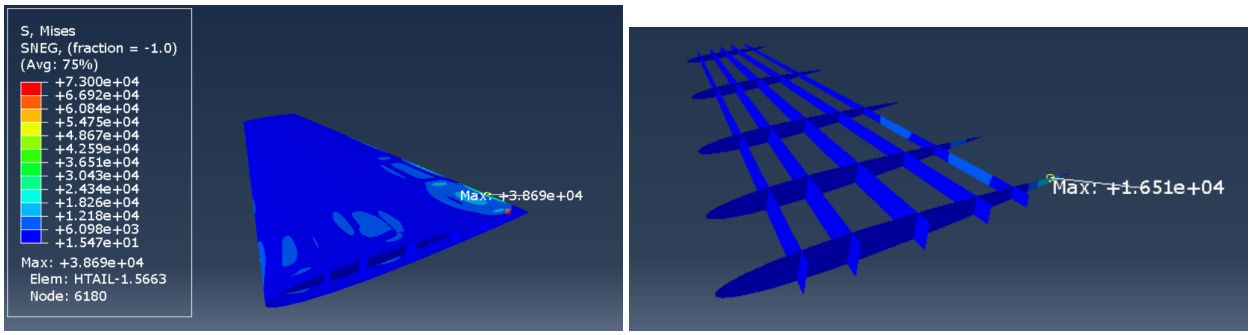

Figure 53. Stress Concentration with Ultimate Loading on Horizontal Tail

H. Combat Survivability

The structural layout of the Dragonfly, comprising a semi-monocoque fuselage, reinforced wing and tail structures, and strategically distributed load paths, contributes to combat survivability. The semi-monocoque fuselage with skin, frames, and longerons offers redundancy and damage tolerance; even if one structural element is compromised, others can continue to carry load and preserve airframe integrity. The wing's design, validated through FEA, incorporates multiple spars and ribs, and actuator reinforcements to localize and manage stress concentrations, improving resistance to structural failure from high-G maneuvers or combat damage. The tail structures, with multiple spars and strategically placed ribs, provide additional redundancy in control-critical areas, enhancing the aircraft's ability to maintain stability and maneuverability even after sustaining localized damage.

I. Fatigue

Using Basquin's law of fatigue, the life service of the Dragonfly is analyzed through cyclic loading until failure. Fatigue properties for aluminum were derived from [30]. Assuming the applied stress amplitude was the highest stress from FEA results at 54,600 psi (see Section IX.G.2), the number of cycles to failure is 3,100. This is a conservative estimate as it is for the worst-case loading scenario of 12g per cycle, which exceeds the requirements of any specific mission profile. Based on this analysis, it is reasonable to conclude that the structure can endure at least 2,000 hours of operational life, especially with routine maintenance.

X. Mass Properties

A. Methodology

To begin the mass properties analysis, the Dragonfly's component weights were determined using Siemens NX CAD, Raymer Chapter 15 Fighter/Attack Weights section [9], Roskam Part V General Dynamics (GD) Class II methods [22], and actual weights provided in the RFP or manufacturer data sheets. Major structural components (e.g. fuselage, wing, tail) were modeled in Siemens NX with assigned thickness and material properties to calculate CAD-based weights. Using CAD is the preferred method for obtaining weights, as it provides the most accurate representation of the Dragonfly's structural configuration. To validate the CAD weights, statistical methods presented in Raymer and Roskam were used as baseline guidelines to assess whether the components were within a reasonable range. In most cases, the CAD-derived weights were similar to the statistical estimates, and in some instances, even lower, indicating that the statistical methods may tend to overestimate component weights.

For the subsystem components that could not be precisely modeled in CAD, statistical methods were used to estimate their weights. It is important to note that the average weight was taken from Raymer and Roskam, as these equations have inherent limitations that can lead to either underestimation or overestimation of certain components. While averaging helps account for potential deviations between the methods, often, the weights from Raymer and

Roskam were already similar, which provides additional confidence in the estimates. In instances where Roskam did not provide estimation methods for specific subsystems, Raymer's equations were used solely. For Raymer's methodology, several assumptions were made. Specifically, the engine cooling shroud length was approximated based on the selected engine specifications and the Dragonfly's dimensions. Additionally, the flight controls equation in Raymer is directly dependent on the number of crew members. While the aircraft is remotely piloted and does not have a physical crew, it was assumed to have a single crew member to account for the necessary flight control systems. Lastly, the fuel system and tanks equation assumes to have all self-sealing integral tanks, with three located internally in the fuselage, and two conformal tanks. The self-sealing integral tank weights were determined through statistical methods, however, the fuel volume capacity was found using CAD.

Actual component weights were used where available. Specifically, the RFP calls for the use of Government Furnished Equipment (GFE), and the Dragonfly incorporates the RFP specified electrical system, vehicle management system, APU, ICNIA, Data bus, INEWS, IRSTS, and Active Radar. Additionally, the RFP provides the weight of the AIM-120 AMRAAM, and the Dragonfly is equipped to carry up to four missiles. Lastly, the camera system used is the L3Harris WESCAM MX-8, and the engine is the F110-GE-129, with these weights obtained from manufacturing data sheets.

The center of gravity (CG) location for each component was determined using the CAD model. The Siemens NX mass properties analysis tool calculates specific CG locations based on the component weight, geometry, and distance from the nose (reference datum point). For sub-systems not represented in CAD, system layout schematics were referenced to approximate realistic placement. Table 49 summarizes the Dragonfly's component weights, CG locations, and methodology sources.

Table 49. Component Weights and CG Locations

Component	Methodology	Weight [lb]	CG [ft. From Datum]
Wing	CAD	2,499	31.27
Horizontal Tail	CAD	294	48.04
Vertical Tail	CAD	588	46.09
Fuselage	CAD	3,468	29.33
Landing Gear (Retracted)	Raymer (Eqs. 15.5, 15.6) & Roskam (Eq. 5.41)	1,352	25.67
Engine Mounts	Raymer (Eq. 15.7)	52	43.03
Engine Section	Raymer (Eq. 15.9)	40	43.03
Air Induction System	CAD	461	23.36
Engine Cooling	Raymer (Eq. 15.12)	141	43.03
Oil Cooling	Raymer (Eq. 15.13)	38	43.03
Vehicle Management System	RFP	50	7.26
Fuel System & Tanks	Raymer (Eq. 15.16) & Roskam (Eq. 6.24)	1,119	27.96
Instruments & Avionics	RFP & Camera Data Sheet	725	5.20
Hydraulics	Raymer (Eq. 15.19)	Included in Flight Control	
Electrical	RFP	220	20.00
Air Conditioning & Anti-Ice	Raymer (Eq. 15.23) & Roskam (Eq. 7.34)	159	25.00
APU	RFP	100	32.41
Flight Control System	Raymer (Eq. 15.17) & Roskam (Eq. 7.10)	1,275	26.00
Engine (Unmounted)	Engine Data Sheet	3,940	43.03
Ordnance	RFP	1,308	34.56
Internal Integral 1 Tank Fuel	CAD	4,627	14.90
Internal Integral 2 Tank Fuel	CAD	4,017	27.23
Internal Integral 3 Tank Fuel	CAD	3,416	40.30
Conformal Tank Fuel	CAD	6,908	31.02

B. Weights and Center of Gravity

In accordance with MIL-HDBK-516C Section 5.5.1 and 14 CFR Part 25 §25.25, the evaluation of mass properties must ensure that the design supports safe operations across all defined mission requirements, payload variations, fuel configurations, and maintenance needs. The component weights and their respective CG locations were used to determine major aircraft weights and their CG. These include defining the operating empty weight (OEW), maximum take-off weight (MTOW), maximum take-off weight without conformal tanks, and maximum zero fuel weight (MZFW), as summarized in Table 50. The aircraft is designed to take into consideration these regulations to ensure safety, stability, and overall compliance.

Figure 54 provides a schematic layout of the component CG locations, as well as the OEW CG. Major structural components and fuel tank locations are highlighted, as these were key contributors to the overall CG and were strategically positioned during the design process.

Table 50. Summary of Key Aircraft Weight Conditions and CG Locations

Weight Definitions	Weight [lb]	CG [ft. From Datum]	CG [%MAC]
OEW	16,520	31.95	53.72
MTOW	36,800	29.99	39.37
MTOW (Without Conformal Tanks)	29,890	29.75	37.63
MZFW	17,830	32.15	55.12

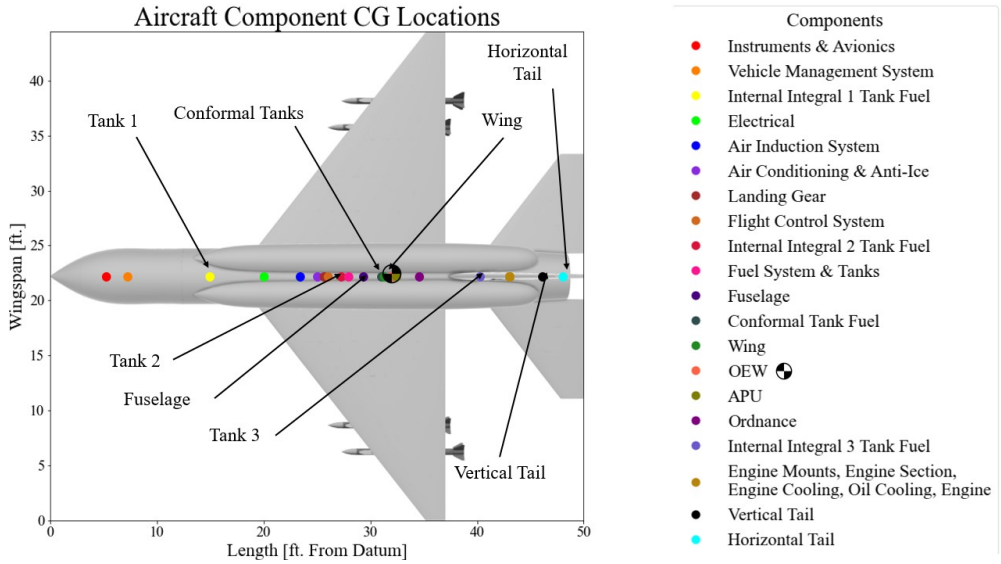

Figure 54. Longitudinal Component CG Layout

C. Loading Conditions

As stated in 14 CFR Part 25 §25.27, the extreme forward and the extreme aft CG limits must be established for each separate operating condition. The following loading conditions address the extreme forward and aft CG limits for each mission specified in the RFP to adhere to these regulations.

1. Defense Counter Air-Patrol Mission

The Defense Counter Air-Patrol (DCAP) mission influenced the fuel tank design, as it is the most fuel demanding mission. For this mission, the Dragonfly requires 18,923 lb of fuel, filling all three internal tanks to capacity and the conformal tanks to capacity. To identify the extreme forward CG limit, the aircraft was loaded from forward to aft in the following sequence: internal tank 1, internal tank 2, conformal tanks, ordnance, and internal tank 3. The Dragonfly's ultimate forward CG extreme occurs at 25.37% MAC, which is reached after tank 2 is loaded. This limit is not driven by the conformal tanks, which were strategically placed to avoid contributing to CG extremes. Similarly, the Dragonfly's extreme aft CG limit was determined by loading in the aft-to-forward sequence: internal tank 3, ordnance, conformal tanks, internal tank 2, and internal tank 1. The aft-most extreme occurs at 64.68% MAC, reached after the ordnance is

loaded. Again, the conformal tanks do not drive this aft limit. It is worth noting that the extended main landing gear is located at 66.81% MAC, ensuring the aircraft remains stable and does not experience tip-back, even under extreme aft-loading conditions. In operating conditions, the aircraft would follow a more realistic loading sequence: conformal tanks, internal tank 2, internal tank 3, internal tank 1, and ordnance. This sequence allows each tank to be fully loaded one at a time while keeping the CG within the allowable ±10% static margin. Figure 55 illustrates the complete loading envelope for the DCAP mission.

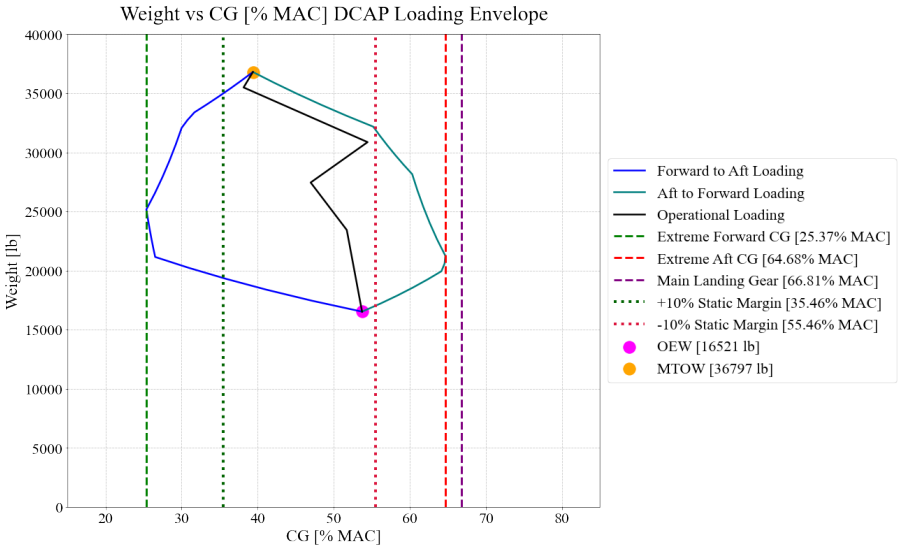

Figure 55. DCAP Mission 1 Loading Diagram

2. Point Defense Intercept Mission

The Point Defense Intercept (PDI) mission requires 6,177 lb of fuel; therefore, the aircraft is only partially loaded to meet the mission requirement. The 6,177 lb is distributed by allocating 50% to internal tank 1, 30% to internal tank 2, and 20% to internal tank 3. It should be mentioned that the Dragonfly configuration for this mission does not incorporate conformal tanks nor does it load any single tank to full capacity. This is because balancing the fuel distribution across the three internal tanks is necessary to remain within the allowable ±10% static margin. For this configuration, the forward-most CG limit is at 32.86% MAC when loaded in the following sequence: internal tank 1, internal tank 2, ordnance, and internal tank 3. This should not be mistaken for the aircraft's ultimate extreme forward CG limit (25.37 % MAC), as it is just the furthest forward CG that occurs when loaded for this specific mission. The aft-most CG limit is at 55.46% MAC when loading in the sequence: internal tank 3, ordnance, internal tank 2, and internal tank 1. Similarly, this is not the aircraft's overall extreme aft CG (64.68 % MAC), but the most aft location reached during loading for this mission. In operational scenarios, the Dragonfly should be loaded in the ideal sequence: internal tank 2, internal tank 3, internal tank 1, and ordnance. This operational loading path allows each tank to be filled one at a time, while maintaining CG within ±10% static margin. Figure 56 demonstrates the complete loading envelope for the PDI mission.

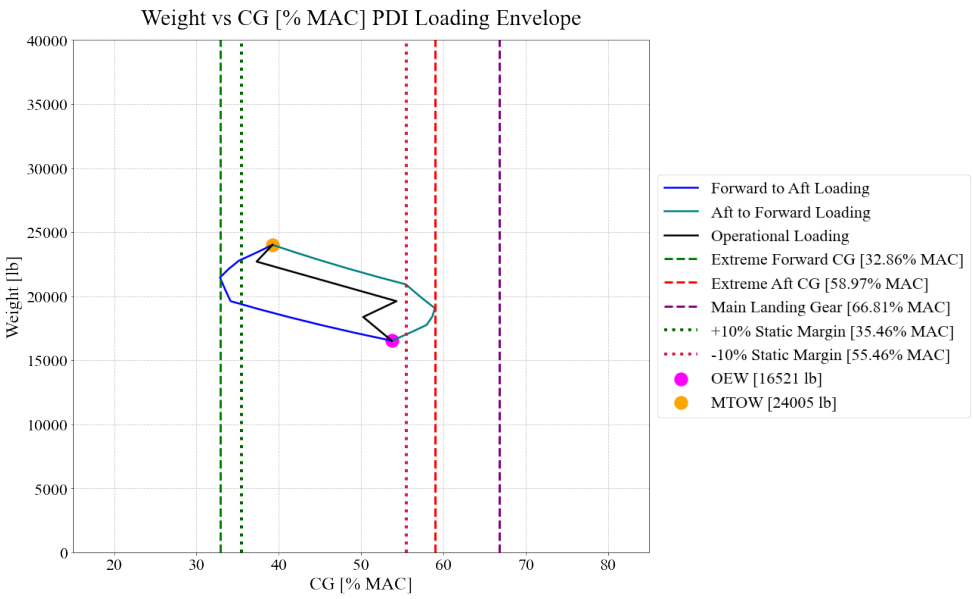

Figure 56. PDI Mission 2 Loading Diagram

3. Intercept/Escort Mission

Unlike the DCAP and PDI missions, which require a specific loading configuration, the Intercept/Escort (IE) mission can be completed for various loading configurations. Namely, the variations being considered for the IE mission are: 1) the minimum requirement of a 200 nmi dash, 2) at maximum total fuel, and 3) at maximum internal fuel.

Starting with the first variation for a 200 nmi dash, the IE mission requires 9,268 lb of fuel. The fuel is distributed 30 % in internal tank 1, 50 % in internal tank 2, and 20% in internal tank 3. This configuration does not utilize conformal tanks, nor does it load any tank to full capacity, ensuring that the fuel is distributed among tanks strategically to remain within ±10% static margin. Using the same forward and aft loading sequences without the conformal tanks as previously discussed, the forward-most CG limit is at 32.62 % MAC and the aft-most CG limit is at 60.71% MAC for this specific loading configuration. The ideal operational loading sequence that meets the static margin requirements is as follows: internal tank 2, internal tank 3, internal tank 1, and ordnance. Figure 57 displays the loading envelope for the IE mission to complete a 200 nmi dash.

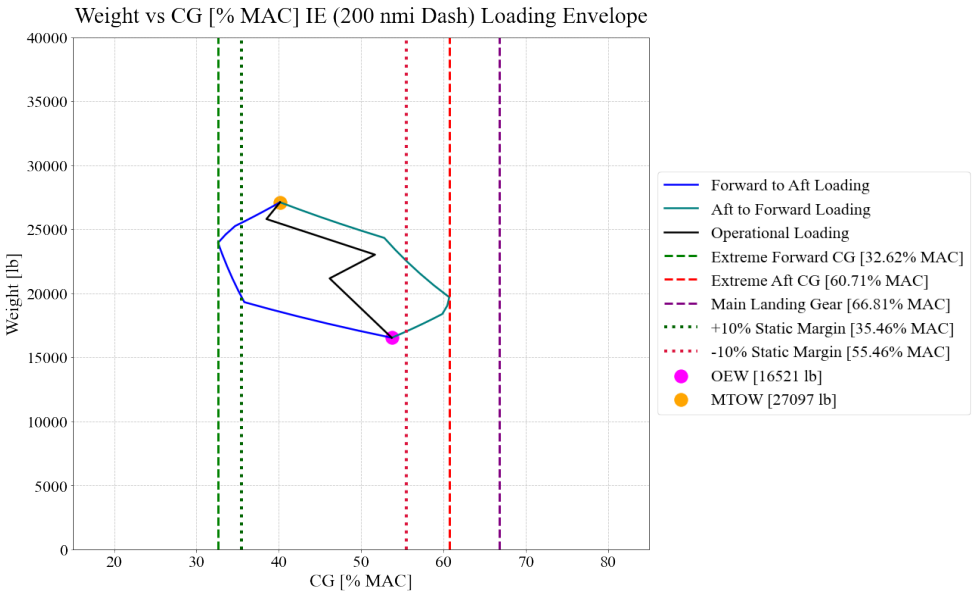

Figure 57. IE Mission 3 (200 nmi Dash) Loading Diagram

Next, the second variation of the IE mission assumes the Dragonfly is loaded to its maximum fuel capacity of 18,969 lb, utilizing all internal and conformal tanks. This configuration aligns with the DCAP mission envelope shown in Fig. 55, as this envelope represents the most fuel-constrained scenario, requiring the maximum takeoff weight (MTOW) configuration.

For the final IE mission variation, the loading configuration assumes maximum internal fuel is loaded, disregarding the conformal tanks. The maximum internal fuel capacity is 12,060 lb. This configuration also meets the ultimate extreme CG limits at 25.37 % MAC and 64.68 % MAC when loaded in the forward and aft sequences. This is because the conformal tanks do not impact the extremes when the internal tanks are loaded to capacity. The internal tanks do not carry the same amount of fuel, therefore, operational loading is slightly more complex to keep the aircraft within static margin limits. If each tank were fully loaded one at a time, the CG would not remain within the allowable ±10% static margin; therefore, the Dragonfly must be operationally loaded in the following sequence: 100% internal tank 2, 50% internal tank 3, 50% internal tank 1, 50% internal tank 3, 50% internal tank 1, and ordnance. By partially loading tanks 3 and 1 at a time, the CG shift is balanced to avoid instability. Figure 58 shows the loading envelope for the IE mission under full internal fuel conditions.

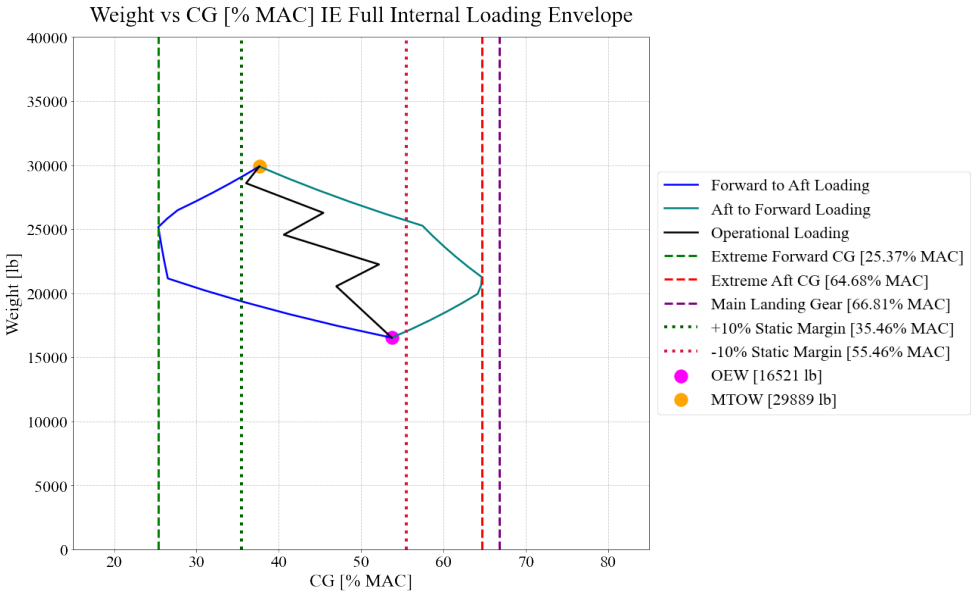

Figure 58. IE Mission 3 Full Internal Fuel Loading Diagram

D. Mission CG Unloading Profiles

The MIL-HDBK-516C states in section 5.5.2 that the aircraft center of gravity must remain within the approved flight envelope for all mission scenarios. Additionally, it is required that a fuel system methodology to determine the weight and center of gravity of the fuel has been defined. The following mission profiles demonstrate how the implemented fuel burn methodology ensures that the Dragonfly operates within the approved ±10% static margin envelope, meeting these requirements.

1. Defense Counter Air-Patrol Mission

Figure 59 plots the CG profile as the Dragonfly burns fuel through each mission segment and accounts for the ordnance drop. Table 51 tracks the fuel consumption path at each mission segment and the location from which tank fuel is being drained. For this mission, the Dragonfly unloads fuel in the opposite sequence was operationally loaded: internal tank 1, internal tank 3, internal tank 2, and then conformal tanks. The conformal tanks do not burn all of the fuel, as the reserves are assumed to be left unburned. The mission profile demonstrates that the Dragonfly remains within the allowable ±10% static margin for the entirety of the mission.

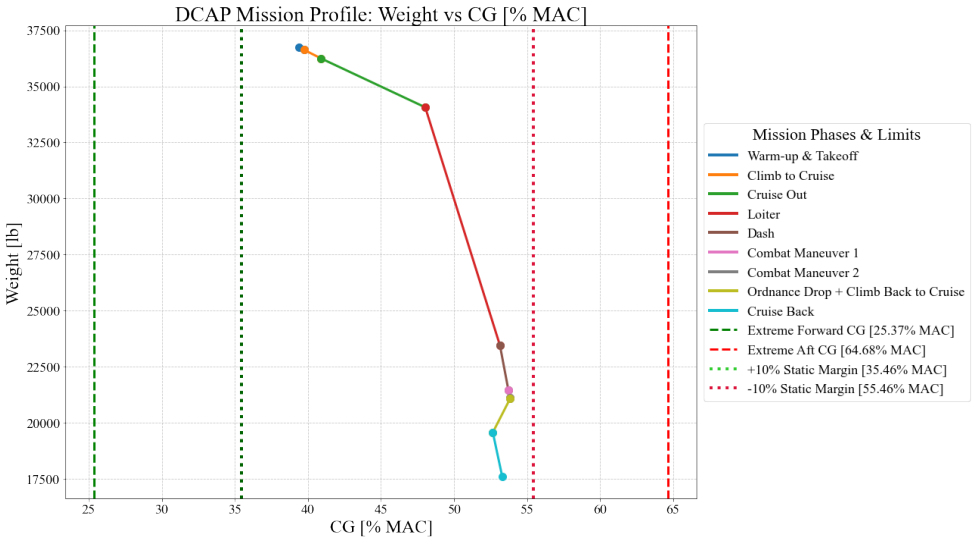

Figure 59. DCAP Mission CG Profile

Table 51. Mission 1 Segment Fuel Burn Log (DCAP)

Mission Segment	**Fuel Tank**	**Fuel Burn [lb]**
Warm-up & Takeoff	Internal Integral 1	126
Climb to Cruise	Internal Integral 1	385
Cruise Out	Internal Integral 1	2,175
Loiter	Internal Integral 1	1,942
	Internal Integral 3	3,416
	Internal Integral 2	4,017
	Conformal Tanks	1,231
Dash	Conformal Tanks	2,009
Combat Maneuver 1	Conformal Tanks	335
Combat Maneuver 2	Conformal Tanks	31
Climb Back to Cruise	Conformal Tanks	203
Cruise Back	Conformal Tanks	1,982
Total Fuel Burned Over Mission		**17,852**
Total Max Static Margin Shift		**14.48%**
Remaining Fuel (Reserves in Conformal Tanks)		**1,070**

2. Point Defense Intercept Mission

Figure 60 plots the CG profile as the Dragonfly burns fuel through each mission segment and accounts for the ordnance drop. Table 52 tracks the fuel consumption path at each mission segment and the location from which tank fuel is drained. For this mission, the Dragonfly unloads fuel in the opposite sequence as it was operationally loaded: internal tank 1, internal tank 3, and internal tank 2. The internal tank 2 does not burn all of the fuel, as the reserves are assumed to be left unburned. The mission profile demonstrates that the Dragonfly remains within the allowable ±10% static margin for the entirety of the mission.

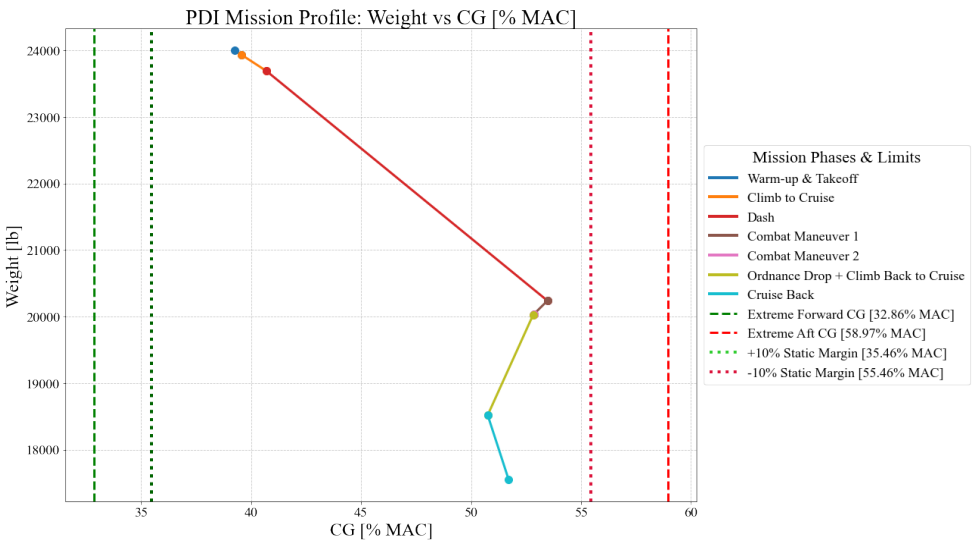

Figure 60. PDI Mission CG Profile

Table 52. Mission 2 Segment Fuel Burn Log (PDI)

Mission Segment	Fuel Tank	Fuel Burn [lb]
Warm-up & Takeoff	Internal Integral 1	71
Climb to Cruise	Internal Integral 1	243
Dash	Internal Integral 1	2,774
	Internal Integral 3	678
Combat Maneuver 1	Internal Integral 3	200
Combat Maneuver 2	Internal Integral 3	14
Climb Back to Cruise	Internal Integral 3	198
Cruise Back	Internal Integral 3	145
	Internal Integral 2	828
Total Fuel Burned Over Mission		**5,151**
Total Max Static Margin Shift		**14.24%**
Remaining Fuel (Reserves in Internal Integral 2)		**1,025**

3. Intercept/Escort Mission

Figures 61,62, 63 plot the CG profile as the Dragonfly burns fuel through each mission segment for the 200 nmi dash, maximum total fuel, and maximum internal fuel variations, respectively. Tables 53, 54, 55 track the fuel consumption path at each mission segment and the location from the tanks being drained for the 200 nmi dash, maximum total fuel, and maximum internal fuel variations, respectively. The IE mission does not include an ordnance drop, and therefore, all missiles remain attached. The three mission variations burn fuel in the opposite sequence as loaded. All CG profiles remain within the required ±10% static margin for the entire IE mission.

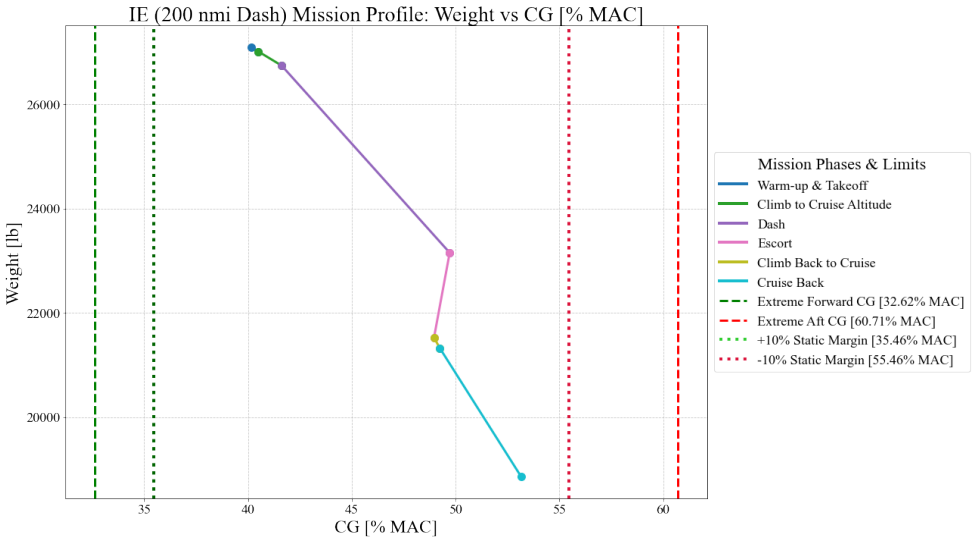

Figure 61. IE (200 nmi Dash) Mission CG Profile

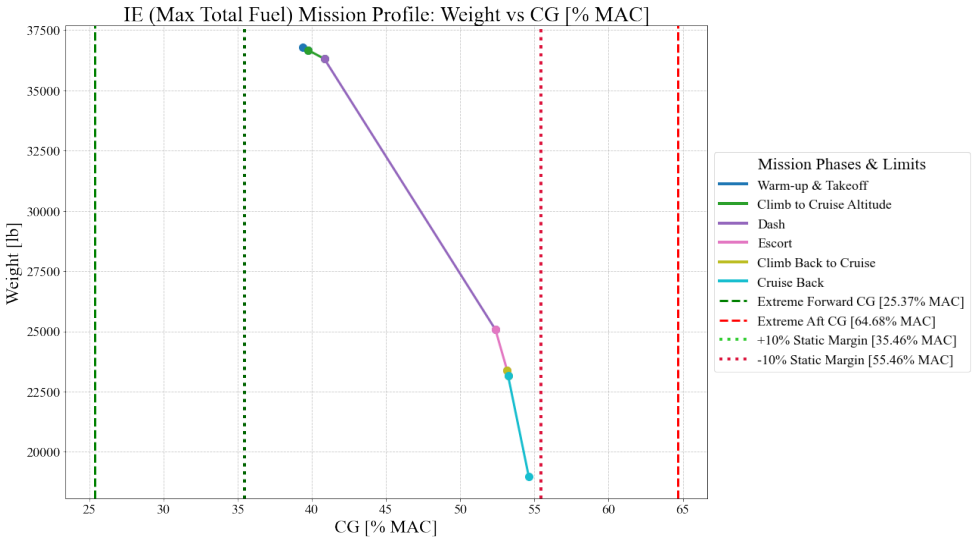

Figure 62. IE (Max Total Fuel) Mission CG Profile

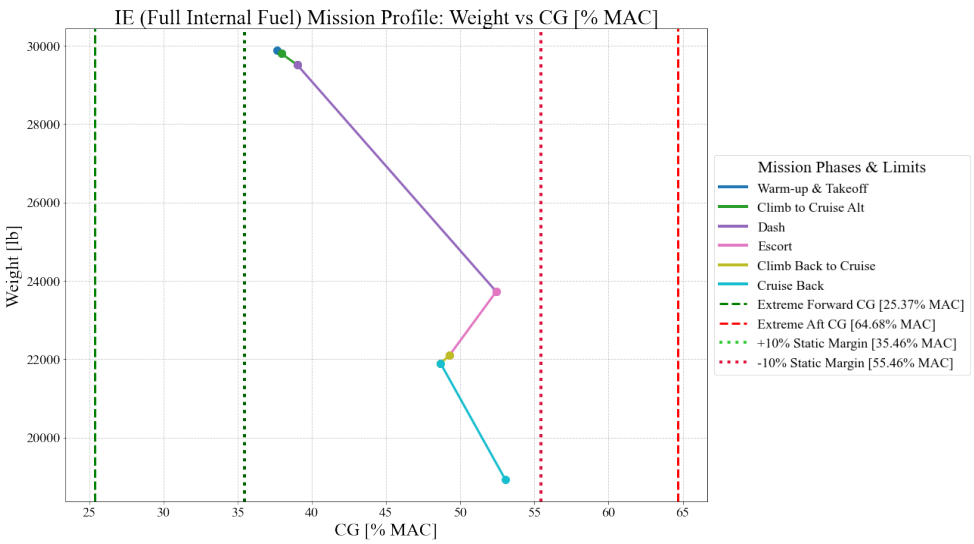

Figure 63. IE (Full Internal Fuel) Mission CG Profile

Table 53. Mission 3 Segment Fuel Burn Log (IE: 200 nmi Dash)

Mission Segment	Fuel Tank	Fuel Burn [lb]
Warm-up & Takeoff	Internal Integral 1	83
Climb to Cruise Altitude	Internal Integral 1	272
Dash	Internal Integral 1	2,425
	Internal Integral 3	1,163
Escort	Internal Integral 3	691
	Internal Integral 2	938
Climb Back to Cruise	Internal Integral 2	205
Cruise Back	Internal Integral 2	2,466
Total Fuel Burned Over Mission		**8,242**
Total Max Static Margin Shift		**13.01%**
Remaining Fuel (Reserves in Internal Integral 2)		**1,026**

Table 54. Mission 3 Segment Fuel Burn Log (IE: Maximum Fuel)

Mission Segment	Fuel Tank	Fuel Burn [lb]
Warm-up & Takeoff	Internal Integral 1	120
Climb to Cruise Altitude	Internal Integral 1	365
Dash	Internal Integral 1	4,142
	Internal Integral 3	3,416
	Internal Integral 2	3,684
Escort	Internal Integral 2	333
	Conformal Tanks	1,369
Climb Back to Cruise	Conformal Tanks	208
Cruise Back	Conformal Tanks	4,200
Total Fuel Burned Over Mission		**17,838**
Total Max Static Margin Shift		**15.25%**
Remaining Fuel (Reserves in Conformal Tanks)		**1,131**

Table 55. Mission 3 Segment Fuel Burn Log (IE: Max Internal Fuel)

Mission Segment	Fuel Tank	Fuel Burn [lb]
Warm-up & Takeoff	Internal Integral 1	90
Climb to Cruise Alt	Internal Integral 1	290
Dash	Internal Integral 1	1,933
	Internal Integral 3	1,708
	Internal Integral 1	2,144
Escort	Internal Integral 1	170
	Internal Integral 3	1,457
Climb Back to Cruise	Internal Integral 3	202
Cruise Back	Internal Integral 3	49
	Internal Integral 2	2,929
Total Fuel Burned Over Mission		**10,972**
Total Max Static Margin Shift		**15.42%**
Remaining Fuel (Reserves in Internal Integral 2)		**1,088**

E. Trade Study

A trade study was conducted to determine the optimal fuel unloading strategy for the Dragonfly. Since the DCAP mission demanded the most fuel and influenced design decisions, it was selected as the basis for this analysis. Three distinct fuel system strategies were evaluated: a basic fixed-order sequence, an intermediate CG-adaptive approach, and an advanced incremental optimization method.

1. Basic Fuel System

The basic fuel system operates on a sequential, fixed-order draining method. As shown in Fig.59, this approach burns fuel from one tank entirely before proceeding to the next. This strategy is simple and requires minimal fuel system complexity. However, it results in a large static margin shift of 14.48%, as the CG movement has a wider range throughout the mission.

2. Intermediate Fuel System

The intermediate fuel system uses a proximity-based strategy to manage fuel consumption. At each mission segment, the fuel system selects tanks to drain based on how close their CG is to the aircraft's current CG, minimizing the CG displacement. To avoid abrupt CG movement, the fuel system will not draw more than 50% of a tank's remaining fuel per burn cycle. By adjusting fuel selection based on CG proximity, this strategy maintains a more linear CG profile compared to the basic fixed-order method by reducing the total static margin shift to 9.68% MAC, as shown in Fig. 64.

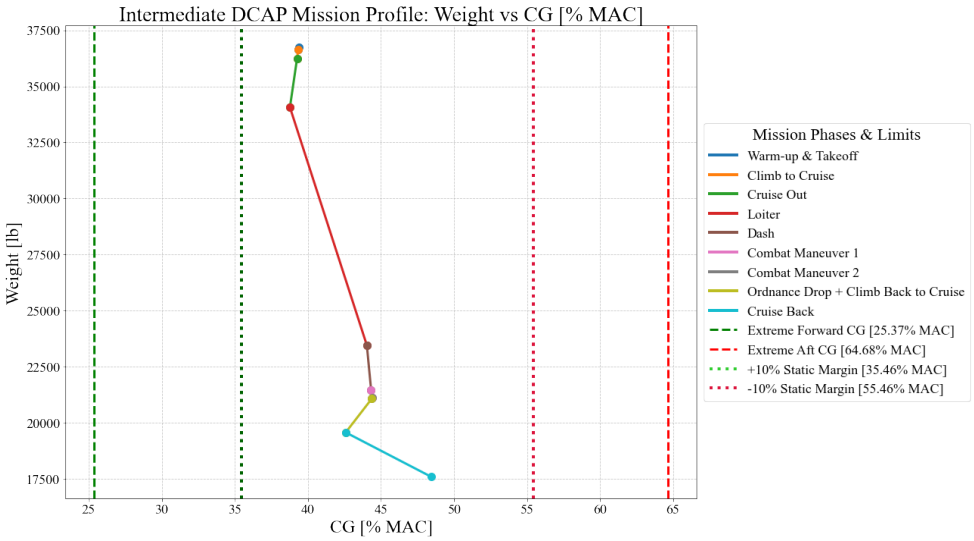

Figure 64. Intermediate Fuel System DCAP Mission CG Profile

3. Advanced Fuel System

The advanced fuel system uses an incremental optimization strategy to minimize CG movement throughout the mission. Instead of relying on proximity or fixed tank order, it evaluates small fuel burns from each tank and simulates the resulting CG shift. The system then selects the tank that results in the smallest deviation from the original CG at maximum takeoff weight (MTOW). Additionally, forward tanks are protected by a minimum reserve level and are not drained until the final phase. By directly targeting minimal CG deviation with every burn, this is the most stable profile, reducing the static margin shift to 7.27% MAC, as shown in Fig.65.

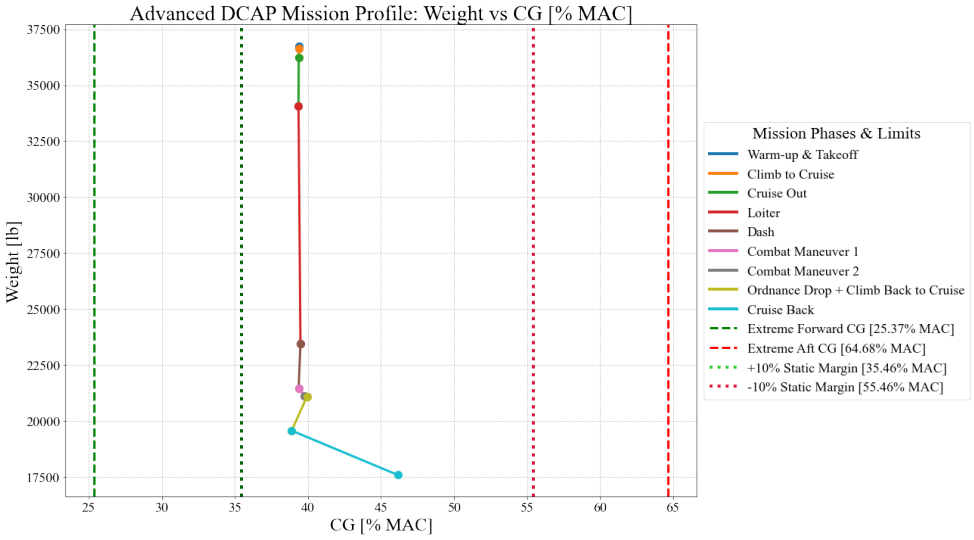

Figure 65. Advanced Fuel System DCAP Mission CG Profile

4. Trade Study Conclusions

Table 56 compares the three fuel management strategies simulated for the DCAP mission. While the advanced fuel system significantly reduced static margin shifts by nearly 50%, its implementation is impractical due to the complexity of continuously executing small incremental burns. In a realistic operation, fuel tanks are not burned all simultaneously in small amounts. In the case of a tank failure, this system would fail to operate as it requires fuel burn from all tanks at the same time. Similarly, the intermediate fuel system provided a noticeable improvement in CG stability, however, it would require additional cost and system complexity, such as advanced sensors or control logic to achieve. This conflicts with the goal of delivering a cost-effective interceptor. Therefore, the fuel system for DCAP is selected to operate at a basic, fixed-order burn sequence. This approach offers simplicity, feasibility, and successfully maintains CG within the required static margin limits throughout the mission.

Table 56. Fuel Burn Strategy Comparison

Fuel System Complexity	Fuel Consumption Logic	Total Static Margin Shift
Basic	Sequential Fixed-Order	14.48%
Intermediate	CG Adaptive (Proximity Ranking)	9.68%
Advanced	Incremental CG Optimization	7.27%

XI. Landing Gear

Dragonfly's landing gear is engineered to optimize weight and space efficiency within the fuselage while effectively accommodating the loads generated during takeoff and landing.

A. Positioning the Landing Gear

Table 57 shows the positions of the landing gear in feet aft of the datum placed at the tip of the nose. These positions are used to evaluate the landing gear geometry in this section. The position of the landing gear was determined from guidelines on landing gear geometry in Raymer Chapter 11 [9]. The positions of the aft and forward C.G. are the operating ranges for the landing gear geometry and are determined later on in this section. Figure 66 shows that the tipback angle is greater than the tailstrike angle and 15°. Figure 67 shows that when Dragonfly is in a five-degree roll at its tailstrike angle, the distance from the wing tip to the ground is greater than six inches. Figure 68 shows that the overturn angle of the Dragonfly is less than 63°. All of these requirements are derived from Raymer [9] and demonstrate that the landing gear geometry is valid.

Table 57. Landing Gear Placement

Main Gear Position	33.83 ft
Nose Gear Position	9.33 ft
Main Gear Offset	5.20 ft
Static Height	6.00 ft

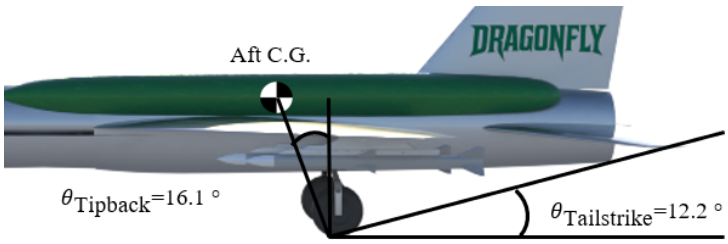

Figure 66. Tipback and Tail-Strike Angle

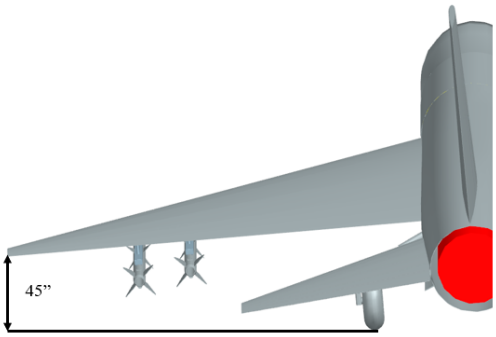

Figure 67. Five Degree Roll

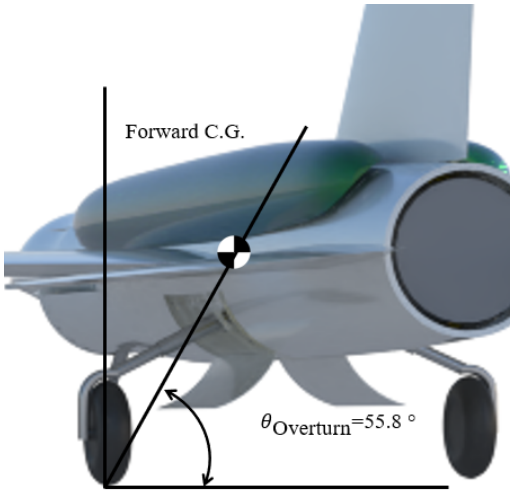

Figure 68. Overturn Angle

Based on the landing gear geometry determined in the previous section, the wheels can be sized. Table 58 lists the constraining landing gear parameters determined from Raymer [9]. The maximum runway speed was determined to be a margin of 1.23 times the stall speed as required by 14 CFR Part 25 §25.103. Additionally, the landing gear loads were increased by seven percent as required by a 14 CFR Part 25 §25.733.

B. Sizing the Tires

The primary factor in wheel selection included ensuring the maximum speed on the runway was below the maximum allowable speed for the tires, verifying that the landing gear loads could be supported by the tires, and selecting a wheel diameter greater than the required braking diameter. Table 58 lists all the constraints required for the tires and wheels, which are all met by the wheel and tire selection as shown in Table 59.

Table 58. Landing Gear Wheel Constraints

Max Runway Speed [ft/s]	246
Max Main Gear Load [lb]	16,200
Max Nose Gear Load [lb]	10,100
Main Tire Inflated Pressure [psi]	125
Nose Tire Inflated Pressure [psi]	150
Main Gear Rolling Radius [in]	10.6
Main Gear Braking Requirement Wheel Diameter [in]	15.2
Nose Gear Braking Requirement Wheel Diameter [in]	15.2
Nose Gear Rolling Radius [in]	10.6
Nose Gear Rolling Radius [in]	10.6
M_f	0.197
M_a	0.071

Table 59. Landing Gear Wheel

	Main Wheel	**Nose Wheel**
Wheel Type	Type VII 36x11	Type VII 30x7.7
Max Speed [mph]	217	230
Max Load [lb]	26,000	16,500
Max Pressure [psi]	235	270
Max Diameter [in]	35.10	29.40
Wheel Diameter [in]	16	16

Figure 69 illustrates the valid center of gravity loading for Dragonfly for dynamically stable landing gear geometry. This plot was created using landing gear geometry considerations outlined in Chapter 11 of Raymer [9].

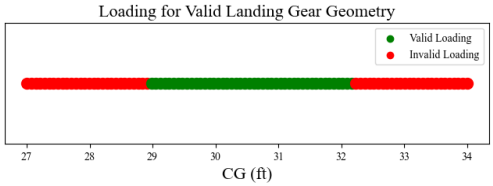

Figure 69. Valid Landing Gear Loading

C. Oleo Sizing

Table 60 tabulates the oleo sizing based on Chapter 11 of Raymer [9].

Table 60. Oleo Sizing

Max Static Load [lbs]	16,200
Max Vertical Landing Velocity [ft/s]	13
Gear Load Factor	3.5
Tire Stroke [in]	0.43
Oleo Stroke [in]	20.43
Oleo Length [in]	51.06
Oleo External Diameter [in]	3.90
Oleo Internal Diameter [in]	3.00
Static Length [in]	33.70

D. Landing Gear Deployment and Retraction System

Figures 70, 71, and 72 show the retracted and deployed positions of the landing gear. The nose gear is stored in a cutout in the inlet. The main gear is stored below the trailing edge of the wing in front of the fuel tanks. The landing gear uses a series of hydraulics for deployment and retraction.

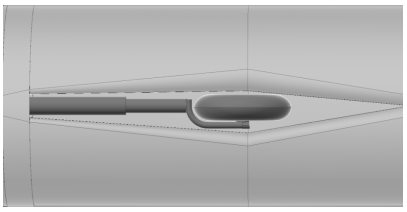

Figure 70. Nose Gear Retracted

Figure 71. Gear Deployed

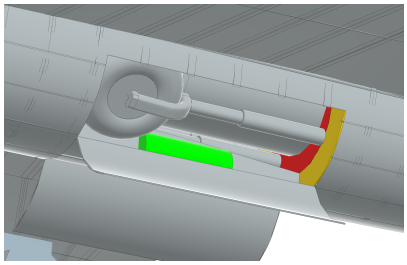

Figure 72. Main Gear Retracted

XII. Systems

The design philosophy for the design of the Dragonfly's systems has two key principles: redundancy and cost. First, redundancy is critical for the aircraft's survivability. For instance, damage to a single hydraulic line should not cause the aircraft to lose control of all control surfaces simultaneously. Second, simplicity is emphasized primarily for cost-effectiveness, but it is also stated in the RFP that the Government Furnished Equipment (GFE) should be used to the maximum extent possible [1]. Because of this requirement, non-GFE systems were only to be utilized if they provided significant benefit to the aircraft in terms of weight, cost, or survivability factors.

A. Flight Controls and Hydraulics

The Dragonfly receives commands from the remote pilot through line-of-sight communication when possible, but it primarily relies on satellite communication when operating beyond line-of-sight range (discussed further in Section XII.E). Once the commands are received from the ground control station, they will be executed using electro-hydraulic actuators.

The Dragonfly's hydraulic system is shown in Fig. 73. All the control surfaces (flaps, slats, ailerons, horizontal stabilizers, and rudder) and landing gear are hydraulically actuated. There are three hydraulic reservoirs, which aid in survivability if one gets damaged, reduce the overall length and weight of hydraulic lines, and improve the system's ability to withstand high g-forces [31]. After leaving the reservoir, hydraulic fluid is pressurized and passed through a filter. A pressure indicator is located downstream of the filter (not shown in Fig. 73). The pressurized hydraulic fluid is then routed to all the actuators via separate feed lines. Military aircraft typically separate individual hydraulic lines in order to increase survivability [31], this is reflected in the aircraft by placing all the lines on separate planes so they cannot all be shot at once (not depicted in the 2D diagram in Fig. 73). The used fluid is then returned to the hydraulic reservoir, completing the cycle. Non-pressurized transfer lines are present to transfer fluid between reservoirs as necessary. In accordance with MIL-HDBK-516C regulations 8.1.1 and 8.1.3, the Dragonfly has a secondary electro-hydraulic backup actuator for each control surface, in case the primary fails. Since the Dragonfly is designed to be more expendable than other fighter jets due to its low cost and remote piloted nature, it was determined that a third actuator is not worth the increase in cost and weight. All the feed and transfer lines also contain shut-off valves (not pictured), so the failure of one system does not affect the others.

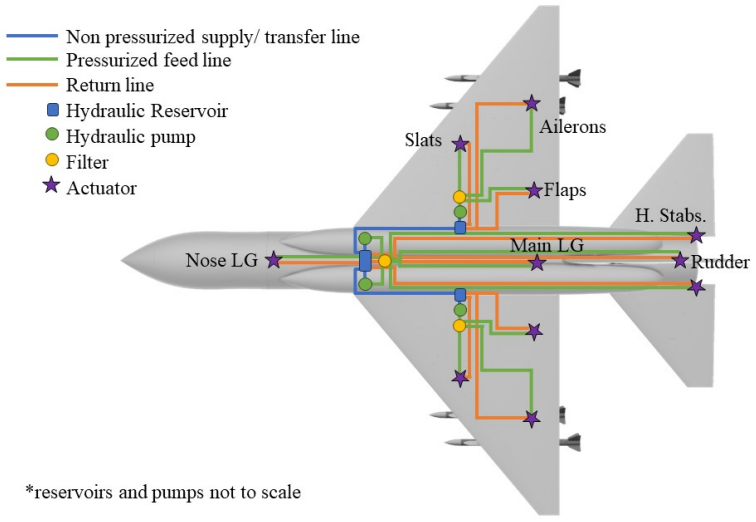

Figure 73. Hydraulic System Layout

B. Fuel System

Since Dragonfly requires significantly more fuel for the DCAP mission than the PDI mission, the decision was made to have removable conformal fuel tanks. The aircraft has five primary fuel tanks shown in Fig. 74: two removable conformal fuel tanks mounted over the wings and three internal tanks, including one that wraps around the engine. All tanks will be self-sealing following the RFP [1] and to increase survivability.

The fuel tanks will be split into two systems (similar to the F-16 configuration [32]) so that failure of one system does not affect the other. Non-pressurized fuel is transferred between tanks as necessary to maintain SM requirements (see Section X.D). Pressure Reducing Valves (PRVs) will be used to maintain the fuel feed sequence via pressure differential, a method typical for fighter aircraft with external tanks [31]. Fuel is pressurized via electrical fuel pumps and then transferred from the forward internal fuel tank (System A) and the central internal fuel tank (System B) to the collector tank. This collector tank feeds into a heat exchanger, then to the engine/ APU. Shut-off valves are installed on the fuel transfer lines between the conformal tanks and internal tanks for when the external tanks are not in use.

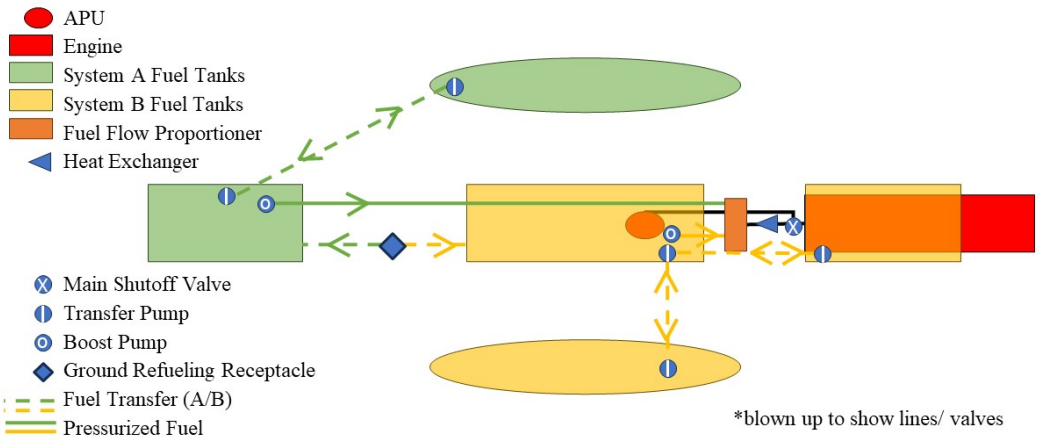

Figure 74. Fuel System Layout

Assuming 14% of the volume of all fuel tanks is being taken up by self-sealing walls and other fuel system components (11% derived from geometric calculations assuming an 11 mm thick wall + 3% for other components), the volume of all fuel tanks is seen in Table 61.

Table 61. Tank Fuel Volumes

Tank	Fuel Volume [lb]
Forward Internal Tank	4,630
Central Internal Tank	4,020
Aft/ Engine Internal Tank	3,410
Combined Conformal Tanks	6,910
Total	**18,970**

C. Electric System

All of the hydraulic actuation of control surfaces, landing gear, and ordnance release is controlled by electric signals. Any hydraulic/ fuel pump motors will also be driven by electrical power. All electronics will use engine-generated power, with the APU serving as a backup. The APU is GFE from the RFP [1]. The GFE APU will be a small turbojet engine responsible for electrical and pneumatic power generation while the aircraft is on the ground. In the event that both the engine and the APU are out, the Dragonfly will revert to using batteries for emergency power. The layout of the electrical system with distinction between AC and DC power is shown in Fig. 75.

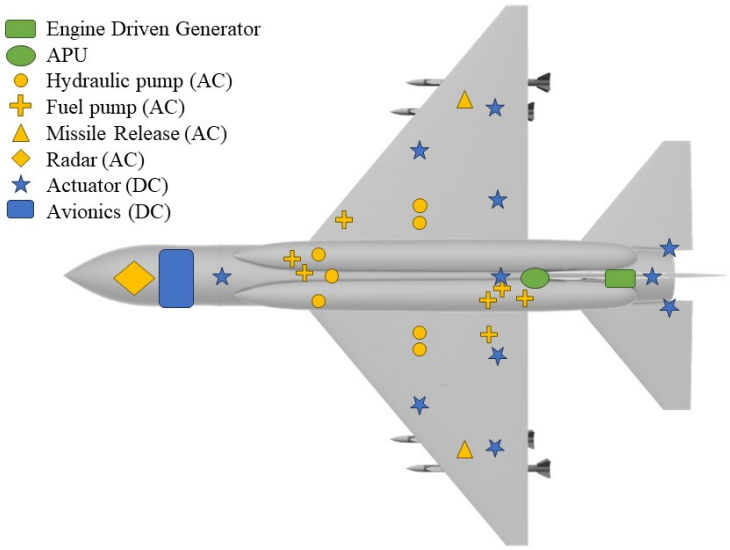

Figure 75. Electric System Layout

All electrical systems for AC and DC were divided into essential and non-essential, as seen in Table 62. Radar is considered nonessential, but it has its own bus. Nonessential AC components are only powered by the main engine generator; essential AC and DC components can be powered by either the main engine generator or the APU. Nonessential DC components receive the same power as the essential DC components, but can be selected on or off. To comply with MIL-HDBK-516C regulation 12.2.5, dual electrical lines will be routed to all electrical power outputs to ensure redundancy.

Table 62. Electrical System Nonessential/ Essential Differentiation

NONESS AC 1	NONESS AC 2	ESS AC 1	ESS AC 2	NONESS DC 1	NONESS DC 2	ESS DC 1	ESS DC 2
-Starboard Missile Release	-Port Missile Release	-System A Fuel Pumps -Starboard Hyd. Pumps	-System B Fuel Pumps - Port Hyd. Pumps	- INEWS	- IRSTS	-Starboard EHA -Nose LG -ICNIA -Cameras	-Port EHA -Main LG -Rudder EHA -VMS

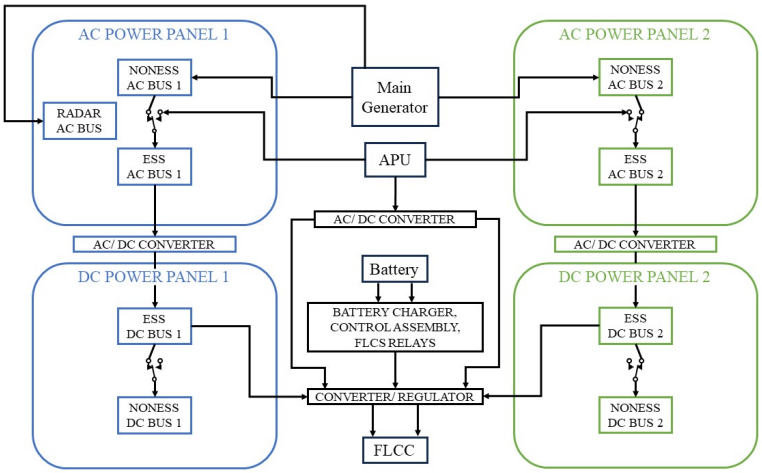

Figure 76. Electric Systems Flow

D. Pneumatics and Environmental Control System

The Dragonfly's pneumatic system distributes bleed air from the engine throughout the aircraft. The bleed air will be used for anti-icing and to pressurize the hydraulic reservoirs to prevent cavitation. The anti-icing schematic is shown in Fig. 77. Hot bleed air is routed along the leading edge of the wing and the engine inlet to prevent buildup. This was included to fulfill the RFP's "all-weather" requirement [1]. Following MIL-HDBK-516C regulation 8.2.12, bleed air shut-offs are located just forward of the engine.

The avionics are cooled using ambient air that enters through a small inlet, located between the radar and the rest of the avionics. This air passes through a heat exchanger before circulating to the avionics and radar components. This configuration, similar to that used in the MQ-9 and MQ-25, minimizes bleed air ducting, which is an advantageous approach for unmanned aircraft that do not require any sort of cabin pressurization.

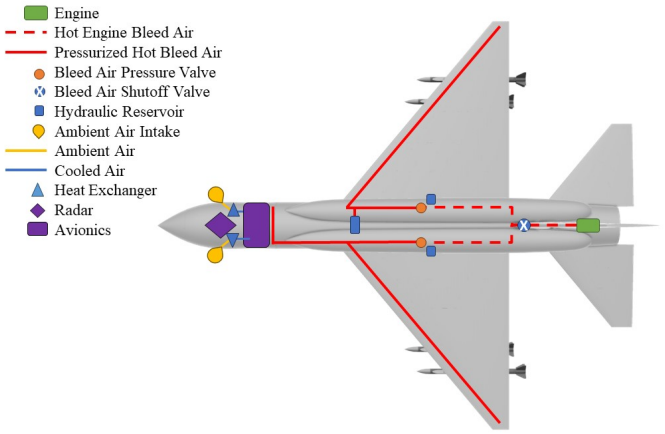

Figure 77. ECS and Pneumatic System Layout

E. Avionics

1. Avionics Selection

As with the rest of the Dragonfly's systems, the approach to avionics was to use as much GFE as possible. Additionally, using an integrated avionics system instead of standalone items results in a reduction of space, weight, power, and cooling requirements along with an increase in reliability and maintainability [33]. The expected capabilities of the GFE avionics are outlined in Table 63. The Northrop Grumman AN/APG-83 Scalable Agile Beam Radar was selected because it is the less expensive variant of what is found on the F-22 and F-35 [34]. Its scalable design also makes it more compatible with the Dragonfly. Additional cameras were also added to support remote piloting.

Table 63. Avionics Size, Cost, Weight, and Capabilities

Avionics	Volume [ft^3]	Weight [lb]	Cost [K$]	Required Capabilities/ Selection Notes
ICNIA	3.0	100	200	See section XII.E.2
Data Bus	0.5	10	10	Must meet MIL-STD-1553
INEWS	3.0	100	500	Signals Intelligence Electronic Surveillance ≥ 20 Threats Tracked Radar/ Comm. Jamming Enemy Radar Warning ≤ 90 dBm Detection Sensitivity Compatible with Chaffs/ Flares ≤ 100 ms Threat Reaction Time
Vehicle Management System	1.0	50	200	Receive pilot/ autopilot inputs Send Commands to Actuators Coordinate All Subsystems Health Monitoring & Shutdowns Autonomous Capabilities
IRSTS	2.0	50	200	Heat Signature Detection ≥ 160 mi Detection Range ≥ 10 Targets Tracked
Active Array Radar	6.0	450	1,000	Northrop Grumman AN/APG-83 SABR
Cameras	0.32	15	350	L3Harris WESCAM MX-8

2. Communications/ Level of Autonomy

The Dragonfly will use a communication architecture similar to the MQ-9 Reaper. Line-of-sight (LOS) communication will be used whenever possible with a combination of L-band, S-band, and C-band frequencies depending on the range and mission requirements. LOS communication effectiveness varies by altitude, but is limited by terrain and the curvature of the Earth. When LOS communication is not feasible, the Dragonfly will rely on satellite communications (SATCOM). The MQ-9 Reaper upgraded its SATCOM system in 2023, doubling the bandwidth and decreasing latency by a factor of 10 [35], so the Dragonfly will incorporate this newly updated system. Using the Reaper's preexisting SATCOM system will also decrease cost. The Tactical Data Link (TDL) that the Dragonfly will use is Link 16, supplemented by Ku-Band datalink. Link 16 was selected because of its standardized use and proven reliability.

In line with the aircraft's philosophy of being low-cost and simple. The Dragonfly's autonomous capabilities are limited to being able to maintain altitude, speed, and heading, as well as waypoint navigation. These autonomous capabilities enable the Dragonfly to self-terminate if necessary. In the event of communication loss, the Dragonfly will either return to the nearest GCS or navigate to a designated crash site if the situation dictates. The Dragonfly will not be capable of autonomous missile release as required by the DoD Directive 3000.09. According to this regulation, autonomous and semi-autonomous weapon systems should be designed to allow commanders and operators to exercise human judgment over the use of force. The Dragonfly is designed to ensure that the remote pilot has full control over weapon release decisions.

XIII. Cost Analysis

A comprehensive cost analysis was completed to ensure the Dragonfly met the financial requirements of $25 million per unit for a production run of 1,000 aircraft. The analysis includes research, development, test, and evaluation (RDT&E), flyaway production, and long-term operating costs, calculated using historical data and the DAPCA IV cost model from Raymer. Throughout the design process, cost was prioritized over other factors, such as structural complexity, material selection, and payload capacity, to ensure the final design aligns with the overall objective of delivering a high-performance yet cost-effective aircraft.

A. Research/ Development/ Test/ Evaluation, Flyaway, and Unit Cost

The DAPCA IV model calculates the flyaway and RDT&E costs based on the total hours required for engineering, tooling, manufacturing, and quality control. The cost for each process is determined by multiplying the respective labor hours by the associated cost rates. The cost rates provided by Raymer are calibrated to 2012 and must be adjusted to 2024 dollars to account for inflation. An inflation rate of 1.36% was assumed for this conversion. Table 64 displays the breakdown for the RDT&E and flyaway costs.

Table 64. Flyaway Cost per Unit Buildup (1,000 Aircraft Purchase)

Category	Cost [Million]	% of Total
Avionics	$3.73	14.9%
Engine	$7.20	28.8%
Manufacturing Materials	$0.09	0.4%
Quality Control	$1.16	4.6%
Manufacturing Labor	$7.92	31.7%
Engineering Labor	$2.43	9.8%
Tooling Labor	$1.59	6.4%
Flight Test	$0.43	1.7%
Development Support Cost	$0.42	1.7%
Total Cost per Unit:	**$24.97**	
Total Cost for 1,000 Units:	**$24,970**	

The unit cost per aircraft for 1,000 units, as shown in Table 64, is $24.97 million. A cost trade of 100, 500, and 1,000 units is shown in Table 65 for comparison.

Table 65. Production Quantity Comparison

Production Quantity	Cost per Unit [Million]	Total Cost [Million]
100	$65.69	$6,569
500	$31.36	$15,680
1,000	$24.97	$24,970

B. Direct Operating Cost

Direct operating costs were also calculated using the DAPCA IV model for a production run of 1,000 aircraft. The operating costs account for the fuel and crew required for missions, as well as maintenance, vehicle depreciation, and insurance expenses. 100 flight hours per year over 20 years of service were used to determine maintenance, crew, and fuel costs. Although current fighter aircraft may exceed 100 flight hours in a given year, pilots operating the Dragonfly can train using simulators. Therefore, the Dragonfly is only flown during operations or after sitting idle for too long.

Since the interceptor is a remotely piloted aircraft, the infrastructure and controls for the vehicle must also be included in the operating costs. Such infrastructure is comprised of the Ground Control Station, Satellite Communications Terminal, and other support equipment. In a 2016 Congressional Research Service report, a package of four MQ-1 Predators and one Ground Control Station cost a total of $20 million [36]. At $4.5 million for each MQ-1, the Ground Control Station cost equates to $2 million. Considering inflation, a 2024 Ground Control Station cost $2.52 million. A similar implementation can be used for the homeland defense interceptor.

Table 66 displays the breakdown of the operating costs per unit for the production of 1,000 aircraft. The total life cycle cost of a single unit is also displayed in Table 67 as the sum of the operating and flyaway costs.

Table 66. Operations, Maintenance, Spares, and Infrastructure (OMSI) per Unit per Life Cycle

Category	Cost [Million]	% of Total O&M
Fuel	$9.38	12.96%
Crew Cost	$5.65	7.81%
Maintenance Total	$26.82	37.08%
Spares	$2.50	3.46%
Infrastructure	$2.52	3.48%
Flyaway	$24.97	34.53%
Total O&M Cost	**$72.34**	**100%**

Table 67. Life Cycle Cost

Category	Cost [Million]	% of Life Cycle
O&M Cost	$69.82	73.7%
Flyaway	$24.97	26.3%
Total Life Cycle Cost	**$94.79**	**100%**

C. Cost Reduction Methods

The primary objective for cost management in the design and development of this aircraft is to minimize total life cycle costs. This encompasses both flyaway and operational costs of the aircraft. Several approaches can be taken to reduce these costs without compromising the aircraft's performance or mission capabilities.

An effective way to reduce overall costs is to increase the production quantities of the aircraft over a specified period of time. As shown in Table 65, larger production runs result in a significant reduction in the unit price of each aircraft. This is mainly due to learning curve effects and bulk procurement of material and parts. The longer a manufacturer produces and particular design, the faster the aircraft can be built and with fewer errors. This method can help reduce per-unit costs and make the overall acquisition more affordable for the operator.

Another way to decrease costs would be to downsize the engine. The engine is the main driver in the Dragonfly's cost. If performance requirements are able to met, and data indicate that the engine is oversized, a cheaper engine can be implemented to further reduce costs.

The material selection for the aircraft can also be adjusted to minimize flyaway costs. Material and design adjustment factors are used to determine the overall flyaway cost of a unit. If a cheaper material can be used with minimal performance loss, the cost can be further reduced.

D. Model Uncertainties

Although the DAPCA IV model is notable for providing reasonable results for most classes of aircraft, it may not be the best model for one specific class. All cost models include some uncertainties and inaccuracies in calculations. A primary uncertainty in the DAPCA IV model includes the assumptions for the operational cost breakdown. Factors such as the exact number of flight hours, crew salaries, and maintenance required for each aircraft remain unknown while in development. These assumptions make it more difficult to accurately calculate the total life cycle costs of the aircraft.

Furthermore, Raymer's use of 2012 hourly rates for labor and other cost factors introduces potential inaccuracies when attempting to calibrate for 2024 costs. The inflation rate is assumed to be constant, but in reality, inflation is not linear and can fluctuate based on a variety of economic factors.

Lastly, the model does account for production or technical delays that might arise during the development of the aircraft. New technologies and designs can also significantly alter cost predictions and design changes.

XIV. Ordnance

One of the major roles of the Dragonfly is the transport of ordnance to the battlespace. As such, a trade study was conducted to determine the quantity of AIM-120 AMRAAM missiles to carry, and if a gun would add sufficient benefit to justify its costs, weights, and implementation concerns.

A. AIM-120 AMRAAM

1. Missile Quantity

In order to determine the number of AIM-120 missiles reasonable for an aircraft of the Dragonfly's class to carry into the modern battlespace, a survey of common missile load-outs on existing aircraft was conducted. It was decided

that four AIM-120 AMRAAMs, whose dimensions are labeled in Table 68, will serve as the primary air-to-air armament of the interceptor. AMRAAMs were selected not only as a requirement per the RFP, but also because they are included in the government-furnished equipment, making them a cost-effective design choice. While only one AMRAAM is sufficient to meet mission requirements, carrying additional missiles ensures redundancy and significantly enhances mission success rates without compromising cost-effectiveness and overall weight of the aircraft. Furthermore, four missiles allow missions to be completed with fewer units, saving operational costs and vehicle liability. If the interceptor was only equipped with one or two AMRAAMs, it is likely that one or more additional units would be required to ensure mission success.

Table 68. AIM-120 AMRAAM Specifications

Parameter	Value
Launch Weight	327 lb
Length	12 ft
Max Span	2.1 ft
Body Diameter	0.6 ft

2. Missile Placement

With limited internal fuselage space, the missiles will be mounted externally on missile rail launchers beneath the wings. The outer missiles are located 16 feet from the centerline of the aircraft, while the inner missiles are located at 13.6 feet. These placements align with adequate structural support between the ribs of the wing and provide sufficient spacing between the missile rail launchers for safe, unobstructed missile release. The missile placement adheres to the stores clearance regulations set by MIL-HDBK-516C 17.2.1, ensuring safe conditions during ground and flight operations and a safe environment for maintenance personnel. LAU-129 rail launchers will be mounted onto the hardpoints at these locations under the wing, and the missiles will be loaded onto the launchers. LAU-129 missile rail launchers were chosen for their proven compatibility with AIM-120 AMRAAMs, as well as their quick and simple release mechanisms. Additionally, the missile launchers include emergency drop capabilities if necessary. Each pylon hardpoint location must be capable of supporting the missile weight at a load factor of 7-g's, per the structural load limit. With a missile weight of 327 pounds, the hardpoints must be capable of supporting 1,635 pounds of force during combat maneuvers. The use of LAU-129 launchers meets the standards in MIL-HDBK-516C section 17.2.2 because safe separation is achieved.

B. M61A1 Vulcan

A cannon like the M61A1 Vulcan was also evaluated for potential inclusion in the Dragonfly's armament. Historically, guns played a dominant role in air-to-air combat, with over 60% of kills attributed to guns in 1965. However, by 2002, this figure had dropped below 5%, while beyond-visual-range (BVR) air-to-air missiles accounted for over 50% of aerial

victories, with short-range missiles and other factors making up the remainder [37]. These trends reflect significant advancements in radar, sensors, and missile technology, which have largely eliminated the need for visual-range engagements in modern aerial warfare.

Anecdotal evidence indicates that shooting down cruise missiles with guns is very difficult [38]. This is made harder once one considers that entering the range to shoot down a flying explosive with a gun can endanger the engaging interceptor, should the flying explosive go off. As such, the viability of guns against cruise missiles seems negligible. From a review of the M61A1 Vulcan's historical utility and modern viability, it can be deduced that it presents little to no additional value for the Dragonfly and so was excluded from armaments.

XV. Survivability

When deciding which survivability and low observability features to implement on the Dragonfly, several considerations were made. First, the aircraft is designed as a homeland defense interceptor, as outlined in the RFP, meaning the most likely combat scenario involves flying from the mainland to intercept an incoming threat. As such, reducing frontal observability was prioritized. Second, the RFP contains minimal survivability requirements, so any potential design choices had to be weighed against more demanding constraints from other disciplines, particularly those impacting weight, cost, or performance. As a result, the selected survivability and observability measures aim to keep the Dragonfly simple and cost-effective, while still providing meaningful protection.

A. Radar Cross-Section Reduction

A study by Chen et al. [39] investigated the effect of leading-edge sweep on aircraft radar cross section and found that increasing sweep angle significantly reduced frontal RCS. In particular, a sweep angle of 39° reduced the frontal signature to around five dBsm, down from an initial, straight wing value exceeding 20 dBsm. Based on open-source estimates, a conventional 4th-generation fighter such as the F-16 exhibits a frontal RCS of approximately ten dBsm. With the Dragonfly's 40° leading-edge sweep, a similar reduction to around five dBsm is expected. Incorporating an S-shaped inlet to obscure the engine fan face—a known high-reflectivity surface—can reduce frontal RCS by an additional 10–16 dB [40]. As a result, the Dragonfly's estimated frontal RCS may approach 0 dBsm. While this does not meet the threshold for true stealth aircraft (typically around –20 dBsm [40]), the design provides meaningful observability reduction appropriate for a homeland defense interceptor. Figure 78 shows the difference in height between the inlet entrance and the fan face of the engine. Additional analysis would have to be made to incorporate the effect of the inlet's wedge on the Dragonfly's RCS.

Radar-absorbing material (RAM) coatings were considered but ultimately excluded from the design due to their significant cost and maintenance burdens, which conflict with the Dragonfly's emphasis on simplicity and affordability. RAM coatings can cost approximately $ 1,000 per gallon [41] and require up to 1,500 man-hours to apply per aircraft

[42], representing a substantial investment in both materials and labor. Additionally, aircraft coated with RAM must often be s d in specialized, climate-controlled hangars to preserve the integrity of the coating—facilities that can cost upwards of $5 million, as seen with the B-2 bomber [43]. Beyond the logistical challenges, RAM coatings primarily offer broad-spectrum RCS reduction, which is more critical for stealth aircraft. In contrast, this aircraft is designed as a homeland defense interceptor, where reducing frontal radar cross-section is the priority. As such, stealth in this design is achieved primarily through shaping features, such as leading-edge sweep and internal inlet design, rather than through maintenance-intensive coatings.

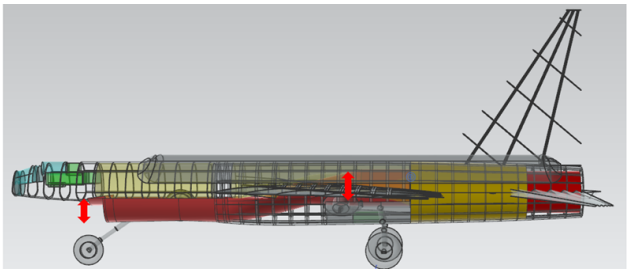

Figure 78. Inlet geometry showing no direct line of sight to the engine fan face

B. Flares and Chaffs

To enhance survivability against radar-guided and infrared threats, an optional rear-fuselage countermeasure dispenser can be integrated into the Dragonfly's design. Utilizing systems like the AN/ALE-47 or M130, which are common on similar fighters [44], these dispensers can deploy chaff and flares to confuse incoming missiles. The rear placement was determined through similarity analysis and ensures coverage of the aircraft's vulnerable aft sector without occupying weapon hardpoints or compromising aerodynamic performance. This modular approach allows end-users to equip the system based on specific mission requirements and threat assessments. The M130 can be adapted with aerodynamic housings designed to reduce drag, as demonstrated in prior system configurations and patents [45].

XVI. Repair and Maintenance

Effective repair and maintenance planning is a critical aspect of aircraft design, particularly for cost-sensitive, high maneuverability aircraft like the Dragonfly. Ensuring maintainability not only reduces life cycle costs but also enhances mission readiness by minimizing downtime. By integrating structured maintenance schedules and strategically placing service hatches for key systems, the Dragonfly can achieve both regulatory compliance and operational efficiency. These features directly support and satisfy the standards in MIL-HDBK-516C Chapter 16 requirements regarding servicing instructions, removal procedures, non-destructive inspections, special inspection procedures, and life-limited parts.

A. Maintenance Approach

The main set of checks that the aircraft will go through includes the pre-flight check, A check, B check, C check, and D check. The pre-flight check will occur before every flight and will consist of a visual check of the aircraft and a general check of the systems and engines. The occurrence of the A, B, C, and D checks will revolve around the design service life of 2,000 flight hours. The A check is the minor inspection which consists of a basic systems check, diagnosing the avionics, lubrication of bearings and gears, and replacement of minor components. This would occur every 50 FH, or every month. Using Raymer's table for MMH/FH, the MMH required for this check is predicted to range from 500 to 750 MMH. The B check is the intermediate inspection and consists of testing of hydraulics and control surfaces, a detailed engine system check, such as the fuel pumps or the afterburner, and fatigue and wear testing. This would occur every 300 FH, or every six months. The MMH required would range from 3,000 to 4,500 MMH. The C check is the major inspection of the aircraft and would mainly consist of Non-Destructive Testing (NDT), engine tear down and rebuild, and subsystem overhaul. This would occur every 1,000 FH, or annually. The MMH required would range from 10,000 to 15,000 MMH. Lastly, the D check would be a total overhaul, and the aircraft would be torn down for maintenance. There will be a replacement of main aircraft components, deep structural inspections, and full avionics and propulsion system refurbishments. This would occur every 2,000 FH, or every four years, and the required MMH would range from 20,000 to 30,000 MMH. The summary of the maintenance checks are as shown below in Table 69.

Table 69. Maintenance Schedule

Check	Interval	MMH Required	Maintenance Tasks
Pre-flight	Every flight	N/A	Light check of engines and systems
A	50 FH / 1 Month	500 - 750	Basic system check, replacement of minor components
B	300 FH / 6 Months	3,000 - 4,500	Detailed engine system check, fatigue and wear testing
C	1,000 FH / 1 Year	10,000 - 15,000	Major inspection, NDT, subsystem overhaul
D	2,000 FH / 4 Years	20,000 - 30,000	Total overhaul, main components replacement

B. Repair Hatches

When repairing the aircraft, strategically placed access hatches are required and help facilitate efficient maintenance and repair operations by allowing ground crews to service critical components without extensive disassembly. Service hatches should be located near key systems and components that require frequent inspection or replacement. Some possible key locations include the forward fuselage for avionics and radar maintenance, the wing roots for hydraulic and fuel system access, and the fuel tanks for inspection of leakage or maintenance. A diagram of the possible service hatch locations is shown in Fig. 79.

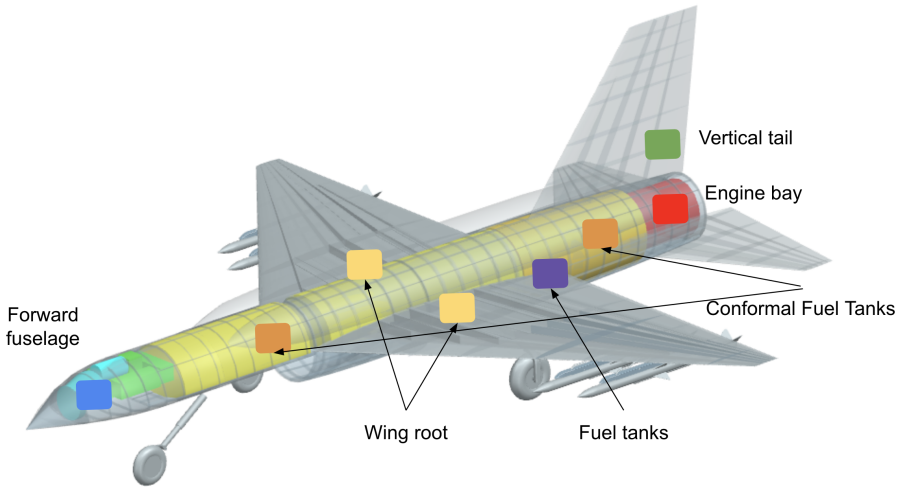

Figure 79. Service Hatches Location

C. Conformal Tanks

The Dragonfly will be using conformal fuel tanks to ensure that enough fuel to complete mission 1. The CFTs are mounted along the upper fuselage spine, extending from the mid-forward section to just ahead of the vertical stabilizer. Using information on the CFT used in the F-16 Block 50/52/60 variants and CAD calculations, the different weights are as shown in Table 70.

Table 70. Weight Data Per Each Conformal Fuel Tank

Tank Volume	Empty Weight	Fuel Weight	Total Weight
598 gallons	210 lbs	3,455 lbs	3,665 lbs

To allow for the CFTs to be securely placed and removed for the different missions, mechanical fasteners such as bolts, screws, and rivets will be used. Mechanical fasteners were chosen as they provide a rigid, load-bearing connection to ensure that the tanks can withstand the high loads and high speeds during flights. Unlike clamps or adhesives, mechanical fasteners help distribute stress across hard points, decreasing the possibility of failure. Another benefit is the simplicity of repair and inspection. Fasteners can be easily inspected for wear, corrosion, and fatigue using non-destructive methods, which also decreases the possibility of failure. However, one main drawback of using mechanical fasteners is the costly and excessive maintenance. Installation of the CFTs may be labor-intensive as bolts often require a secondary locking mechanism such as safety wire or locking washers. In addition, cranes will be required to install and remove the conformal fuel tanks (CFTs). With an empty mass exceeding typical manual handling limits and a fuselage mounting height of approximately 6 ft, mechanical lifting equipment is necessary for safe and efficient installation. Figure 80 shows an ISO-view and a side view of a 5 ft 9 in human standing adjacent to the aircraft for scale.

This visual comparison highlights the significant size and elevation of the CFTs, reinforcing the requirement for external lifting support during maintenance or reconfiguration operations.

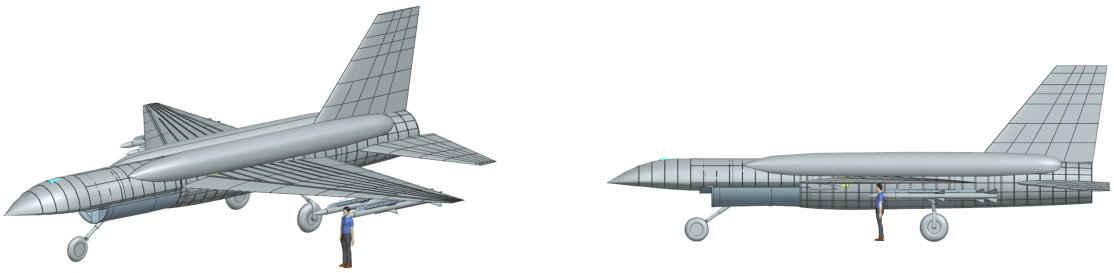

(a) Iso View **(b) Side View**

Figure 80. Human Scale Comparison for Conformal Tank Installation

XVII. Conclusions

Following the tragic September 11th attacks, the United States continues to search for a high-performance yet affordable homeland defense option that does not draw funds away from offensive forces. The QF-49 Dragonfly fulfills this gap in the market with a simple yet effective design, coming in at $24.97 million. The Dragonfly has removable conformal tanks which allow it to perform a variety of missions and meet all performance criteria, including an 18.0 deg/s instantaneous turn rate and Mach 1.6 dash speed set by the AIAA RFP [1]. Since the Dragonfly is remotely piloted and low-cost, it is an ideal first-line-of-defense fighter to minimize losses of more expensive aircraft.

References

[1] "Homeland Defense Interceptor Request for Proposal," Tech. rep., AIAA Undergraduate Design Team Project, 2025.

[2] "F-22 Raptor," U.S. Air Force, 2025. URL https://www.af.mil/About-Us/Fact-Sheets/Display/Article/104506/f-22-raptor/, [cited 9 March 2025].

[3] Decker, A., "F-35's price might rise, Lockheed warns," Defense One, 2024. URL https://www.defenseone.com/business/2024/07/raytheon-hunting-another-us-supplier-solid-rocket-motors/398263/, [cited 9 March 2025].

[4] Taylor, J. W. R., *Jane's All The World's Aircraft*, Sampson Low, Marston and Company LTD, London, 1963.

[5] Taylor, J. W. R., *Jane's All The World's Aircraft*, Sampson Low, Marston and Company LTD, London, 1977.

[6] "Turbojet Aircraft Engine R-15," Aviaru.rf, 2025. URL http://xn--80aafy5bs.xn--p1ai/aviamuseum/dvigateli-i-vooruzhenie/aviamotorostroenie/aviamotory-sssr/turboreaktivnye/turboreaktivnyj-aviatsionnyj-dvigatel-r-15/, [cited 15 November 2024].

[7] "F-16 Fighting Falcon," U.S. Air Force, 2025. URL https://www.af.mil/About-Us/Fact-Sheets/Display/Article/104505/f-16-fighting-falcon/, [cited 1 March 2025].

[8] "F-106A Delta Dart," Museum of Aviation, 2016. URL https://museumofaviation.org/portfolio/f-106-delta-dart/, [cited 4 May 2025].

[9] Raymer, D., *Aircraft Design: A Conceptual Approach*, 6th ed., AIAA, Reston, Virgina, 2018.

[10] Chan, N. Y. S., "Scaling Considerations for Small Aircraft Engines," M.s. thesis, Massachusetts Institute of Technology, June 2008. URL https://core.ac.uk/reader/4409730.

[11] GE Aerospace, "GE Aviation Awarded $707 Million F110 Engine Production Contract," 2022. URL https://www.geaerospace.com/news/press-releases/defense-engines/ge-aviation-awarded-707-million-f110-engine-production.

[12] Nicolai, L., and Carichner, G., *Fundamentals of Aircraft and Airship Design, Volume 1 - Aircraft Design*, 5th ed., AIAA, 2010.

[13] NASA, "Design and performance study of a parametric diverterless supersonic inlet," 2022.

[14] Jung-Ho Park, S.-O. P., Dae-Cheol Kim, "RCS Analysis of the Jet Engine Inlet using the Physical Optics Method," Tech. rep., 2002. URL https://citeseerx.ist.psu.edu/document?doi=c47e242c24c03e2d6e9248dbf421313b07368f26.

[15] Hehs, E., "JSF Diverterless Supersonic Inlet," *Code One Magazine*, 2000. URL https://www.codeonemagazine.com/article.html?item_id=58.

[16] GlobalSecurity.org, "Diverterless Supersonic Inlet (DSI)," 2024. URL https://www.globalsecurity.org/military/systems/aircraft/dsi.htm.

[17] IPCC/GRIDA, "Aircraft engine efficiency and emissions," https://www.grida.no/climate/ipcc/aviation/097.htm, 1999. Accessed May 2025.

[18] Lednicer, D., "The Incomplete Guide to Airfoil Usage," UIUC Applied Aerodynamics Guide, 2025. URL https://m-selig.ae.illinois.edu/ads/aircraft.html, [cited 9 February 2025].

[19] James A Weiberg, R. E. D., "Section Characteristics of an NACA 0006 Airfoil with Area Suction near the Leading Edge," Tech. rep., National Advisory Committee for Aeronautics, 1954. URL https://ntrs.nasa.gov/citations/19930083969.

[20] Torenbeek, E., *Advanced Aircraft Design: Conceptual Design, Technlogy, and Optimization of Subsonic Civil Airplanes*, John Wiley Sons Incorporated, 2013.

[21] Bernard Etkin, L. D. R., *Dynamics of Flight: Stability and Control*, John Wiley Sons Inc., 1995.

[22] Roskam, J., "Airplane Design Part V: Component Weight Estimation," Design, Analysis and Research Corporation (DARcorporation), Lawrence, Kansas, 2018.

[23] Bruhn, E. F., "Analysis and Design of Flight Vehicle Structures," Tri-state Offset Company, 1973.

[24] Staley, J. T., and Lege, D. J., "Advances in aluminium alloy products for structural applications in transportation," *Journal de Physique. 4*, Vol. 3, No. 7,pt.1, 2025.

[25] Figge, F. A., and Bernhardt, L., "Air Superiority Fighter Wing Structure Design For Improved Cost, Weight, and Integrity," 1975.

[26] "MatWeb: Online Materials Information Resource," MatWeb LLC, 2025. URL `https://www.matweb.com`, [cited 9 February 2025].

[27] Roskam, J., *Airplane Design Part III: Layout Design of Cockpit, Fuselage, Wing and Empennage: Cutaways and Inboard Profiles*, Design, Analysis and Research Corporation (DARcorporation), Lawrence, Kansas, 1986.

[28] Megson, T., *Aircraft Structures for Engineering Students, 5th ed.*, Elsevier Ltd., Massachusetts, 2013.

[29] Howe, D., *Aircraft Loading and Structural Layout*, Professional Engineering Publishing Limited, London and Bury St Edmunds, UK, 2004.

[30] *DesignLife Theory Guide*, GlyphWorks, 2013.

[31] Moir, I., and Seabridge, A., *Aircraft Systems*, John Wiley & Sons Ltd, 2008.

[32] Corporation, L. M., "F-16A/B Flight Manual," Tech. rep., United States Air Force, 2003.

[33] Camana, P., "Integrated communications, navigation, identification avionics (ICNIA)-the next generation," *IEEE Aerospace and Electronic Systems Magazine*, 1988.

[34] "AN/APG-83 Scalable Agile Beam Radar (SABR)," Tech. rep., Northrop Grumman, 2025. URL `https://www.northropgrumman.com/what-we-do/air/sabr-scalable-agile-beam-radar-apg-83-aesa`.

[35] "AATC tests enhanced intelligence gathering capabilities with MQ-9 Reaper upgrade," Tech. rep., US Air Force, 2023. URL `https://www.af.mil/News/Article-Display/Article/3406025/aatc-tests-enhanced-intelligence-gathering-capabilities-with-mq-9-reaper-upgrade/`.

[36] Congressional Research Service, "Veterans' Benefits: The Impact of Military Service on Social Security," Tech. Rep. R42136, Congressional Research Service, 2024. URL `https://crsreports.congress.gov/product/pdf/R/R42136`, accessed: March 10, 2025.

[37] STILLION, J., "Trends in Air-to-Air Combat: Implications for Future Air Superiority," Tech. rep., Center for Strategic and Budgetary Assessments, 2015.

[38] Nicholls, D. J., *Cruise Missiles and Modern War Strategic and Technological Implications*, Center for Strategy and Technology Air War College, 2000. URL `https://www.airuniversity.af.edu/Portals/10/CSAT/documents/OP/csat13.pdf`.

[39] Zhang, S., Wang, L., Li, H., and Zhou, B., "Numerical Simulation on the Radar Cross Section of Variable-Sweep Wing Aircraft," *Journal of Aerospace Technology and Management*, Vol. 7, No. 2, 2015, pp. 217–226. https://doi.org/10.5028/jatm.v7i2.468, URL https://www.scielo.br/j/jatm/a/3tgYcYGvbHDqknRTQtBLC7d/?lang=en.

[40] Chung, S. M., and Tuan, S.-C., "Efficacy of an S-Shaped Air Inlet on the Reduction of Front Bistatic Radar Cross Section of a Fighter Engine," *Progress In Electromagnetics Research*, Vol. 172, 2021, pp. 1–12. https://doi.org/10.2528/PIER21060803, URL https://www.jpier.org/ac_api/download.php?id=21060803.

[41] MachineDesign, "Robots Keep F-22 Raptor Fighters Healthy and Stealthy," 2022. URL https://www.machinedesign.com/markets/robotics/article/21251522/robots-keep-f-22-raptor-fighters-healthy-and-stealthy.

[42] U.S. Air Force, "Luke AFB Unveils Newest Heritage Jet," 2022. URL https://www.luke.af.mil/News/Article-Display/Article/3076055/luke-afb-unveils-newest-heritage-jet/.

[43] Osborn, K., "Why the B-2 Spirit Stealth Bomber Is the Most Expensive Plane Ever," 2023. URL https://nationalinterest.org/blog/buzz/why-b-2-spirit-stealth-bomber-most-expensive-plane-ever-207195.

[44] BAE Systems, "ALE-47 Airborne Countermeasures Dispenser System," , Accessed May 2025. URL https://www.baesystems.com/en/product/ale47-airborne-countermeasures-dispenser-system.

[45] McNeal, T., "Countermeasure Dispenser System," https://patents.google.com/patent/US5136951A/en, Accessed May 2025. U.S. Patent No. 5,136,951, Issued August 11, 1992.

Appendix

Configuration Drawings

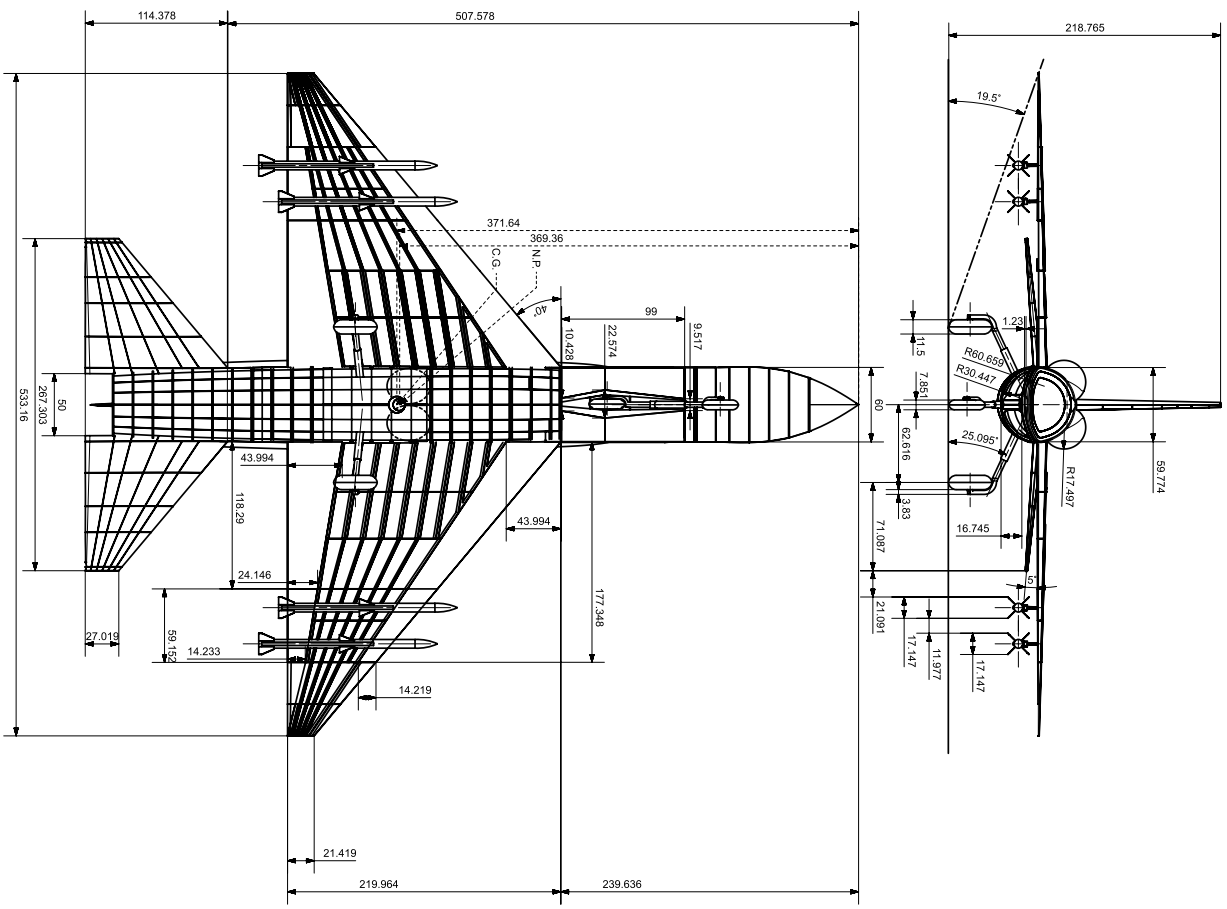

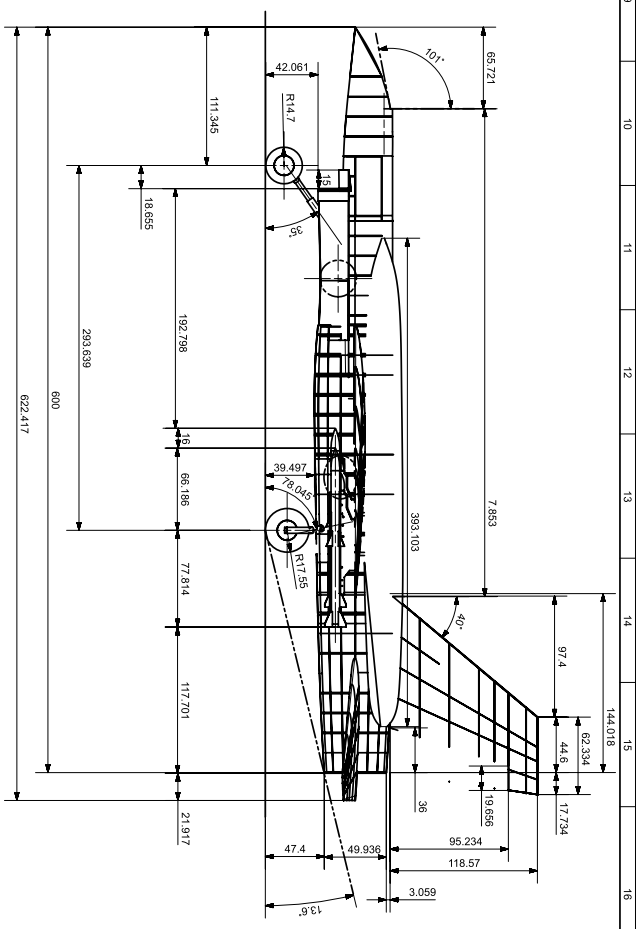

ALL DIMENSIONS IN INCHES

			FIRST ISSUED	05-Oct-2020
			DRAWN BY	Thomas Frain
			CHECKED BY	
			APPROVED BY	
SIZE	DRG NO.			
D				
SCALE 1:1				
SHEET 2 OF 2				
SHEET REV				
A				

SIEMENS

TITLE

Dragonfly_Assembly_drawing

THIS DRAWING HAS BEEN PRODUCED USING AN EXAMPLE TEMPLATE PROVIDED BY SIEMENS PLM SOFTWARE

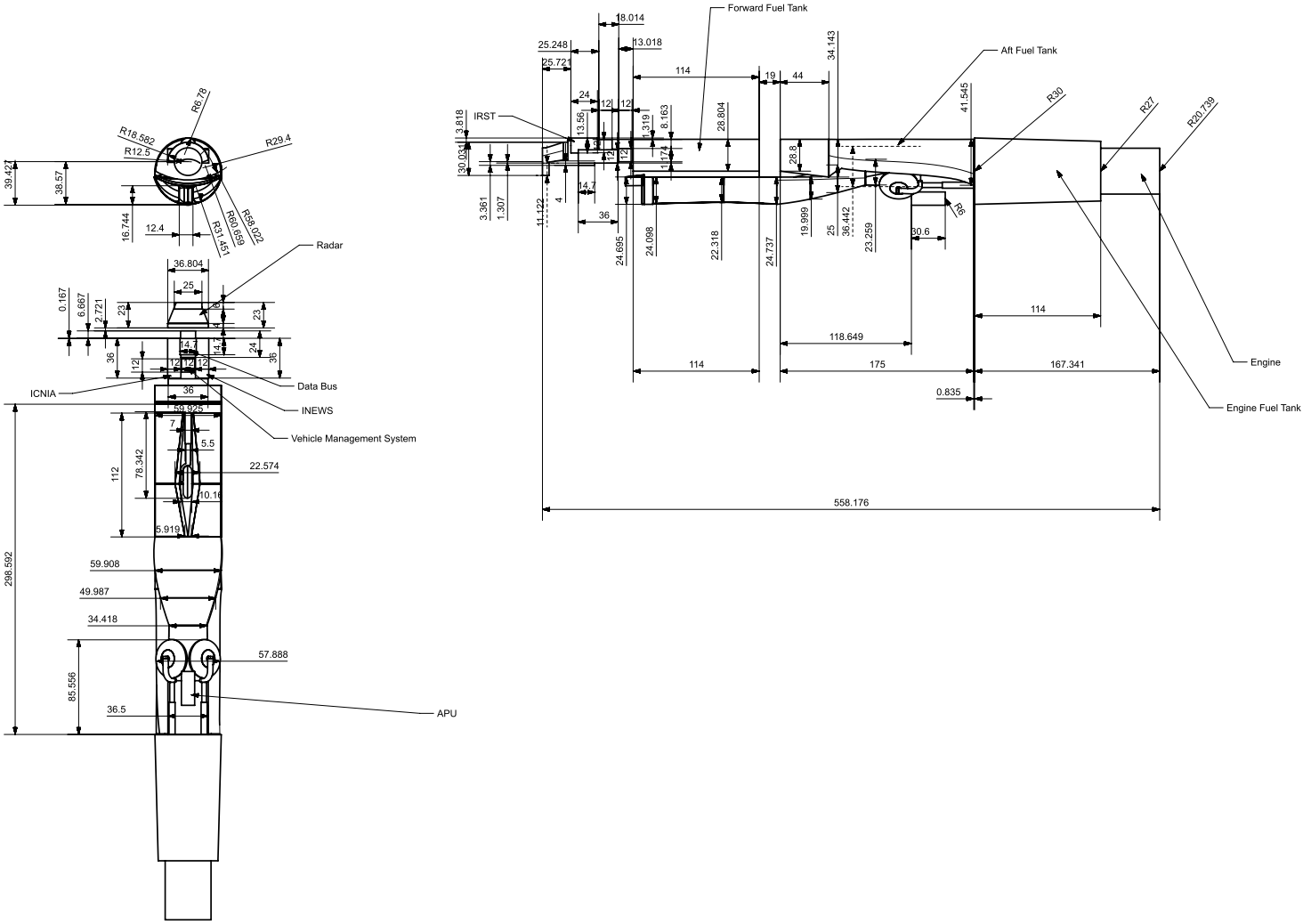

ALL DIMENSIONS IN INCHES

SIEMENS		THIS DRAWING HAS BEEN PRODUCED USING AN EXAMPLE TEMPLATE PROVIDED BY SIEMENS PLM SOFTWARE
FIRST ISSUED	05-05-2025	TITLE
DRAWN BY	Thomas Folan	
CHECKED BY		
APPROVED BY		SIZE D | DRG NO. Dragonfly_Internal_Configuration | SHEET REV A
		SCALE 1:1 | SHEET 2 OF 2